Attenuation in silica-based optical fibers

Wandel, Marie; Rottwitt, Karsten; Povlsen, Jørn Hedegaard

Publication date:
2006

Document Version
Publisher's PDF, also known as Version of record

Attenuation in silica-based optical fibers

Marie Wandel

PhD Thesis
Industrial PhD program (EF 954)

December 2005

ATV
Danish Academy of Technical Sciences

Preface

This thesis has been prepared at COM, Department of Communications, Optics & Materials, Technical University of Denmark and at OFS Denmark.

The work has been financed partly by Oticon Fonden, administered by the Danish Academy of Technical Sciences (ATV) and partly by OFS Denmark under the project number: EF 954.

The supervisors for this project are: Lars Grüner-Nielsen (OFS), Karsten Rottwitt (COM), Jørn Hedegaard Povlsen (COM) and David DiGiovanni (OFS labs).

The work has primarily been carried out at OFS Denmark from August 2002 to November 2005. 3 months were spent at OFS laboratories and a 3 month leave from the project was given from November 2004 to January 2005 in order to commercialize one of the products developed during this project.

Lyngby, December 2005

Marie Wandel

Abstract

In this thesis on attenuation in silica based optical fibers results within three main topics are reported.

Spectral attenuation measurements on transmission fibers are performed in the wide wavelength range 290 nm – 1700 nm. The measured spectral attenuation is analyzed with special emphasis on absorption peaks in order to investigate the cause of an unusual high attenuation in a series of transmission fibers. Strong indications point to Ni^{2+} in octahedral coordination as being the cause of the high attenuation.

The attenuation of fibers having a high core refractive index is analyzed and the cause of the high attenuation measured in such fibers is described as being due to scattering of light on fluctuations of the core diameter. A novel semi-empirical model for predicting the attenuation of high index fibers is presented. The model is shown to be able to predict the attenuation of high index fibers having viscosity profiles similar to those for which the model was calibrated but not of fibers having dissimilar viscosity profiles. The model is improved by including the viscosity profiles of the fibers. A set of fibers is produced demonstrating that by carefully designing the index profile as well as the viscosity profile a lower attenuation of high index fibers can be obtained.

The design of dispersion compensating fibers using the super mode approach is described, the object being to design dispersion compensating fibers for dispersion compensating fiber modules having a low attenuation, described by a high figure of merit. The major trade offs encountered when designing dispersion compensating fibers with high figure of merit are to obtain a very negative dispersion, low attenuation and low micro bend loss at the same time. The model for predicting the attenuation of high index fibers is used for the optimization process and results are reported of a dispersion compensating fiber having a record high figure of merit of 470 ps/(nm dB).

Resume (in Danish)

Denne afhandling beskriver dæmpning i silicabaserede optiske fibre indenfor tre områder.

Målinger af transmissionsfibres spektrale dæmpning er foretaget i et bredt bølgelængdeområde (290 nm – 1700 nm). For at undersøge årsagen til en usædvanlig høj dæmpning målt i en serie transmissionsfibre lægges der særlig vægt på undersøgelse af de observerede absorptionstoppe i det målte spektrum. Analysen peger på at en forurening af glasset med Ni^{2+} i oktaederisk koordination er skyld i den høje dæmpning målt for disse fibre.

Den høje dæmpning der måles i høj-index fibre er beskrevet som forårsaget af forskydning af materiale under trækprocessen. En semi-empirisk model der beregner dæmpningen i høj-index fibre ud fra oplysninger om indexprofil og trækbetingelser bliver præsenteret. Modellen kan beregne dæmpningen for fibre hvis viskositetsprofiler ligner dem for hvilke modellen blev kalibreret. En forbedring af modellen introduceres hvori der bliver taget højde for forskelle i viskositetsprofiler. Ved hjælp af den forbedrede model demonstreres det hvordan dæmpningen i optiske fibre kan forbedres ved ikke kun at designe indexprofilen men også viskositetsprofilen af fibrene.

I sidste del af afhandlingen beskrives hvordan dispersionskompenserende fibre kan designes ved hjælp af super mode teorien. Målet er at designe en dispersionskompenserende fiber der kan bruges til dispersionskompenserende fibermoduler med lav dæmpning. Denne lave dæmpning kan opnås for fibre med en høj ”figure of merit”.
Under designprocessen opleves forskellige begrænsninger især med hensyn til på samme tid at opnå både en meget negativ dispersion, lav dæmpning og lavt mikrobøjningstab. Modellen der er blevet udviklet til at beregne dæmpning i høj-index fibre anvendes til at optimere designet af dispersionskompenserende fibre med høj ”figure of merit”. Resultatet er en dispersionskompenserende fiber med den rekordhøje ”figure of merit” på 470 ps/(nm dB).

Acknowledgements:

For their supervision I would like to acknowledge: Lars Grüner-Nielsen (OFS), Karsten Rottwitt (COM), Jørn Hedegaard Povlsen (COM) and David DiGiovanni (OFS laboratories).

Oticon Fondet and OFS are acknowledged for financing this project and the Danish Academy of Technical Sciences for administering it.

I acknowledge the help and support from colleagues at OFS Denmark. Among these: Poul Kristensen, Carsten G. Jørgensen, Dan Jakobsen, Torben Veng, Tommy Geisler. Technicians and operators at OFS Denmark are acknowledged for their help with the manufacturing of the fibers described in this project.

During my stay at OFS laboratories a number of people helped me with my experiments: Man Yan, Patrick Wisk, Robert Windeler, Eric Monberg and Frank DiMarcello.

For proof reading of the manuscript I would like to thank Kirsten Wandel and Oluf Damsgaard Henriksen.

Table of contents

1. Introduction

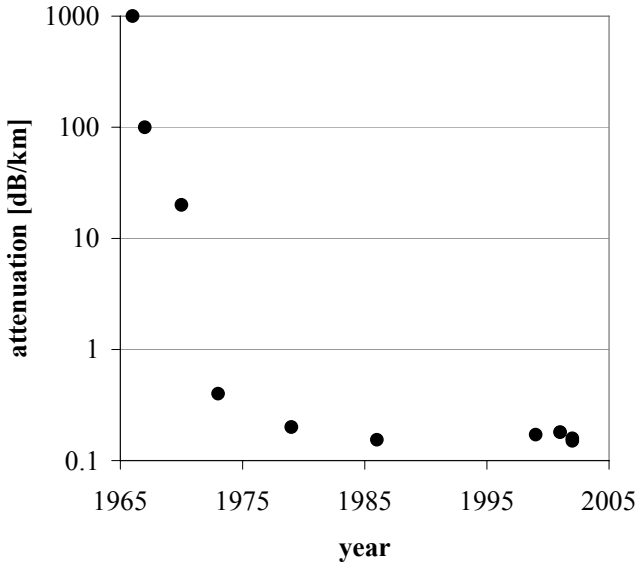

Figure 1 –The reduction in the attenuation of optical fibers from 1965 to present times.
Data from Kapron [1970], Miya [1979], Kanamori [1986], Nagel [1989], Kato [1999], Tsukitani [2002], Nagayama [2002].

Silica based optical fibers constitute the backbone of optical communication systems and carry much of the information that is being transmitted around the world. One of the properties of optical fibers that make them a preferred medium for data transmission is their high transparency, making the attenuation, or loss of light small. A typical attenuation coefficient of optical fibers for transmission is 0.2 dB/km.

Optical fibers are not only used as a transmission medium, but also for components within an optical communications system. Typically fibers used for components have attenuation coefficients several times larger than the transmission fibers. Even though the fiber loss is compensated by the introduction of amplifiers to a system, a low fiber attenuation is always desired since by reducing the attenuation, the number of amplifiers in a system can be reduced, thereby reducing the cost and complexity of the system and also improving the signal to noise ratio.

A common reaction to the title of this work "Attenuation in silica-based optical fibers" is: Wasn't that done many years ago? And true, a lot has happened since the results on the first optical fibers with attenuation coefficients in the order of 1000 dB/km were reported (Figure 1). In 1970 results were reported on fibers having an attenuation coefficient of approximately 20 dB/km at 632 nm [Kapron et.al 1970]. An attenuation coefficient of 0.2 dB/km at 1550 nm was reported in 1979 [Miya et.al

1979]. Now transmission fibers are routinely manufactured with an attenuation of less than 0.2 dB/km and a fiber having an attenuation coefficient of 0.151 dB/km at 1568 nm was recently reported [Nagayama 2002]. These results have been obtained by constant improvement of processes, materials and fiber designs and are approaching the theoretical lower limit of the attenuation in silica-based optical fibers. However, some phenomena regarding the attenuation in silica based optical fibers still deserve some attention.

Among these phenomena is the measurement of the spectral attenuation of optical fibers. Chapter 4 will present spectral attenuation measurements on transmission fibers manufactured at OFS Denmark and it will be demonstrated how these measurements can be a valuable tool in analyzing the causes of unusually high attenuation sometimes observed in these fibers.

Another phenomenon worth further investigation is the attenuation of fibers having a high core refractive index. This type of fiber is presently being used in optical communication systems as dispersion compensating fibers, nonlinear fibers and fibers for Raman amplification. For these fibers it is not possible to obtain as low an attenuation as that demonstrated for low core index fibers such as transmission fibers. When the core index is increased, the attenuation increases faster than can be fully explained by the known loss mechanisms. This will be the subject for chapter 5 in which a novel semi-empirical model predicting the attenuation of high index fibers will be introduced. By an expansion of the model, further insight into the mechanisms causing the high attenuation is gained, and improved designs for high index fibers having a lower attenuation are tested.

When looking to dispersion compensating fibers used for dispersion compensating fiber modules, the attenuation coefficient of the fiber is not as interesting as the total attenuation in the module, which is described by a figure of merit (FOM). The design of dispersion compensating fibers for low loss dispersion compensating fiber modules will be discussed in chapter 6. The model for predicting attenuation of high index fibers presented in chapter 5 will be used for optimizing the fiber design and results on two manufactured dispersion compensating fibers with FOM as high as 430 ps/(nm dB) and 470 ps/(nm dB) will be presented in chapter 6.

Initially the thesis will present an introduction to optical fibers and attenuation in optical fibers in chapter 2 and 3.

2. Optical fibers

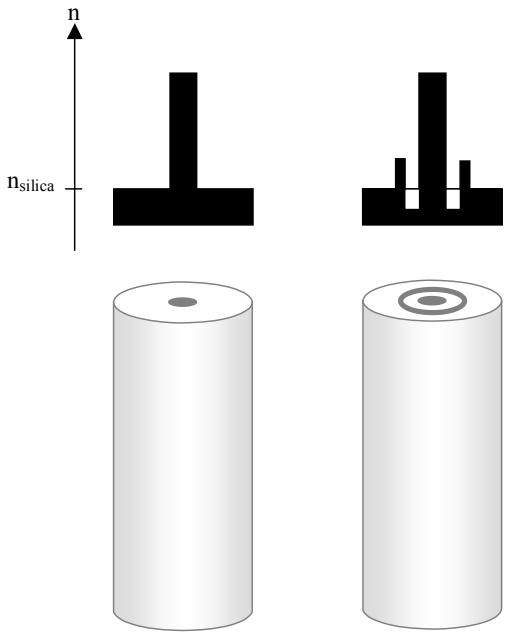

Figure 2 – Refractive index profiles and cross sections of optical fibers with single-clad and triple-clad index profiles.

2.1 Introduction

The fibers discussed in this work are all silica-based and manufactured using the Modified Chemical Vapor Deposition (MCVD) process. The light guiding properties of an optical fiber are determined by the refractive index profile (n(r)), which for the fibers presented here is either a single-clad or a triple clad refractive index profile (Figure 2).

The fiber with a single-clad index profile has a core with a refractive index (n) that is higher than that of the surrounding cladding (n_{silica}). The fiber with triple-clad index profile has a core with a high refractive index surrounded by a trench with a lower refractive index followed by a ring having a higher index than the cladding. The triple clad refractive index profile is by some authors described as a dual concentric core refractive index profile.

Refractive indexes given in this work will be given as refractive index differences (Δn) with reference to the refractive index of pure silica (n_{silica}):

$$\Delta n = n - n_{silica} \qquad \text{Equation 1}$$

2.2 Manufacturing of optical fibers.

In the MCVD process, high-purity material is deposited inside a horizontally mounted rotating silica tube [MacChesney 1974]. The material deposited inside the tube can be either pure or doped silica. Typical dopants include Fluor (F) that decreases the refractive index of the silica, Germanium (Ge) that increases the refractive index of the silica and Phosphor (P) that increases the refractive index and lowers the viscosity of the glass. The sources of Si, Ge and P are typically the chlorides $SiCl_4$, $GeCl_4$, $POCl_3$, which at room temperature are liquids having a high vapor pressure.

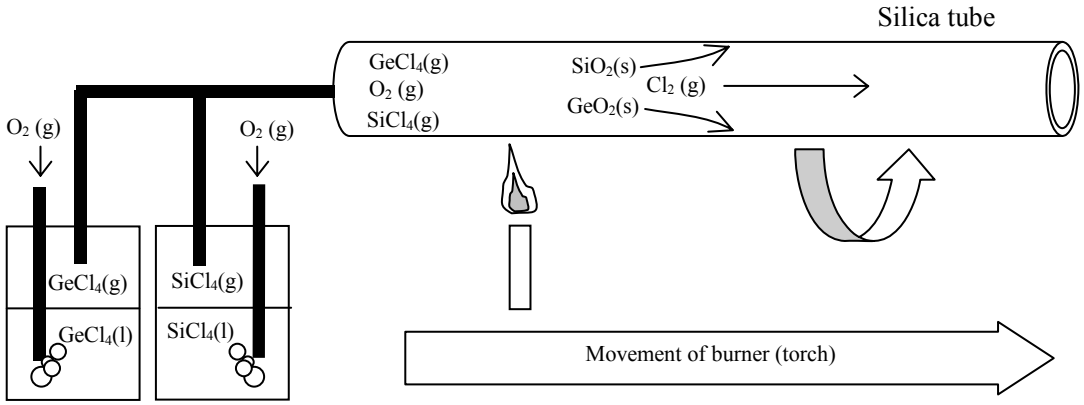

Figure 3 – The Modified Chemical Vapor Deposition (MCVD) process. The source materials, here exemplified with $GeCl_4$ and $SiCl_4$, are liquids having a high vapor pressure at room temperature. They are introduced into the horizontally mounted, rotating high purity silica glass tube with a flow of O_2. When the gas mixture is heated by the traversing oxy-hydrogen torch, the source materials are oxidized and sub-micrometer glass particles are formed. Through thermophoresis, the glass particles deposits on the cooler down stream wall. When heated by the torch, the sub-micrometer glass particles sinter into a thin layer of glass.

The reactant gasses are introduced into one end of the silica tube with a flow of oxygen (O_2). As the gas mixture is heated by a traversing oxy-hydrogen torch, the gasses are oxidized and sub-micrometer glassy particles are formed. Through thermophoresis, the glassy particles deposit on the inside wall of the tube as a layer of silica soot. When the traversing torch heats this soot layer, the glassy particles will sinter into a thin layer of glass with a well-defined refractive index. New layers of glass can now be deposited and sintered on top of the first. By controlling the ratio of $SiCl_4$ to the ratio of the dopant sources, the concentration of dopants, and consequently the refractive index of the glass is controlled.

When the innermost layer has been deposited, the tube is collapsed into a rod by heating the glass above its softening temperature at which point the preform shrinks due to the surface tension of the material.

The refractive index profile of the preform is measured and the preform is now either jacketed with an additional silica tube (to increase the ratio of cladding area to core area) or it can be drawn directly into fiber.

When the preform is drawn into fiber, the diameter is reduced by as much as a factor of 1000. The reduction of the diameter is uniform across the preform, so the resulting fiber has a refractive index profile that is a miniature replica of the refractive index profile of the preform. The outer diameter of the fibers presented here is 125 μm.

The draw process is a vertical process in which the preform is lowered into a furnace having a temperature around 2000 °C. The glass is softened and a drop of melted glass is formed at the lower end of the preform. When this drop falls, it is caught and the fiber is threaded through the coating applicator and onto a take-up spool. Two layers of protective coatings are applied before the fiber reaches the take-up spool.

The three main parameters characterizing the drawing process are the draw tension (F_{draw}), the draw temperature (T_{draw}) and the draw speed (v_{draw}) [Paek 1975, Vasiljev et.al 1989]. These three parameters are not independent, but will depend on each other through the relation for a given configuration of the draw tower [Paek 1986]:

$$v_{draw} \propto \frac{F_{draw}}{3A\eta(T)} \qquad \text{Equation 2}$$

A is the cross sectional area of the fiber and $\eta(T)$ is the viscosity of the glass at the end of the neck-down region where the fiber reaches its final diameter. Equation 2 assumes a Newtonian flow, i.e. that the viscosity of the glass is independent of the applied force. Since silica is the prototype of a strong glass [Angell 1995], the temperature dependence of the viscosity can be described with an Arrhenian expression [Shelby] as:

$$\eta = B\exp\left(\frac{E_a}{RT}\right) \qquad \text{Equation 3}$$

B is the pre-exponential factor, E_a the activation energy and R the gas constant.
A linear relationship between $\log(F_{draw})$ and $1/T_{draw}$ for fibers drawn at constant speed has been confirmed by several groups [Paek et.al 1988, Vasiljev et.al 1989, Choudury et.al 1998, Cheng & Jaluria 2000].

It is interesting to notice that for a given furnace configuration, T_{draw}, fiber diameter and preform diameter, there is a limit as to how fast a fiber can be drawn in a stable process without rupture of the fiber or large variations of the fiber diameter [Choudury et.al 1998, Choudury et.al 1999].

An overview of the fiber manufacturing process is given in Figure 4.

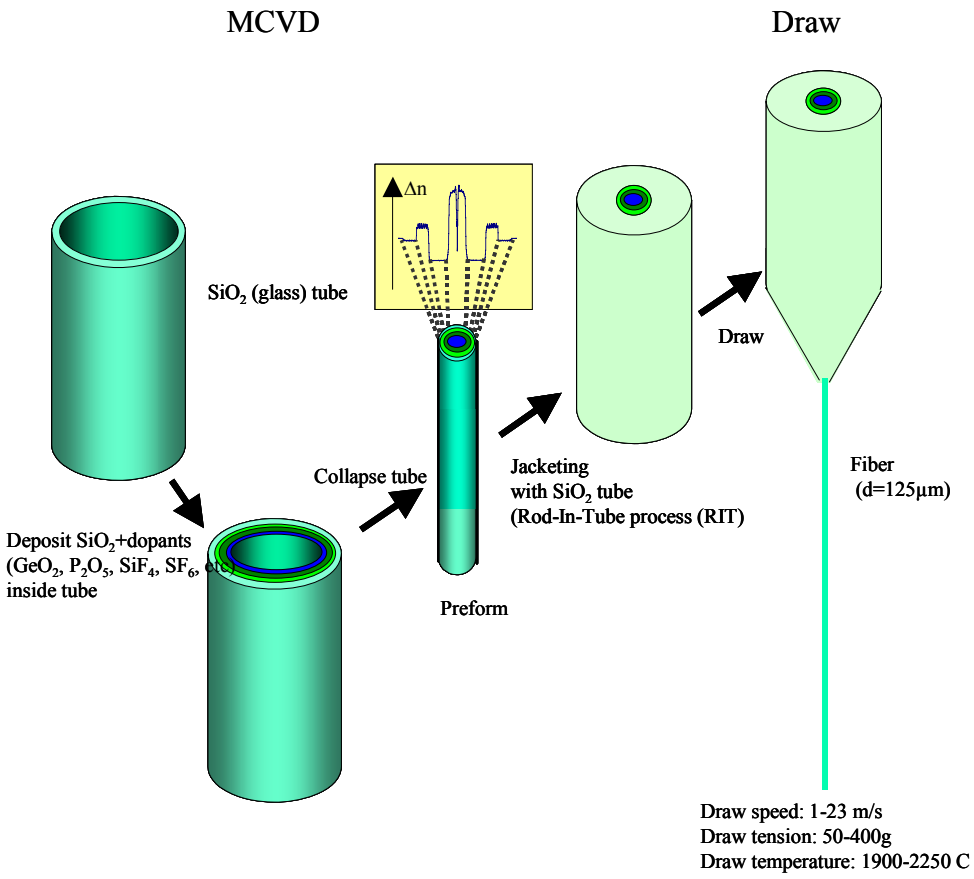

Figure 4 – the manufacturing process for optical fibers. The refractive index profile of the fiber is determined during the MCVD process in which layer upon layer of pure or doped silica is deposited inside a silica tube. The tube is collapsed and is either jacketed with an additional silica tube in order to increase the ratio of cladding area to core area or directly drawn into fiber.

2.3 The material

The optical fibers discussed in this work are made of silica-based glass.
Even though glass has been known through centuries, there exists no universally accepted definition of a glass. One possible definition is that given by Shelby [2005] that a glass is: An amorphous solid lacking long-range periodic atomic structure and exhibiting a region of glass transformation behavior.

If a crystal is being heated above its melting temperature (T_m) an abrupt change in enthalpy will be observed. When the melt is cooled below T_m the material will normally rearrange to obtain crystalline order and the enthalpy will drop to the value for the crystal. If however crystallization does not occur, a supercooled liquid is obtained. Upon further cooling, the viscosity of this liquid will increase (fluidity will decrease) and the structural rearrangements will slow down. At some point, the viscosity of the liquid will be so high that the atoms can no longer be completely rearranged to obtain the equilibrium structure, and the enthalpy will thus begin to deviate from the equilibrium. Eventually the viscosity of the liquid will become so high that no rearrangements are possible and the enthalpy reaches the value of the frozen liquid. The temperature region in which the enthalpy of the glass is neither that

of the equilibrium liquid, nor that of the frozen solid is the glass transformation region.

An important concept of glasses is the fictive temperature (T_f). The fictive temperature of a glass is the temperature for which the glass has the same structure as a supercooled liquid at equilibrium. T_f is thus a measure of structural disorder in the glass with a high T_f signifying a high degree of disorder.

In most optical fibers, the main component is vitreous (or glassy) silica (SiO_2). The basic building block of SiO_2 is the SiO_4 tetrahedron. The tetrahedron has a silicon atom at the center forming bonds to four oxygen atoms. Each of the four oxygen atoms can form bonds to neighboring silicon atoms thus creating a network that in the case of silica glass is highly disordered. The average Si-O bond distance is 1.6 Å and the average angle of the O-Si-O bond is 109.3°.

The structure of the silica network can be described in terms of the size of ring structures of connected tetrahedra found in the network. The typical ring structure found in silica consists of 3 – 9 membered rings. Looking at the bond angles and bond lengths for silica, it can be shown that 6-membered rings are the most energetically favored followed by the 5-membered rings while the 3- and 4-membered ring structures experiences some strain due to the small bond angles necessary to close the rings [Pasquarello 1998]. It has further been shown that if a silica glass is cooled very fast (quenched) the ratio of the 3-membered to 6-membered rings increases [Geissberger et.al 1983].

In order to control the refractive index of silica, dopants are introduced during the production of optical fibers. The most commonly used dopants are Germanium (Ge) and Fluor (F). Ge is incorporated by substituting for the Si atom in the silica tetrahedron. F is incorporated into the glassy network by substituting one of the bridging O-atoms. Since F cannot like the oxygen atoms form a bridge between two Si-atoms, the result of introducing F is a loser network with fewer oxygen bridges connecting the silica tetrahedrons.

3. Attenuation in optical fibers.

3.1 Definition.

The attenuation coefficient describes the loss of optical power inside an optical fiber. The attenuation coefficient (α) expressed in units of dB/km is defined as:

$$\alpha = \frac{10}{L}\log\left(\frac{P_{in}}{P_{out}}\right) \qquad \text{Equation 4}$$

P_{in} is the power launched into the fiber, P_{out} is the output power from the fiber and L is the length of the fiber [km].

3.2 The impact of fiber attenuation on an optical communication system.

Understanding the mechanisms causing attenuation in optical fibers is important since the attenuation in optical fibers limits the performance of optical communication systems. Even though the attenuation can be compensated by amplification, this will degrade the optical signal-to-noise ratio (OSNR) thus limiting the transmission distance.

In a 10Gb/s system with a bandwidth of 0.1 nm the OSNR must be larger than 16 dB [Nelson et.al 2005]. For a system with N amplification stages separated by equal lengths (L) of fiber having an attenuation coefficient (α), the OSNR (dB) is given by [ITU-T G.692]:

$$OSNR = P_{in} - L\alpha - NF - 10\log N - 10\log(h\nu\Delta\nu_0) \qquad \text{Equation 5}$$

With P_{in} being the power into the transmission fiber, NF the external noise figure of the amplifier, $\Delta\nu_0$ the optical bandwidth, h Planck's constant and ν the optical frequency.

If the amplifier spacing is 150 km, the input power 3 dBm, the attenuation coefficient of the optical fiber 0.2 dB/km, the noise figure of the amplifier 5 dB and the optical bandwidth 0.1 nm, the maximum transmission length in the 1.55 μm band will be 10 x150 km in a 10Gb/s system.

Figure 5 illustrates the importance of a low attenuation coefficient of optical fibers. If the attenuation coefficient of the transmission fiber is increased to 0.22 dB/km, the

limit for the OSNR of 16 dB is reached after 5 spans. With an attenuation coefficient of 0.24 dB/km the limit is reached after 2 spans. A high attenuation coefficient of the transmission fiber thus severely limits the transmission distance.

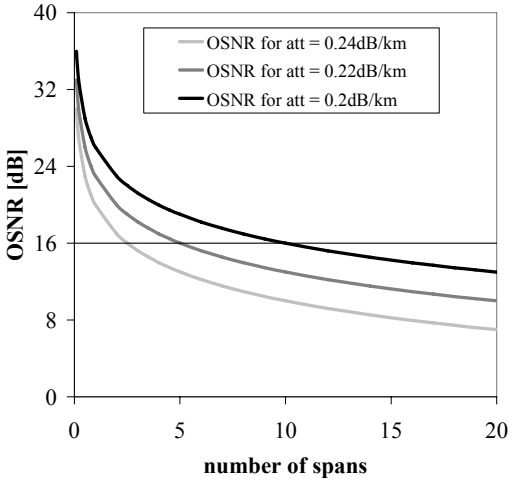

Figure 5 – OSNR as a function of N with P_{in} =3 dBm, L = 150 km and NF = 5dB (Equation 5).

3.3 Loss mechanisms

The attenuation, or the loss of light in optical fibers is due to several mechanisms. The wavelength range that will be discussed in this work ranges from the UV (290 nm) to the IR (1700 nm). The total loss in this wavelength range can be expressed as a sum of the contributions:

$$\alpha = \alpha_{UV} + \alpha_{IR} + \alpha_{Rayleigh} + \alpha_{Abs} + \alpha_{waveguide} \qquad \text{Equation 6}$$

with α_{uv} being the attenuation due to the Urbach absorption edge in the UV region of the spectrum, α_{IR} the attenuation due to vibrational absorptions in the IR region of the spectrum, $\alpha_{Rayleigh}$ is the Rayleigh scattering loss, α_{Abs} the attenuation due to absorption and $\alpha_{waveguide}$ the waveguide dependent attenuation.

3.3.1 Scattering losses

At 1550 nm, the dominant contribution to the attenuation coefficient of silica-based optical fibers is from scattering. Light is scattered by all spatial fluctuations of the permittivity ($\Delta\varepsilon(r)$). ε is related to the refractive index n of the material through: $\varepsilon^2 = n$. Using the formalism of scattering of unpolarized light by an oscillating dipole, the intensity of the scattered light at a distance R from the scatterer and at an angle θ to the direction of incident radiation is expressed as:

$$I(R,\theta) = \frac{I_0 \pi^2 (1+\cos^2\theta)}{2\lambda^4 R^2} \left\langle (\Delta\varepsilon)^2 \right\rangle v \qquad \text{Equation 7}$$

With I_0 being the intensity of the incident radiation, $\langle(\Delta\varepsilon)^2\rangle$ the mean squared fluctuation of the permittivity and v the correlation volume [Lines 1984]. The angular

dependence of the scattering as expressed by Equation 7 has been confirmed by measurements of the angular Rayleigh scattering in optical fibers [Mazumder et.al. 2004; Guenot et.al. 1999; Neeves et.al.1992].

The four main scattering mechanisms in optical fibers are elastic scattering on density ($\alpha_{density}$) or concentration fluctuations ($\alpha_{concentration}$), inelastic scattering on acoustical phonons (Brillouin scattering, $\alpha_{Brillouin}$) or optical phonons (Raman scattering, α_{Raman}) [Lines 1994] with the total scattering loss ($\alpha_{Scattering}$) given by:

$$\alpha_{Scattering} = \alpha_{density} + \alpha_{concentration} + \alpha_{Brillouin} + \alpha_{Raman} \qquad \text{Equation 8}$$

In pure silica glass $\alpha_{concentration} = 0$ and the main contribution to the scattering loss is from $\alpha_{density}$. In a pure silica glass, fluctuations of the permittivity can be induced by fluctuations in the density of the material. The density fluctuations are caused by fluctuations in the liquid state of the glass, frozen in when the glass melt is cooled. As discussed previously, the degree of disorder (density fluctuations) in the material depends on the cooling rate of the glass with a high cooling rate resulting in a large degree of disorder and a slow cooling rate resulting in a smaller degree of disorder. The degree of disorder is expressed through T_f and since a high T_f signifies a high degree of disorder, glasses with a high T_f have a high $\alpha_{density}$. An expression for $\alpha_{density}$ is [Lines 1994]:

$$\alpha_{density} = \frac{5 \cdot 10^{-5} n_0^8 p^2 K_T T_f}{\lambda^4} \qquad \text{Equation 9}$$

With n_0 being the refractive index, p the photoelastic constant, and K_T the isothermal compressibility. For pure silica having T_f = 1450 K, $\alpha_{density}$ = 0.11 dB/km at λ = 1550 nm. The contributions to the scattering loss from $\alpha_{Brillouin}$ and α_{Raman} at λ = 1550 nm for pure silica glass have been calculated to 0.006 dB/km and 0.009 dB/km respectively [Lines 1994].

Adding dopants to the glass affect all scattering components since the dopants not only introduces concentration fluctuations but also affects the density and the vibrational states of the material.

When dopants are added to the silica glass, concentration fluctuations on which the light scatter are present as well. The addition of dopants to the silica will however decrease the viscosity of the glass and consequently T_f ,resulting in lower $\alpha_{density}$. This effect was investigated by Lines [1994] who showed that theoretically the attenuation of silica due to scattering at λ=1550 nm can be reduced by adding an alkali metal oxide such as Na, K or Rb in low concentrations making the reduction in $\alpha_{density}$ is larger than the increase of $\alpha_{concentration}$.

The effect on the Rayleigh scattering loss of adding dopants to the silica has been investigated experimentally and the following expression for the Rayleigh scattering loss as a function of dopant concentration has been found for silica glass doped with a single dopant (either Ge or F) [Shiraki et.al1992, Ohashi et.al1992]:

$$\alpha_{Rayleigh} = A_{Rayleigh} \frac{\left(1 + C_{Rayleigh} \Delta n_i\right)}{\lambda^4} \qquad \text{Equation 10}$$

With $A_{Rayleigh}$ and $C_{Rayleigh}$ being empirically determined constants and Δn_i the refractive index change induced by doping the silica with dopant i. If $\Delta n_i = 0$, $\alpha_{Rayleigh} = A_{Rayleigh}/\lambda^4$ so $A_{Rayleigh}$ is a measure of the Rayleigh scattering in pure silica. Both $A_{Rayleigh}$ and $C_{Rayleigh}$ have been experimentally determined for silica glass doped with Ge or F as listed in Table 1.

Ref	**i**	$A_{Rayleigh}$ **[dB µm^4/km]**	$C_{Rayleigh}$
[Ohashi et.al.1992a]	Ge	0.8	30
[Shiraki et.al 1992]	F	0.8	28
[Dianov et.al 1997]	Ge	0.79	48
[Nagayama et.al 2000]	-	0.75	

Table 1 – Experimentally determined Rayleigh scattering coefficients for pure as well as Ge and F doped silica glass optical fibers

Investigations of the Rayleigh scattering from silica glass doped with both Ge and F showed a dependence of the dopant concentration as [Tsujikawa et.al 1994]:

$$\alpha_{Rayleigh} = A_{Rayleigh} \frac{\left(1 + 42\Delta n_{GeO_2} + 41\Delta n_F^2 + 31\Delta n_{GeO_2}\Delta n_F^2\right)}{\lambda^4} \qquad \text{Equation 11}$$

Tsujikawa et.al [2000] measured the effect of the drawing temperature on the Rayleigh scattering loss and found that a reduction in the drawing temperature of 200 °C reduced the Rayleigh scattering coefficient for Ge-doped fibers from 0.90 to 0.78 dB µm^4/km.

3.3.2 UV absorptions

The attenuation in the UV region of the optical spectrum is dominated by defect absorptions and the Urbach absorption.

Urbach absorption:

In amorphous materials, localized band tails extends into the otherwise forbidden energy gap between the valence and conduction band of the material. These states contribute to the absorption of the material at energies below the band gap (Figure 6). This phenomenon was originally described by Urbach [1953] and has been further investigated by Dow [1975] who gave the empirical expression for the Urbach edge:

$$\alpha_{UV} = A_{Urbach} \exp\left[g\left(E - E_0\right)\right] \qquad \text{Equation 12}$$

With A_{Urbach} giving the strength of the absorption (dB/km), g being a temperature dependent constant (eV^{-1}) and E_0 a constant (eV) having an energy comparable to the bandgap. Structural disorder is believed to influence the Urbach edge, with a larger degree of disorder resulting in more extended band tails and consequently a less steep edge in the absorption spectrum.

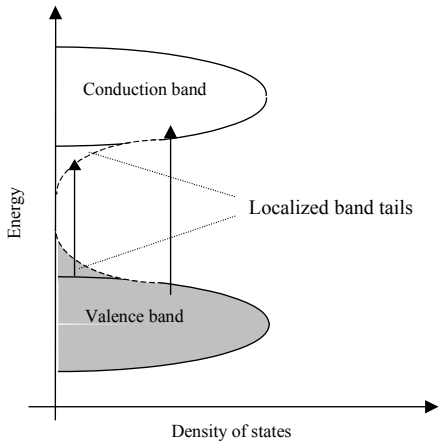

Figure 6 – Schematic representation of the electronic structure in an amorphous material such as vitreous silica. Due to disorder, localized band tails can be observed in the optical spectrum.

Schultz [1977] quoted through Garrett & Todd [1982] measured the attenuation in the wavelength range 150 –250 nm for bulk silica glass doped with GeO_2. It was found that the spectral absorption from the Urbach edge could be expressed as a function of GeO_2 concentration as:

$$\alpha_{UV} = \frac{1.07 X_{Ge}}{44.6 X_{Ge} + 6000} \exp\left(\frac{4.63}{\lambda}\right) \qquad \text{Equation 13}$$

This expression is widely quoted and has been used to predict the absorption in a very wide spectral range [Dianov 1997]. Whether the expression can accurately be extrapolated to wavelengths as high as 1550 nm has never been experimentally confirmed. Since it has not been possible to obtain the original paper it has not been possible to investigate how the absorption bands due to Ge-defects at 190 and 240 nm (Table 2) has affected the determination of the Urbach absorption from measurements of the absorbance in the 150 – 250 nm spectral region.

In the analyses of the spectral attenuation of Ge-doped optical fibers that will be presented in this work, the Urbach absorption will be modeled with the following expression, which is based on Equation 12 and the assumption that the Urbach absorption depends linearly on the GeO_2 concentration in the optical fiber.

$$\alpha_{UV} = A_{Urbach} \Delta n_{core} \exp\left[g\left(E - E_0\right)\right] \qquad \text{Equation 14}$$

In which Δn_{core} is an expression for the GeO_2 concentration. Whether the Urbach absorption actually has a linear dependence of the GeO_2 concentration is uncertain. Since the Urbach edge of pure silica glass has a much lower intensity than that of Ge-doped silica due to the higher energy of the bandgap, it seems reasonable, that the Urbach edge observed in Ge-doped silica glass is primarily due to Ge and that the intensity of the Urbach edge is proportional to the Ge-concentration.

Skuja et.al [2004] have investigated the effect of F doping on the Urbach absorption of silica glass and found that as the concentration of F increased, the Urbach

absorption decreased. They explained this by a decrease in the structural disorder of vitreous silica upon doping with F.

3.3.3 IR absorptions

In the IR region of the spectrum, the absorption bands related to the vibration of silica oxygen bonds are responsible for the appearance of the spectrum. At wavelengths up to 1700 nm only the tail of the vibrational absorptions is observed.

The vibrations in silica and germania are well described [Hass 1970, Bell et.al 1971, Bell et.al 1975]. An expression for the tail of the vibrational absorptions that are observed in the attenuation spectrum of optical fibers has been given:

$$\alpha_{IR}(\lambda) = \sum X_i C_i \exp\left(\frac{-c_i}{\lambda}\right) \qquad \text{Equation 15}$$

With X_i being the mole fraction of each component i, C_i and c_i being wavelength independent material parameters characterizing the components. For pure silica, C_i= $6x10^{11}$ dB/km and c_i = 48 μm [Lines 1994].
The frequency (v_{vib}) of the vibrations in a material is given by:

$$v_{vib} = \frac{1}{2\pi c}\sqrt{\frac{k_{vib}}{\mu_{vib}}} \qquad \text{Equation 16}$$

With k_{vib} being the force constant of the bond, which can be obtained from the second derivative of the potential energy with respect to the coordinates of the atoms involved in the vibration. μ_{vib} is the reduced mass of the vibrational mode calculated from the masses of the involved atoms. When silica is doped with Ge, the reduced mass of the vibration will increase due to the higher atomic mass of Ge and the frequency will decrease. Consequently, the attenuation in optical fibers caused by vibrational absorptions will decrease at 1550 nm as the concentration of Ge is increased.

3.3.4 Absorption bands

The mechanisms responsible for attenuation in optical fibers described so far all extend over wide wavelength ranges. The last contributions to the attenuation of optical fibers that will be described here is the attenuation due to absorptions caused by defects or contaminations of the glass.

Defects

The structure of crystalline materials can ideally be described by translations of the unit cell. Any deviation from this description is a defect including extended defects such as dislocations or grain boundaries in which the long-range order of the crystal is perturbed. The defects of interest in vitreous silica (doped with Ge) are point defects that occur at isolated atomic position. The defects occurring in Ge doped silica have been subjects to detailed studies since some of them are involved in the mechanism for UV-induced refractive index changes. Furthermore, some of the defects absorb light thereby causing attenuation. The values given in Table 2 for the optically active

defects that are normally observed in Ge-doped silica are from two review papers: [Neustruev 1994, Skuja 1998].

	center wavelength [nm]	oscillator strength
Si-ODC	180	0.20
Ge(ODC)	190	0.20
Ge oxygen vacancy	240	0.05
Ge divacancy	330	1.20E-05
NBOHC	630	4.00E-04
Peroxy radical	630	5.70E-04
Peroxy radical	260	4.00E-04
Interstitial O_2	770	1.00E-08
Interstitial O_2	1280	1.20E-08
Interstitial ozone	260	5.00E-08

Table 2 – Defects found in Ge-doped silica based optical fibers.
Data from Neustruev [1994] and Skuja [1998]

With ODC being an oxygen-deficient-center and NBOHC a non-bridging-oxygen-hole-center. Even though none of these defects absorbs in the 1550 nm wavelength region, they cause additional loss in optical fibers through their reaction with hydrogen.

Reactions with hydrogen

The exposure of optical fibers to hydrogen, causes the attenuation to increase partly due to dissolved unreacted hydrogen in the silica glass and partly due to the reaction between hydrogen and defects in the silica glass [Stone 1987].

Through reactions between the peroxy defect and hydrogen, a Si-O-OH and a Si-H group are formed with the Si-O-OH group absorbing around 1385 nm and the absorption from the Si-H group having a center wavelength of 1530 nm and tails of the absorption extending into the 1550 nm region [Chang et.al 1999]. The NBOHC will also react with hydrogen and form a Si-OH group absorbing light having wavelengths around 1385 nm as well.

Water peak

The absorption observed around 1385 nm in optical fibers is due to overtone vibrational absorption of the Si-OH band or the Ge-OH band. Several groups have investigated these absorption peaks [Bredol et.al 1990, Stone & Walrafen 1982, Humbach et.al 1996]. The assembly of vibrational absorption peaks around 1385 nm is termed the water peak. In Table 3 the five main absorption bands of the water peak are given as described by Bredol et.al [1990].

The water peak has been described as a combination of both Gaussian and Lorentzian components [Bredol et al. 1990]. This combination was chosen since it gave the best fit to measured data. However, the authors argue that neither Gaussian nor Lorentzian line shapes are likely to give the best representation of the water peak, since the physical mechanism of randomly distributed absorbers are more likely to yield a Voigt line shape. Throughout this work, absorption bands will be modeled as having Gaussian line shapes.

Center wavelength [nm]	Relative intensity	Function
1412	0.142	Lorentzian
1391	0.606	Lorentzian
1381	0.542	Gaussian
1352	0.020	Lorentzian
1247	0.059	Lorentzian

Table 3 – Parameters describing the five main absorption bands of the water peak

Other contaminants:

Transition metals are easily incorporated in the silica network in which the transition metal ions can either form complexes using the oxygen atoms of the silica network as ligands or they can act as network formers with the transition metal forming bonds to the oxygen atoms of the network. Another possibility is that the transition metal is dissolved in the glass either as a complex or as a free ion [White et.al 1986]. Due to the partly filled d-orbitals of the transition metals, they have high absorption coefficients in the visible to infrared part of the optical spectrum. In high concentrations the transition metals are highly appreciated as colorants for optical filters or for decorative purposes, while they even in very low concentrations significantly increases the attenuation of optical fibers.

Figure 7 shows the effect of the different loss mechanisms on the spectral attenuation of an optical fiber.

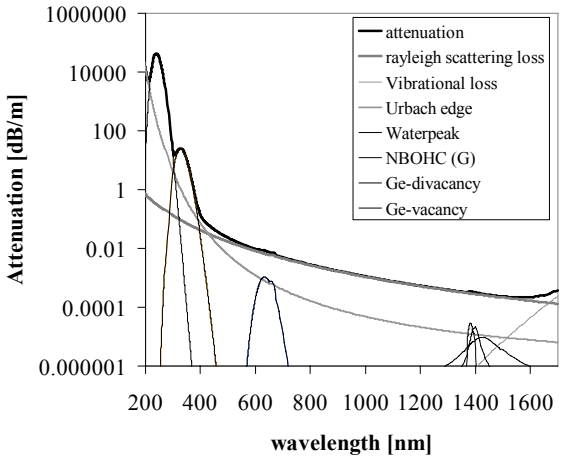

Figure 7 – Spectral attenuation of optical fibers in the wavelength range 200 – 1700 nm. The contributions to the total attenuation from the most common loss mechanisms described in this chapter are included.

The last term of Equation 6, $\alpha_{waveguide}$ will be described in section 6.2 in which the introduction to design of dispersion compensating fibers are given.

This concludes this introductory chapter on attenuation in optical fibers. In the next chapter measurements and analyses of the spectral attenuation of optical fibers having an unusually high attenuation will be presented.

4. Spectral investigation of the attenuation in transmission fibers

4.1 Introduction

It has been observed that some fibers have a high attenuation at 1550 nm i.e. for transmission fibers, an attenuation well above 0.2 dB/km. In this section, the spectral attenuation of high attenuation fibers ($\alpha > 0.25$ dB/km) as well as low attenuation fibers ($\alpha < 0.22$ dB/km) will be measured in the wavelength range 290 – 1700 nm, the object being to determine the cause of the high attenuation at 1550 nm observed in some fibers. The measured attenuation will be analyzed with special emphasis on the absorption peaks.

4.2 Measuring the attenuation

The measurement of the spectral attenuation of optical fibers in the wavelength range has been described in [Wandel & Grüner-Nielsen 2004]. The spectral attenuation has been measured for a number of transmission fibers in the wavelength range 290 – 1700nm. Since the attenuation in this wavelength range varies from below 0.0002 dB/m at 1550 nm to more than 20 dB/m at 330 nm, different lengths are needed in different spectral regions. Furthermore, since this wavelength range spans from the UV to the IR part of the spectrum, different light sources and detectors are needed as well.

4.2.1 The setup:

The 3 different setup used for measuring the spectral attenuation of the fibers are summarized in Table 4.

Wavelength range	Light source	Detector	Fiber length
290 – 380 nm	Deuterium lamp	OSA, Spektro 320, Instrument systems	0.5 – 5 m
350 – 700 nm	Ando White light source	OSA, Spektro 320, Instrument systems	5 – 1000m
600 – 1700 nm	Spectral fiber attenuation measurement system from Photon Kinetics model PK2500		1000 – 50000m

Table 4 – The three setup used for the measurement of the spectral attenuation

Figure 8 and Figure 9 show the setup used for measuring the spectral attenuation in the two low wavelength ranges (290-380 nm and 350-700 nm) The light source used is either the deuterium lamp (290-380nm) or the Ando white light source (350 –

700nm) and the detector is an optical spectrum analyzer (Spektro 320, Instrument systems). The Fiber Under Test (FUT) is connected to the light source and to the detector, by means of pure silica core fibers to which the FUT is fusion spliced. Pure silica core fibers have been chosen since at the lower wavelengths they contribute with less loss to the set-up than a Ge-doped fiber. The mode field diameter of the silica core fibers being different from that of the FUT, a reproducible splice loss cannot be obtained. A dummy splice is introduced within the FUT to eliminate this source of uncertainty to the measurement (SP2). For the reference measurement, the FUT is cut after the mode filter and between splice 2 (SP2) and splice 3 (SP3). In this way, the two splices between the silica fibers and the FUT remain intact, and the only splice that needs to be re-spliced is the one within the FUT, which can be reproduced with high accuracy (SP4). For the wavelength range 600-1700 nm, the spectral attenuation has been measured using a commercially available setup: A Photon Kinetics, PK2500.

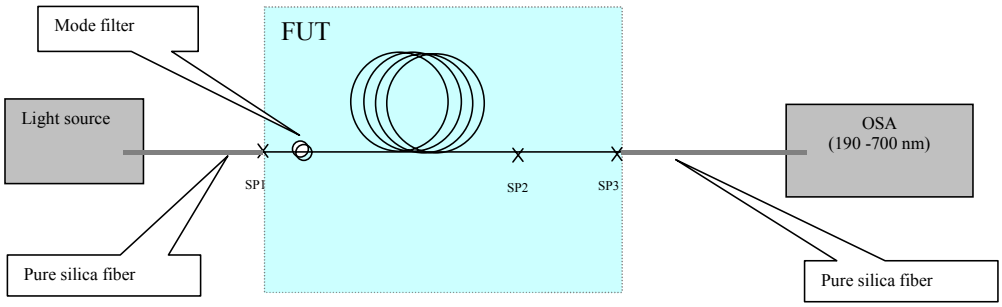

Figure 8 – The set up for measuring the attenuation of optical fibers in the wavelength range 290 nm – 700 nm

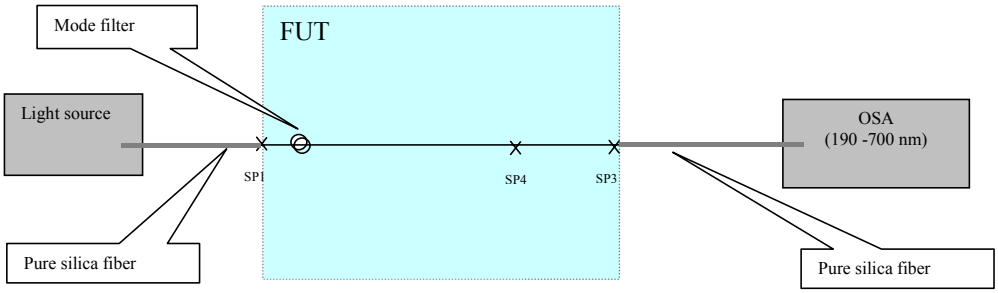

Figure 9 – The set up for measuring the reference

The measurement includes two types of transmission fibers: standard single mode optical fibers (SSMF) and non-zero dispersion-shifted single-mode optical fibers (NZDSF) [ITU-T, G.652, ITU-T G.655]. See Table 5 for the optical properties of either type of fibers at 1550 nm. Within each fiber type, fibers with both a low and a high attenuation at 1550 nm have been measured. For each fiber at least 3 measurements have been made for each spectral region in order to check the reproducibility of the measurements.

	Dispersion [ps/(nm km)]	Attenuation [dB/km]	Mode field diameter [µm]
NZDSF (TrueWave RS)	4.5	0.20	8.4
SSMF (AllWave)	16.5	0.19	10.4

Table 5 – Optical properties of NZDSF and SSMF transmission fibers measured at 1550 nm

4.3 Analyzing the spectral attenuation

In order to obtain a continuous spectrum, an adjustment of each part of the spectrum is allowed within the uncertainty of the measurement. The uncertainty is due to the splice within the FUT being reproduced for the reference measurement and due to uncertainty of the fiber length. The resulting spectrum is then analyzed by fitting Equation 6 to the data using a least squares fitting routine.

Both the Rayleigh scattering and the Urbach edge increases rapidly on going to shorter wavelengths. This can make them difficult to distinguish from each other, especially when other loss components are present in the spectrum. At longer wavelengths, the loss spectrum is dominated by the tail of the IR vibrational absorptions and the waveguide dependent losses such as micro- and macro bend losses. Both types of losses depend exponentially on wavelength, which impedes distinction between them.

Since the object of this study is to analyze the attenuation due to absorption peaks, the loss contributions mentioned above, i.e. the Rayleigh scattering, the Urbach edge, the IR tail and the waveguide dependent losses, will only be used for subtracting the background from the absorption peaks. The magnitude of these loss components will not be analyzed further.

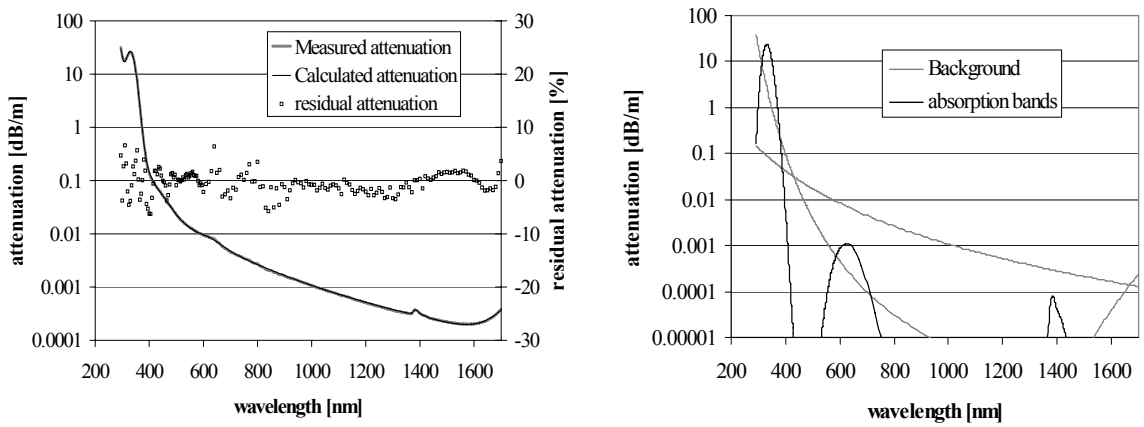

Figure 10 – a) Measured, calculated and residual attenuation of a low attenuation fiber.
b) Background attenuation and absorption bands

Figure 10a shows the measured and calculated attenuation for a transmission fiber with a normal attenuation at 1550 nm of 0.2 dB/km. The calculated attenuation is found by fitting Equation 6 to the measured attenuation. The residual attenuation, which is the difference between the calculated and measured attenuation, can also be seen in Figure 10a. Figure 10b shows the different components of the attenuation of a low loss transmission fiber. The absorption peaks of this fiber are centered at 330 nm, 630 nm and the water peak at 1385 nm. The attenuation of this fiber is fully explained by the loss components described in Equation 6.

If the same fitting routine is used for any one of the high loss fibers, the best possible fit results in a residual attenuation as the one shown in Figure 11. Of the absorption bands only the intensities are allowed to vary.

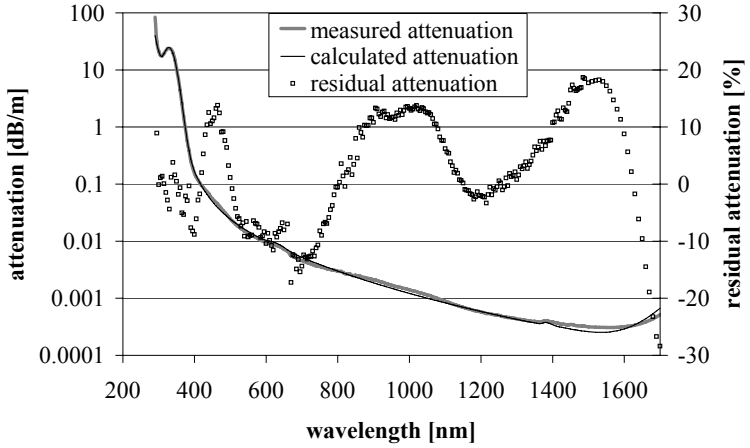

Figure 11 – Measured, calculated and residual attenuation for a high loss fiber

As shown in Figure 11, Gaussian absorption bands with center wavelengths at 435 nm, 870 nm, 1050 nm and 1700 nm can be added to the fitting routine, resulting in a lower residual attenuation as shown in Figure 12. Of the four additional absorption bands, the band at 435 nm has the highest peak intensity.

These four absorption bands were observed in all high attenuation transmission fibers but in none of the low attenuation transmission fibers for which the spectral attenuation was measured. The exact position of the absorption band around 1050 nm is somewhat uncertain as a cut off wavelength for some of the fibers is close to 1050 nm which makes the spectral attenuation measurement uncertain. As the absorption band around 1700 nm is at the edge of the measured wavelength range and furthermore at a wavelength where bend induced losses play a significant role, the exact position and intensity of this absorption band is uncertain as well. Therefore only the absorption bands at 435 nm and 870 nm will be discussed in the following.

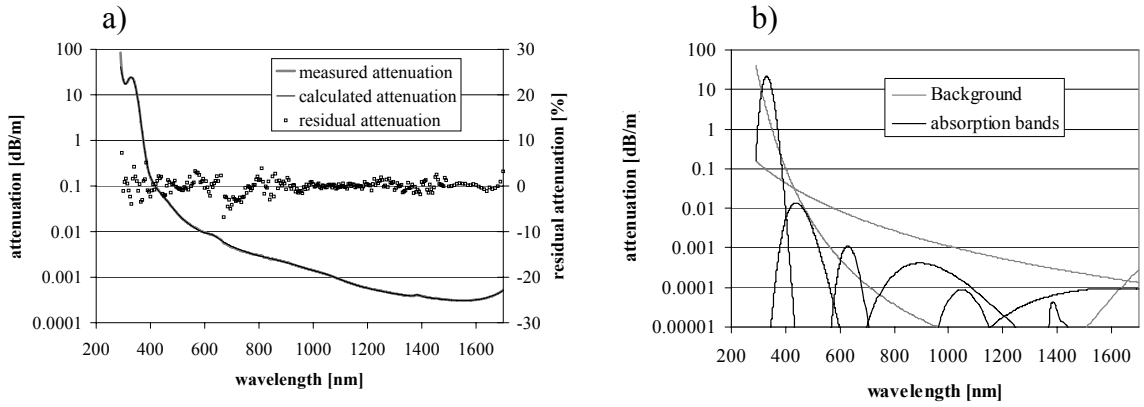

Figure 12 – High loss fiber - fit including novel absorption bands

4.4 Results

Table 6 lists the parameters describing the absorption bands found in the wavelength range 300 nm– 1000 nm for 9 high loss transmission fibers. This includes the absorption bands at 330 nm and 630 nm found in all silica-based optical fibers and the two novel absorption bands at 435 nm and 870 nm.

Fiber	330nm		435nm		630 nm		870 nm	
	Wave length (nm)	Peak intensity (dB/m)	Wave length (nm)	Peak intensity (dB/m)	Wave length (nm)	Peak intensity (dB/m)	Wave length (nm)	Peak intensity (dB/m)
1	329	21.56	420	0.0135	626	0.00114	880	0.000409
2	330	23.77	442	0.0099	623	0.00111	872	0.000632
3	330	14.90	438	0.0168	631	0.00198	852	0.002134
4	330	16.40	448	0.0024	629	0.00169	864	0.000212
5	330	19.21	439	0.0053	631	0.00161	855	0.000213
6	328	15.32	422	0.0171	627	0.00165	880	0.000924
7	330	15.79	436	0.0243	638	0.00155	863	0.003301
8	Not measured		432	0.0053	635	0.00066	868	0.001232
9	Not measured		439	0.0202	636	0.00141	881	0.002244

Table 6 – Center wavelengths and peak intensities of absorption bands found in the high loss optical fibers

The absorption bands with center wavelengths around 330 nm and 630 nm are well described while the bands at 435 nm and 870 nm are rarely mentioned in the optical fiber literature. An increase in intensity of the 435 nm band has been observed during UV exposure [Kristensen 2003; Antonyuk et.al.2000], which is the reason why this absorption band has previously been described as associated with a defect involved in the UV-induced index change in germanium doped silica. Antonyuk describes the defect as a drawing induced defect (DID) associated with germanium-doped silica.

The observation of an absorption peak at 870 nm has been described previously as well. In [Bauch et.al, 1987] the absorption band is observed in pure silica fibers and is believed to be due to a radiation-induced defect in oxygen rich silica, while Kaiser

[1977] speculates whether the absorption band at 870 nm could be due to a contamination of the silica.

Even though both the absorption bands at 435 nm and at 870 nm have been reported in the literature, the spectral attenuation was only measured within limited wavelength ranges. The studies of UV-induced index changes are mainly concerned about attenuation changes up to 700 nm while the measurements of the pure silica fibers do not go below 500 nm. Consequently a possible correlation of the two absorption bands has not been investigated in the optical fiber literature.

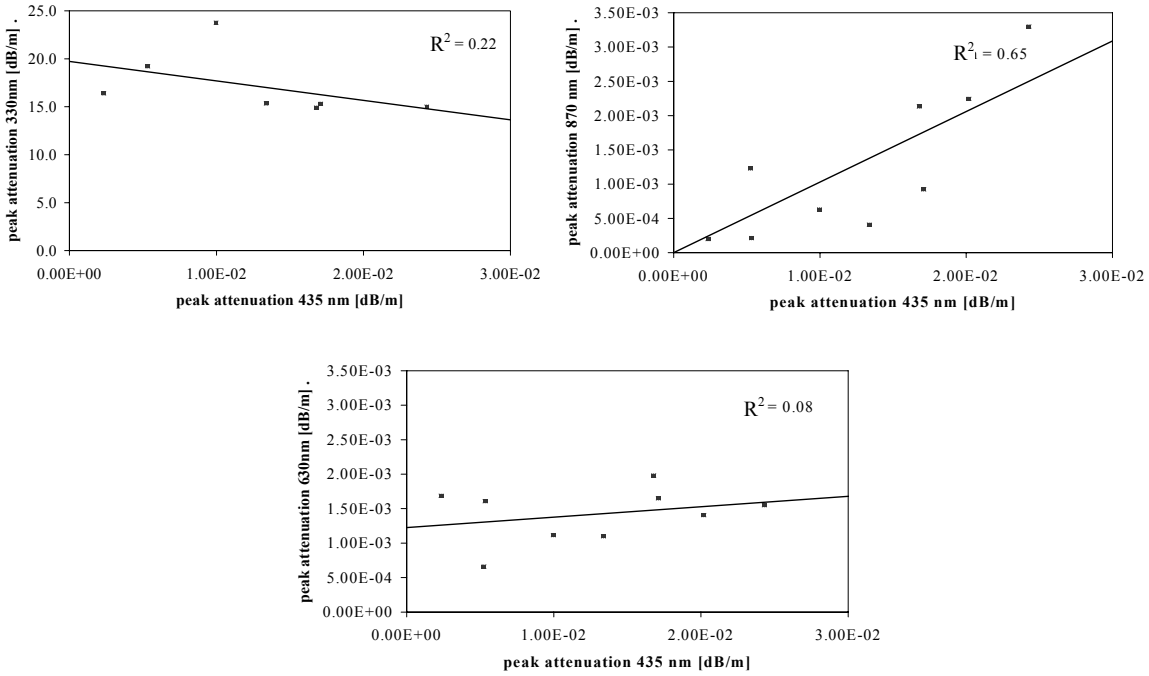

Figure 13 – Correlations between peak intensities of absorption band at 435 nm with bands at 330 nm, 630 nm and 870 nm

Figure 13(a-c) shows the correlation of the intensities of the 435 nm absorption band to the absorption bands at 330 nm, 630 nm and 870 nm respectively. If the absorption at 435 nm is associated with a drawing induced defect, a correlation with the intensity of the silica- drawing induced defect at 630 nm is to be expected.

Figure 13 shows the correlation of the peak intensity of the 435 nm absorption band to be much stronger with the intensity of the 870 nm band than with the intensity of the 330 nm or 630 nm band making it likely that the 435 nm and the 870 nm absorption bands are related. This raises some questions regarding the previous assignments of the absorption bands at 435 nm and 870 nm.

As the 870 nm absorption band has been observed in pure silica fibers it is not likely that this absorption is associated with a Ge-defect like the one believed to be causing the 435 nm absorption band, but rather with either an oxygen rich silica defect or a contamination. The 435 nm absorption has not been observed in pure silica fibers

having the 870 nm absorption band, as the attenuation of these fibers has not been measured below 500 nm.

Since it has now been shown that the 435 nm and the 870 nm absorption bands are likely to be associated with the same defect or contamination, it will further be assumed that the absorptions at 1050 nm and 1700 nm are associated with the same defect or contamination since the four novel absorption peaks are always seen together in the high attenuation fibers. Figure 14 shows the added attenuation spectrum for some of the measured fibers.

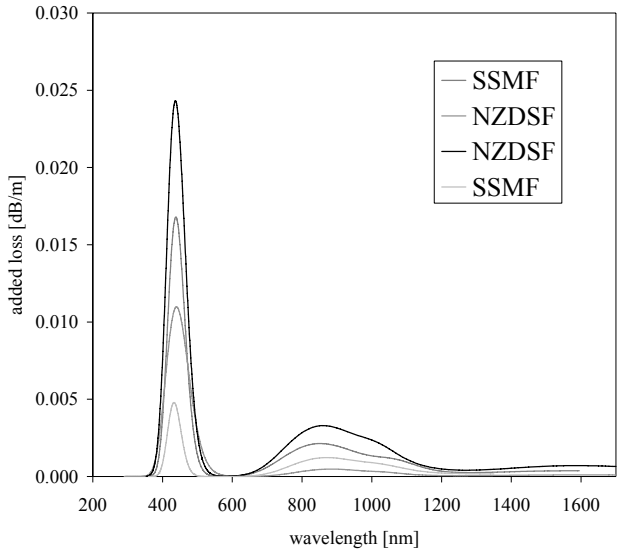

Figure 14 – Added attenuation spectrum of high attenuation fibers. The added attenuation spectrum for SSMF and NZDSF fibers are very similar.

Similar added attenuation spectra have been observed in both the NZDSF and the SSMF transmission fibers (Figure 14). Noticing the different wave guiding properties of these fibers (Table 5) it is unlikely that the added attenuation should be due to coupling to cladding modes or other loss mechanisms defined by the wave guiding properties. In the next sections strong evidence that the added attenuation spectra are due to absorptions caused by contamination will be presented.

4.4.1 Finding a match.

The broad peaks in the visible and near IR region suggests a contamination by a transition metal. The classical work by Schultz [1973] describes the absorption spectra in silica optical fibers doped with oxides of the first row transition metals. However, none of the spectra shown in the work by Schultz matches the one shown in Figure 14.

A study of the glass literature on transition metals in glasses, disclosed a spectrum matching that of Figure 14, viz that of Nickel (Ni) in a dodecahedral or octahedral coordination [Gitter & Vogel, 1979]. Calculations in this paper show that the spectrum reported by Schultz [1973] matches that of tetrahedrally coordinated Ni.

The findings reported by Nelson & White [1993] support the assignment of the added attenuation spectrum of the high attenuation fibers to that of octahedrally coordinated Ni based on an analysis of Ni in several host glasses and theoretical calculations of expected band energies.

Turner & Turner [1972] investigate the absorption spectra of Ni in different host glasses and it is found that Ni is either in octahedral or tetrahedral coordination. The octahedral coordination matches that of the added attenuation spectrum with absorption bands at 445 nm, 865 nm, 1100 nm and 1850 nm.

Möncke et.al [2002a, 2002b, 2003] have a number of papers on the coordination of Ni in glass. They show that the coordination geometry of Ni in the glass depends on the basicity (the number of non-bridging oxygens) of the glass. They show that upon quenching a glass containing octahedrally coordinated Ni, an increase of the levels of tetrahedrally or dodecahedrally coordinated Ni can be found. Their work supports the assignment of the added loss spectrum to that of octahedrally coordinated Ni with absorption bands at 420 nm, 870 nm and 1090 nm.

Other matches to the added attenuation spectrum include the spectrum of an “as cast” zinc-alumina-silicate glass doped with Ni [Suzuki et al.2004] showing broad absorption peaks centered at 440 nm, 860 nm and 1760 nm. When this glass is annealed, the spectrum is changed. As opposed to the other publications mentioned, where the added attenuation spectrum of Figure 14 could be found to match that of octahedrally coordinated Ni, the authors of this paper believe that the spectrum of the “as cast” glass is due to tetrahedrally coordinated Ni while the spectrum of the annealed glass is due to octahedrally coordinated Ni. However, the spectra of the “as cast” and annealed glasses showed in the paper are very similar except for the splitting of the bands. This could indicate that the Ni in both “as cast” and the annealed glass have the same coordination geometry, but that the splitting of the energy levels changes due to different distance to or identity of the ligands between the “as cast” and annealed glass.

By comparison to published spectra of Ni in different glasses it can be concluded that a strong resemblance can be found between the added attenuation spectra measured here and the spectrum of octahedrally coordinated Ni^{2+} in glass.

The concentration of Ni^{2+} in the fiber can be estimated from Turner & Turner [1972] where a 0.2 wt% concentration corresponds to an absorbance of 5.5 cm^{-1} at 435 nm for a lead silicate glass with octahedrally coordinated Ni^{2+}. On the basis of that, an attenuation of 0.013 dB/m at 435 nm in the high attenuation fibers will correspond to a concentration of 25 ppb Ni^{2+} in the glass.

4.5 The nickel experiment.

To investigate the behavior of Ni in germanium doped silica glass, a fiber intentionally doped with Ni was made at OFS laboratories. The fiber has a core doped with Ge as well as Ni.

Since the added attenuation is primarily seen in fibers having an unusual temperature history during draw, this study will investigate whether the temperature history of the

fiber affects the optical absorption spectrum. This is inspired by several of the papers showing that quenching a Ni-doped glass influences the coordination geometry and consequently the absorption spectrum.

The core of the preform has 9 Ge-doped layers. Layer # 5 was deposited as a soot layer, which was then solution-doped with a solution of $Ni(NO_3)_2$ in water and isopropanol. The soot layer was dried under an inert atmosphere and then sintered. The remaining core layers were deposited on top of the Ni layer, and then the preform was collapsed. The preform was then stretched and some of it jacketed. Figure 15 shows the resulting refractive index profile of the preform.

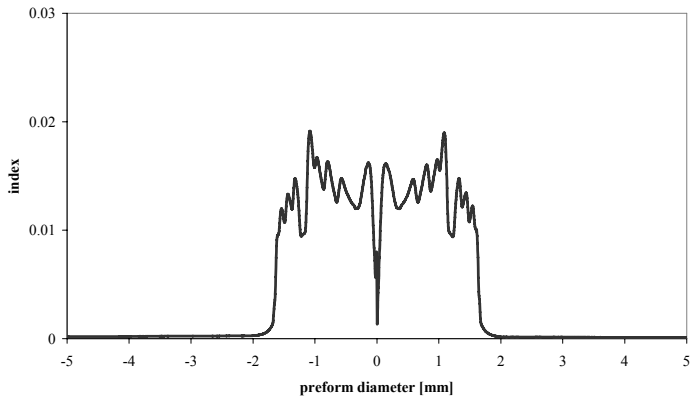

Figure 15 – Refractive index profile of Ni-doped preform

To test whether the temperature history of the preform affects the optical spectrum, the first part of the preform was drawn under various draw conditions using the OFS lab draw tower. Another part of the preform was heated and quenched before the fiber was drawn. A cut was made in the original preform dividing it into two pieces. The two pieces were joined before jacketing the preform, the idea being that during draw, the region where the two preform ends are joined will experience a different temperature profile due to the reflections of light and heat from the preform end faces.

The last part of the preform was drawn at the production facilities at OFS Denmark, to investigate the effect of a different draw tower configuration on the attenuation spectrum.

Table 7 lists the processing conditions. Figure 16 shows the attenuation spectra of the resulting fibers.

	Draw speed [m/s]	**Draw tension [g]**	**Furnace temp [°C]**
Standard – OFS labs	2.5	100	1980
Low tension – OFS labs	2.5	80	2020
Plasma heated – quenched	2.5	100	1970
Below preform joint	2.5	100	1980
Drawn at OFS Denmark	20	100	2030

Table 7 – Processing conditions for the fiber intentionally doped with Ni.

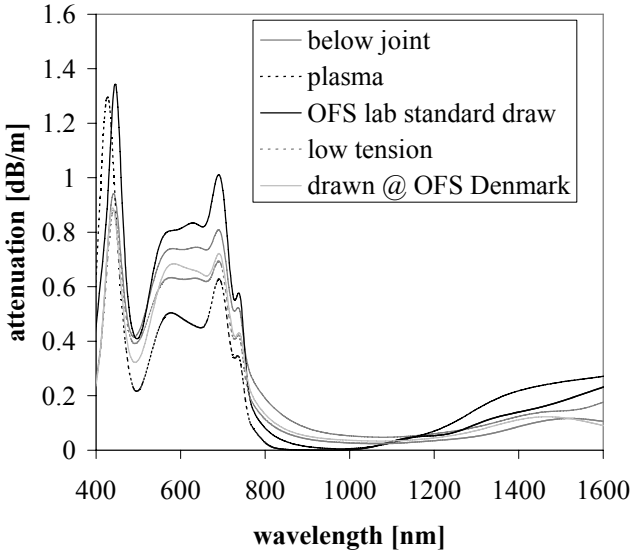

Figure 16 – Attenuation spectra of the fiber intentionally doped with Ni

The attenuation spectra of the fibers from the Ni-preform are very similar even though they have been subjected to different processing conditions. They all have intense and broad absorption peaks centered at 440nm, 570nm, 670 nm, and less intense narrow peaks at 700 nm and 740 nm. At wavelengths longer than 1000 nm a number of broad absorption peaks can be observed. Comparing them to the added attenuation spectrum of the high loss fibers shows only a few similarities: The absorption peak centered at 440nm and the broad absorption peaks at wavelengths > 1000 nm (Figure 14+ Figure 16).

4.6 Optical spectra of Ni-doped glasses

In order to explain the appearance of the optical spectra of Ni-doped glasses, some understanding of coordination chemistry of the first row transition metals is needed.

4.6.1 Coordination chemistry of Ni in glass

Ni is a first row transition metal with 8 d-electrons. The partly filled d-orbitals are responsible for the appearance of the absorption spectrum in the visible to infrared wavelength range.

For an isolated Ni-atom, the five d-orbitals have the same energy. When Ni is embedded in a glass matrix or in any other way surrounded by other atoms, the energy levels of the d-orbitals become affected by the surroundings. Especially the oxygen atoms of the silica network affect the energy levels of the Ni d-orbitals as the oxygen atoms act as ligands to the Ni atom. Depending on the symmetry of the surrounding ligands (oxygen atoms), the energy levels of the Ni d-orbitals split up as they are affected differently by different coordination geometries [Cotton et al., 1995]. In Gitter & Vogel [1979] a systematic study of the coordination geometries of Ni in different glasses from absorption spectra and paramagnetic moments has been

performed. Their results will be used as a basis for understanding the Ni absorption spectra found in this work.

For Ni in glass, the two main geometries are tetrahedral and octahedral. A third geometry to consider is the dodecahedral. It is sometimes referred to as pseudo-tetrahedral as the energy level splitting is comparable to that of the tetrahedral coordination with the same relative spacing between the energy levels.

Figure 17 shows the tetrahedral, dodecahedral and octahedral coordination geometries while Figure 18 gives the splitting of the energy levels of the d-orbitals as well as the resulting energy diagram for octahedrally and tetrahedrally coordinated Ni.

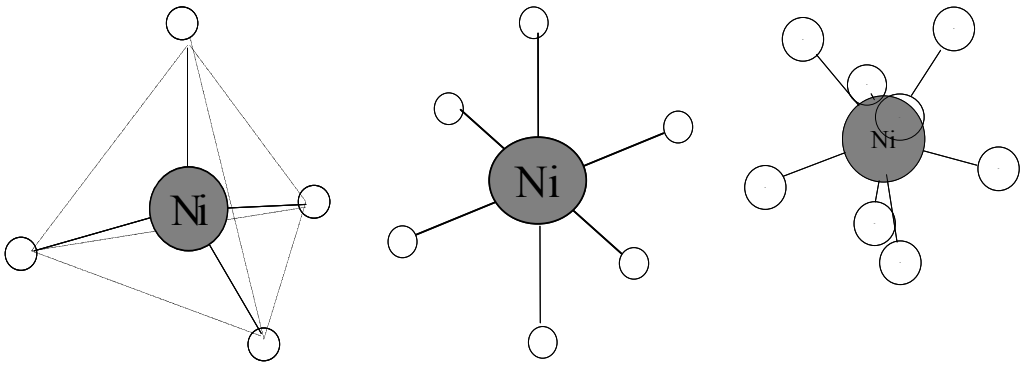

Figure 17 – Tetrahedral, octahedral and dodecahedral coordinated Ni

D_q is the ligand field splitting parameter giving the separation between the highest and lowest energy of the d-orbitals. D_q depends on the coordination geometry as well as on the nature of and the distance to the ligands. For complexes with the same ligands and equal distance to the ligands but different geometries the relation between the ligand field parameters would be:

$$D_q(o) = 2D_q(t^4) = \frac{9}{8} D_q(t^8) \qquad \text{Equation 17}$$

with $D_q(o)$ being the ligand field splitting parameter for the octahedral complex, $D_q(t^4)$ the ligand field splitting parameter for the tetrahedral complex and $D_q(t^8)$ the ligand field splitting parameter for the dodecahedral complex.

The nature of the ligands will affect D_q as well. The value of D_q for a Ni atom coordinated to a non bridging oxygen will thus be different from that of a Ni atom coordinated to a bridging oxygen.

The Racah parameters (*B* and *C*) are integrals related to the electron-electron repulsion. For Ni the free ion Racah parameter *B* is 1130 cm^{-1} and *C* is 4752 cm^{-1}. When Ni is coordinated to the oxygen atoms of the silica (or any other ligands), the area in which the electrons can move increases, thereby decreasing the electron-electron repulsion and consequently the Racah parameter.

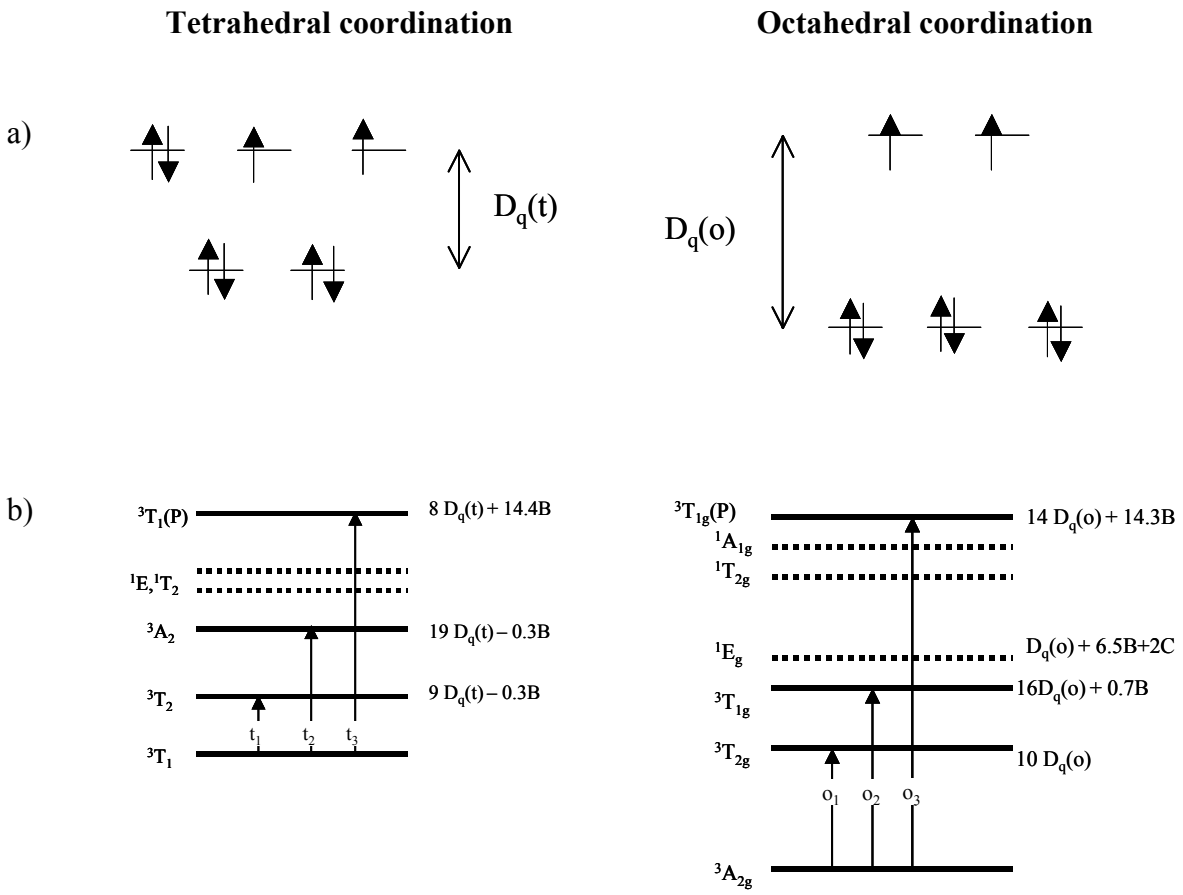

Figure 18 – a) Splitting of the energy levels for tetrahedral and octahedral coordinations. b) Resulting absorption energies for tetrahedral and octahedral coordinations. The absorption energies for dodecahedral coordination can be found using the diagram for tetrahedral coordination but with different values for D_q and B.

4.6.2 Data analysis

In Gitter & Vogel [1979], the energy-level diagrams for Ni in tetrahedral and octahedral coordination are given as shown in Figure 18b. It is further stated that the dodecahedral energy levels can be calculated from the tetrahedral energy level diagram but with different values for D_q and B. The energy levels described, enables the absorption bands of the spectra from the Ni preform and the added attenuation spectra to be resolved.

Gaussian absorption peaks have been fitted to the measured spectral attenuation of the fibers using the energy levels described in Figure 18. Figure 19 and Figure 20 show the spectra together with the absorption bands. The ligand field splitting parameter and the Racah parameters found for each spectrum are given in Table 8 that also lists the values found by Gitter & Vogel [1979] for Ni in various phosphate or borate glasses. The main difference between the borate and phosphate glasses is the basicity or the number of non-bridging oxygens. The values are given as intervals since they were determined for a series of both borate and phosphate glasses. No values are

given for D_q and the Racah parameters for tetrahedrally coordinated Ni for the added loss spectrum, since the intensities of the absorption peaks for Ni in tetrahedral coordination in these fibers are very low compared to those of Ni in octahedral or dodecahedral coordination.

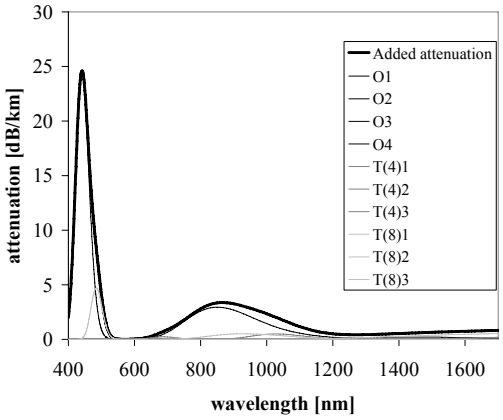

Figure 19 – Added attenuation of high loss fibers

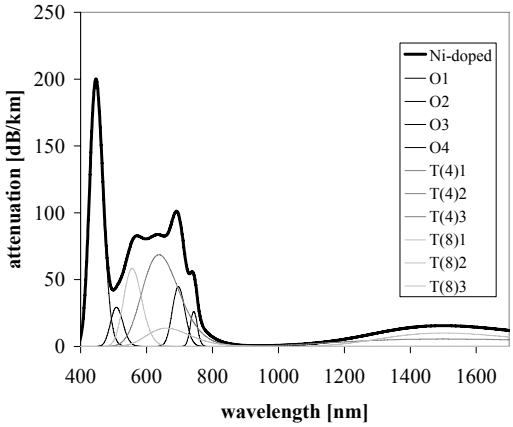

Figure 20 – Attenuation spectrum of fiber intentionally doped with Ni

	Added loss spectrum of high loss fibers	**Fibers intentionally doped with Ni**	**Ni^{2+} in phosphate glasses [Gitter & Vogel, 1979]**	**Ni^{2+} in Borate Glasses [Gitter & Vogel, 1979]**
$D_q(o)$ [cm^{-1}]	695	815	720-745	750-790
$B(o)$ [cm^{-1}]	890	810	860-920	925-955
$C(o)$ [cm^{-1}]	4100	4200	4070-4100	4150-4320
$D_q(t^4)$ [cm^{-1}]		455	485-495	500-515
$B(t^4)$ [cm^{-1}]		865	830-850	850-920
$D_q(t^8)$ [cm^{-1}]	585	650	595-600	620-650
$B(t^8)$ [cm^{-1}]	1110	900	1120-1160	1070-1130

Table 8 – Ligand field splitting parameters and Racah parameters for the Ni doped fibers measured in this work, compared to the values determined for Ni-doped phosphate and borate glasses.

The values for the ligand field splitting parameter and the Racah parameters found for the Ni spectra in this study is comparable to those found for various phosphate and borate glasses by Gitter & Vogel [1979]. Some difference between the values is expected since the oxygen atoms found in borate or phosphate glasses can be expected to have ligand properties that differ from those of oxygen atoms in silica glass. Another difference could be the distance between the oxygen atoms and the Ni atom in the different glasses.

Added attenuation

Contrary to the assumption in section 4.4 that the absorption bands of the added attenuation spectra consisted of four bands with center wavelengths at 440 nm, 870 nm 1050 nm and 1700 nm it can now be seen in Figure 19 that the proposed four bands are actually a combination of a larger number of absorption bands caused by Ni in octahedral (o) and dodecahedral (t^8) coordination. The absorption band at 440 nm is a combination of the o(1) absorption band centered at 438 nm and the $t^8(1)$ absorption band centered at 482 nm. The absorption band at 870 nm is a combination of the o(2) absorption band at 850 nm and the $t^8(2)$ absorption band centered at 930 nm. The weak absorption band at 1050 nm could be due to the $t^4(1)$ absorption at 1028 nm. The absorption peak originally believed to be centered at 1700 nm is a combination of the o(3) absorption band at 1625 nm and the $t^8(3)$ absorption band at 2030 nm. That the originally proposed four absorption bands are actually combinations of a larger number of bands can also explain the low correlation between the intensities of the absorption bands at 435 nm and 870 nm as shown in Figure 13.

Fiber intentionally doped with Ni

The absorption spectrum of the fiber intentionally doped with Ni is shown in Figure 20. Beside the absorption bands from octahedrally and pseudo tetrahedrally coordinated Ni, absorption bands from tetrahedrally coordinated Ni are seen as well. The relative concentration of tetrahedrally to octahedrally coordinated Ni can not be determined directly from the spectrum since the absorption bands from tetrahedrally coordinated Ni is expected to be much more intense than those from octahedrally coordinated Ni due to the symmetry of the complexes (no center of inversion in tetrahedral complexes). The fibers drawn under different conditions have very similar attenuation spectra. The differences seen between the fibers are mainly in the relative intensities of the peaks. Some of the difference in intensity is due to the fact that the Ni concentration along the preform is not likely to be uniform. Whether some of the Ni in the fibers has actually experienced a change in coordination geometry due to the changes in the temperature history cannot be concluded on the basis of available data.

4.7 Discussion

The main difference between the added attenuation spectra and the spectra from the fiber intentionally doped with Ni, is the presence of tetrahedrally coordinated Ni in the latter.

It is a general trend for the metals of the first transition series that the lower coordination numbers are preferred if the ligands are highly polarizable. In the case of Ni dissolved in a glass, the coordination geometry with the lower coordination

number is the tetrahedral in which four oxygen atoms are coordinated to Ni. Both in the spectrum of the fibers intentionally doped with Ni and in the spectrum measured by Schultz [1973] on silica based fibers doped with Ni, absorption peaks are observed proving the presence of Ni in tetrahedral coordination. In the fibers with the added attenuation the presence of tetrahedrally coordinated Ni could not be confirmed. This suggests that the oxygen atoms in the two glasses intentionally doped with Ni are more polarizable than the oxygen atoms in the glass of the fibers with the added attenuation.

The polarizabilty of the oxygen atoms in the glass network is affected by both temperature history and chemical composition of the glass. As the glass is heated the oxygen atoms become more polarizable. If the glass is quenched, the oxygen atoms can be caught in the highly polarizable state. So difference in temperature history could be an explanation for the differences in the optical spectra. However, the intentionally doped fiber has not only been subjected to very differing heat treatments, it has also been drawn under the exact same conditions as the fibers showing the added attenuation spectrum. No matter which temperature history the intentionally doped fiber has been subjected to, the absorption peaks indicative of tetrahedrally coordinated Ni has been present. Furthermore, no absorption peaks indicative of tetrahedrally coordinated Ni have been observed in fibers that are not intentionally doped with Ni.

This suggests that the difference in the spectra of the intentionally doped fibers and the fibers with the added attenuation spectrum is not due to differences in temperature history, but rather due to differences in the chemical composition of the glasses.

In the intentionally doped fibers, some of the Ni is tetrahedrally coordinated while in the contaminated fibers all Ni is either octahedrally or dodecahedrally coordinated. One possible explanation of this is that the contaminated fibers are not only contaminated with Ni but also with some other contaminant.

The effect of another contaminant could be to occupy tetrahedral sites in the glass or to decrease the polarizability of the oxygens in order to make the higher coordination number more favorable.

Ni has a high preference for octahedral sites while metals such as Ca and Zn prefers tetrahedral sites in the glass. It was shown how the addition of Ca or Zn to the glass melt drastically reduces the fraction of Ni in tetrahedral sites in the glass [Burns & Fyfe 1964].
The other possible effect of a codopant that can explain the complete absence of tetrahedrally coordinated Ni in the fibers with the added attenuation spectrum is if the number of non-bridging oxygen atoms are greatly reduced. Codopants having this effect on the glass could be Al or B [Shelby 2005]. The concentration of non-bridging oxygen atoms can be estimated from the intensity of the 630 nm absorption band. It is not possible to compare the intensity of the 630 nm band in the contaminated and the intentionally Ni-doped fibers since the Ni concentration in the intentionally doped fibers is so high that the Ni-absorption bands masks that of the non-bridging oxygens at 630 nm. There is no difference between the intensities of the 630 nm absorption band in the contaminated and the low loss fibers, so it seems unlikely that any

additional contamination reducing the number of non-bridging oxygen atoms should be present in the contaminated fibers.

4.8 Conclusion on spectral investigation

Through spectral attenuation measurements in the wavelength range 290 –1700 nm on a series of high attenuation transmission fibers strong evidence has been found to point to the source of the added attenuation to be a contamination of the fibers with Ni.

Even though at a first glance the added attenuation spectra of the high loss fibers do not resemble those of the Ni doped silica based fibers as shown by Schultz [1973] and confirmed by experiment, a detailed spectral analysis reveals that the added attenuation spectra can indeed be due to the presence of Ni. The main difference between the added attenuation spectra and that of a fiber intentionally doped with Ni is the coordination geometry of Ni. In the added loss spectra, the main coordination geometries are octahedral and dodecahedral while Ni in the fibers from the intentionally doped Ni preform is octahedrally, tetrahedrally and dodecahedrally coordinated. The difference in coordination geometry in the two fibers could be due to an additional contaminant in the contaminated fibers.

This concludes the section on attenuation of transmission fibers. The remaining part of this work will be dealing with optical fibers with high core refractive index.

5. Attenuation in fibers with high Δn_{core}

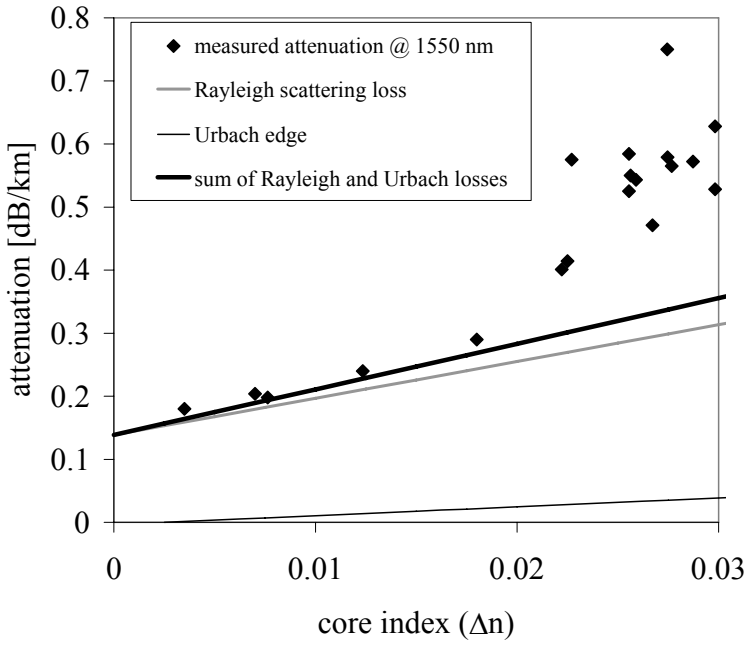

Figure 21 – Attenuation of optical fibers as a function of index difference between the core and the cladding (Δn_{core}). The dots represent measured attenuation; the solid lines the contributions to the attenuation given by Equation 10 and Equation 14.

5.1 Introduction

One of the central subjects of this thesis has been the understanding of the attenuation of fibers having a high index difference between the core and the cladding (Δn_{core}). OFS has chosen that some of the results obtained must be kept confidential. Consequently some of the equations presented in this chapter will only be fully disclosed and/or discussed in the confidential part of this report. Furthermore, the relations between layer indexes and layer widths in the refractive index profiles shown are altered to secure that they are not reproducible. The alterations of index profiles do not affect the conclusions.

5.2 Background

The mechanisms causing the attenuation of fibers with low index difference between the core and the cladding (Δn_{core}) is well understood and the main contribution to the

attenuation at 1550 nm is found to be the Rayleigh scattering loss. However, when it comes to fibers with a high Δn_{core}, neither Rayleigh scattering losses (Equation 10) nor the Urbach edge (Equation 14) can completely account for the high attenuation observed in these fibers.

Figure 21 shows the relation between Δn_{core} and the measured attenuation of Ge-doped silica based optical fibers. The attenuation of fibers with low Δn_{core} is adequately described as a sum of the Rayleigh scattering and the Urbach absorption loss. But as Δn_{core} is increased, the deviation between the calculated and measured attenuation increases rapidly.

For transmission fibers, this is hardly an issue, since the desired wave guiding properties for these fibers can be obtained with a low Δn_{core}. Some fiber types such as dispersion compensating fibers, nonlinear fibers or fibers for Raman amplification must however have high Δn_{core} in order to obtain the desired optical properties. Consequently, the very high attenuation measured in these high Δn_{core} fibers has been investigated in the literature for several decades. A short review of the literature on attenuation in fiber having a high Δn_{core} is given in the following section.

5.2.1 Literature review.

The connection between drawing conditions and the excess loss of high index optical fibers has long been recognized [Ainslie et.al 1981, Ainslie et.al 1982, Ainslie et.al 1983, Brehm et.al 1988, Davey et.al 1989, Guenot et.al 1999]. The three main parameters characterizing the drawing process are the draw tension (F_{draw}), the draw temperature (T_{draw}) and the draw speed (v_{draw}). These three parameters are not independent, but will as described in section 2.2 depend on each other through Equation 2.

Since a given T_{draw} can be achieved by more than one combination of v_{draw} and F_{draw}, in order to analyze the effect on the excess loss of varying one of the draw parameters, the other two parameters must be given as well.

The data presented by Ainslie et.al [1982] show a linear relation between $\log(\alpha_{excess})$ and both v_{draw} and T_{draw} with increasing excess loss upon increased v_{draw} and increased T_{draw}. Data from the same group [Ainslie et.al 1983] show an almost linear relation between the excess loss and $1/F_{draw}$ with the deviation from the linear relation being most pronounced at low tensions. Brehm et.al [1988] concludes that the drawing induced losses depend mainly on temperature since the same loss values are measured for fibers drawn at the same T_{draw} but at differing combinations of v_{draw} and F_{draw}.

It has already been mentioned that the excess loss depends on Δn_{core}. The effect of other parameters of the refractive index profile on the excess loss has been studied as well and it was found that the excess loss increases on decreasing core diameter (r_{core}) [Ainslie et.al 1982, Mashinsky et.al.1994, Lines et.al.1999]. With the index profile described using the formalism of Equation 18, the excess loss has been shown to depend on the core exponent (γ) as well, with the excess loss decreasing with a decreasing core exponent [Ainslie et.al. 1983, Davey et.al. 1989, Lines et.al. 1999]

$$n(r) = n_{core}\left(1 - \left(\frac{r}{r_{core}}\right)^{\gamma}\right), \quad for\ r < r_{core}$$

Equation 18

Figure 22 shows the effect of varying γ from ∞ (step index profile) to 2.

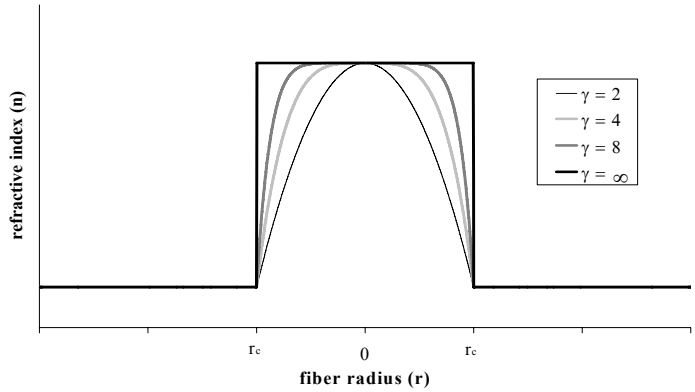

Figure 22 – The effect on the refractive index profile of varying the core exponent *(γ)*

Lines et.al [1999] found the following relation between parameters of the index profile as described in Equation 18 and the excess loss, which they call anomalous loss:

$$\alpha_{anomalous} = A_{anomalous}\Delta n_{core}^2 \frac{\gamma^2}{d_{core}^m \lambda^k (\gamma+2)^2}$$

Equation 19

$A_{anomalous}$ being the strength of the scattering, γ the exponent of the core profile, d_{core} the core diameter, Δn_{core} the index difference between the core and the cladding and λ the wavelength. The exponents *m* and *k* were shown to depend on γ as shown in Table 9.

γ	***m***	***k***
2 (quadratic index profile)	1.6	2.4
∞ (Step index profile)	1	3

Table 9 – Exponents for the anomalous loss expression (Equation 19)

Measurements have were performed of the angular dependence of the scattered light of optical fibers having differing profile parameters [Lines et.al.1999, Likhachev et.al 2003] or drawn under differing draw conditions [Guenot et.al. 1999]. The measurements show that the anomalous loss is due to a small angle forward scattering phenomenon that is highly dependent on profile parameters as well as draw conditions. All three groups explained the angular dependence of the anomalous loss by light scattering on fluctuations of the core diameter as described by Rawson [1974]. The same scattering mechanism is believed to cause loss in photonic fibers with a hollow core [Roberts et.al. 2005]. In these fibers, the fluctuations of the core diameter are due to capillary waves frozen into the surface of the glass at the core

interface. For the photonic fibers with hollow core, the excess scattering loss was found to depend on wavelength as $1/\lambda^3$.

Mazumder et.al. [2004] fabricated an optical fiber having a Δn_{core} of 0.015 and d_{core} of 4.3 μm for which they measured and analyzed the angular scattering. They found, based on the analysis of Lines et.al. [1999], Guenot et.al. [1999] and Rawson [1974] that the anomalous loss is caused by random perturbations in both axial and radial directions. The intensity of the scattering is proportional to the power of the guided mode at the core-clad interface of the fiber. For their fiber, they determined the anomalous loss to depend on wavelength as $1/\lambda^{2.06}$.

Likhachev et.al [2003,2004] supports the theory of the anomalous loss being caused by fluctuations of the core diameter. By studying few-mode fibers with high Δn_{core} they found that modes having a high fraction of power at the core-cladding interface would experience a larger scattering loss than modes having a lower fraction of power in this region. They speculate that the fluctuations of the core diameter are due to large differences between the viscosities in the core and cladding region. Mashinsky et.al [1994] suggest that the core fluctuations are due to turbulence in the boundary layer between the low viscosity core and the high viscosity cladding. They propose that a reduction of the viscosity of the cladding can diminish the fluctuations of core diameter.

The effect of the viscosity at the boundary between the core and the cladding has also been investigated by Tajima et.al [1997], Tateda et.al [1992] and Ohashi et.al. [1993]. Fibers with a low Δn_{core} of 0.006 were manufactured and it was described how matching the viscosities of the core and cladding through co-doping of the glass with F and P_2O_5 resulted in a reduction of the imperfection loss, described as the loss caused by variations of the core diameter.

To summarize the findings in the literature: It has been experimentally tested that by drawing the fibers with high Δn_{core} at high tension and low temperature, the attenuation can be decreased. Furthermore it has been shown that the loss will be reduced if the core index is graded. Through measurements of angular scattering loss it has been shown that the anomalous loss is a small angle scattering phenomenon that can be explained as scattering on fluctuations of the core diameter. Likhachev et.al. [2003,2004] and Mashinsky et.al. [1994] speculate that the core fluctuations could be caused by a viscosity mismatch between the core and the cladding.

5.3 Viscosity matching experiment

To test the theory of Likhachev et.al. [2003,2004] and Mashinsky et.al [1994], that the anomalous loss is caused by abrupt changes in the viscosity between the core and the cladding region, an experiment has been set up to compare the attenuation of two fibers with similar refractive index profiles but different viscosity profiles. Both fibers have triple clad refractive index profiles as are normally seen in dispersion compensating fibers (chapter 6).

In order to make a viscosity matched preform, some knowledge on viscosity of glass is required. The viscosity of silica glass depends on the dopant level in the glass. The effect on the viscosity of doping the glass with F and Ge has been studied extensively

by several groups [Ohashi et.al 1992b, Tateda et.al 1992, Kyoto et.al. 1993, Shiraki et.al 1993, Tajima et.al. 1994]. Both F and Ge decrease the viscosity (increases the fluidity) of the silica glass.

As described by Equation 3, the viscosity of pure silica glass is highly temperature dependent. The same is true for doped silica glass. Shiraki et.al [1993] have shown that the ratio of the viscosity of pure silica to the viscosity of a F- or Ge-doped silica is constant over a large temperature range (1700 -2000°C). Consequently, the viscosity of a doped silica glass can at any temperature in this range be expressed as:

$$\log\eta = \log\eta_{silica} + K_{Ge}\Delta n_{Ge} + K_F\Delta n_F \qquad \text{Equation 20}$$

η_{silica} is the viscosity of pure silica glass at a given temperature, Δn_{Ge} and Δn_F are the changes in refractive index induced by doping the glass with Ge and F. K_{Ge} and K_F are the viscosity sensitivity coefficients having the values -1 (log(Pa s)) and 0.3 (log(Pa s)) for Ge and F respectively [Shiraki et.al 1993]. The viscosity of the glass can be calculated provided the contributions from Ge and F to the refractive index are known. With a small dopant concentration, the refractive index changes linearly with dopant concentration and the total Δn of the glass can be expressed as a sum of the contributions from Ge and F as [Kirchhof et.al.1994]:

$$\Delta n = \Delta n_{Ge} + \Delta n_F \qquad \text{Equation 21}$$

So, if the dopant profiles are known, the viscosity profiles can be determined. During deposition (MCVD process) layers are doped with F to reduce the refractive index of silica (in the trench region of the index profile) while Ge is used to increase the refractive index (in the core). So when looking at the index profile of the preform, a first approximation in order to determine the dopant profiles could be to assume that $\Delta n>0$ is only due to Ge-doping and $\Delta n<0$ only due to F-doping. Since both dopants are known to diffuse, this would lead to a large overestimation of the viscosity in regions of the refractive index profile where $\Delta n\approx 0$ (interface between core and trench - Figure 2). With the object of the experiment being to make a fiber with viscosity match across the core-trench interface, the exact concentration of the dopants and consequently the diffusion of the dopants at the core boundary must be determined.

The diffusion of F and Ge in silica has been described in Kirchhof et.al. [1987], Kirchhof et.al. [1994] and Kirchhof et.al.[1995]. In the following, the determination of the viscosity profiles of optical fibers through diffusion calculations will be described. In order to simplify the otherwise complicated calculation of the diffusion of the dopants, some assumptions are made:

1. The calculations will be performed on the basis of the preform profile instead of on the fiber profile, since the available method for obtaining fiber profiles is not accurate enough for diffusion modeling. It has been shown that the dopants will diffuse during draw [Lyytikäinen et al. 2004] so this assumption will be a source of error in the calculation resulting in an underestimation of the viscosity at the core boundary.
2. The diffusion will mainly take place during the MCVD process before the preform is completely collapsed when the diffusion length is small. A layer

just outside the core boundary with a thickness of 0.01 mm before collapse will correspond to a thickness of 0.2 mm after collapse.
3. The F doped trench region is seen as an endless reservoir of F for diffusion.
4. Since the diffusion length (in the order of 0.01 mm) is small compared to the radius of curvature of the tube, the calculation of the concentration profiles is reduced to a one dimensional diffusion problem.
5. The diffusion coefficients are independent of the concentration of co-dopants.

Since the diffusion is assumed to be in one dimension, Fick's second law, relating the rate of change of concentration of the dopants at a point to the spatial variation of the concentration at that point, will apply [Crank, 1995]:

$$\frac{\partial C}{\partial t} = D\frac{\partial^2 C}{\partial x^2} \qquad \text{Equation 22}$$

With C being the concentration of the diffusing dopant, D the diffusion coefficient, t the time and x the position. The temperature (T) dependence of the diffusion coefficient is given as:

$$D = D_0 \exp\left(-\frac{E_a}{RT}\right) \qquad \text{Equation 23}$$

With D_0 being the pre-exponential term, E_a the activation energy and R the gas constant. The values for D_0 and E_a for F and Ge are given in Table 10. The diffusion coefficient of Ge has been found to depend on Ge concentration. The values in Table 10 are given for a Ge-concentration of 15 mol% [Kirchhof et al.1994].

	D_0 [cm^2/s]	E_a [kJ/mol]
F	1.74	383
Ge (15mol%)	1.09	55.7

Table 10 – Pre-exponential term and activation energies for the diffusion of F and Ge in silica glass

Since F diffuses more readily than Ge in silica, only the diffusion of F will be calculated in the following. The concentration profile for Ge will be determined from the calculated concentration profile of F and the refractive index profile.

For a system in which the diffusing substance occupies an extended region having a concentration C_s that is in contact with another region where the concentration of the diffusing substance is C_0, the solution for Equation 22 is found to be [Crank, 1995]:

$$C(x,t) = \tfrac{1}{2}(C_s - C_0)\,erfc\left(\frac{x}{2\sqrt{Dt}}\right) + C_0 \qquad \text{Equation 24}$$

With *erfc* being the complementary error function defined as:

$$erfc(z) = \frac{2}{\sqrt{\pi}} \int_{z}^{\infty} \exp\left(-x^2\right) dx$$ Equation 25

The concentration of the diffusing dopants at any position can thus be calculated for any diffusion time or temperature from Equation 23, Equation 24 and the values given in Table 10.

Even though the diffusion coefficients are assumed to be independent of the concentration of co-dopants, the diffusion is difficult to model in the regions of the index profile in which both F and Ge diffuses (in opposite directions) since they have opposite effects on the refractive index of the glass.

In order to test whether the above described model for diffusion is valid for the diffusion taking place in the preform during the MCVD process, the model is tested on a preform where the Ge doped core and the F doped trench are separated by a layer of pure silica. In this case the dopant diffuses into a region where the initial concentration of the dopant (C_0) is 0.

Equation 24 have been fitted to the index profile in Figure 23a of fiber preform with a silica layer separating the core and the trench region allowing the initial concentration C_s and the time t to vary and assuming a temperature of 2300°C. From the contributions of F and Ge to the refractive index as shown in Figure 23a, the dopant concentration profiles and consequently the viscosity profile ($\eta(r)$) can be calculated from Equation 23 and Equation 24. The resulting viscosity profile is given in Figure 23b.

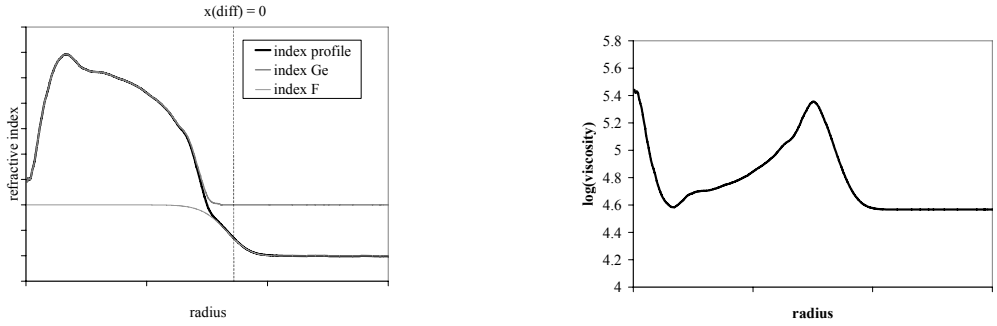

Figure 23 – a) contributions from F and Ge to the refractive index profile after diffusion. x(diff) = 0 marks the outer position of the deposited silica layer. b) the resulting viscosity profile

Using the methodology described above, the dopant profiles and consequently the viscosity profiles can be determined on the basis of the refractive index profile of the preform. This knowledge is used to design a refractive index profile for which the viscosity across the core-trench interface is matched. The viscosity matching is achieved by doping the outer layers of the core with F and the innermost layer of the trench with Ge. A reference fiber is made with an identical index profile but with a dopant profile and consequently a viscosity profile as is normally seen for triple clad index profiles, that is except for the index changes induced by diffusion of the

dopants, $\Delta n<0$ is achieved through F-doping and $\Delta n>0$ is achieved through Ge-doping.

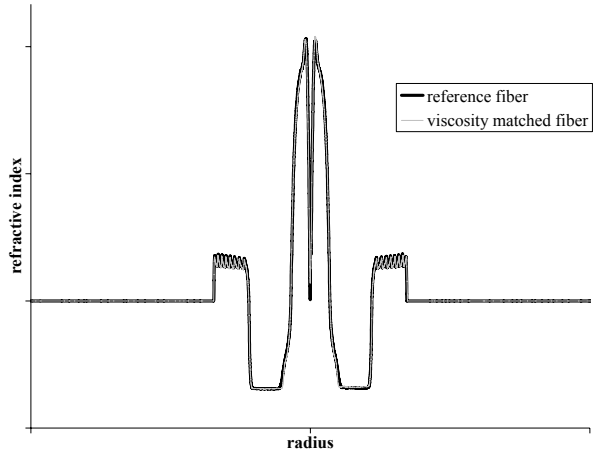

Figure 24 – Refractive index profiles of reference and viscosity matched fibers

The refractive index profiles of the two fibers are given in Figure 24, the dopant profiles in Figure 25 and the resulting viscosity profiles at 1900°C in Figure 26. The refractive index profiles of the two fibers are very similar while there is a clear difference between the dopant profiles and consequently of the viscosity profiles of the two fibers.

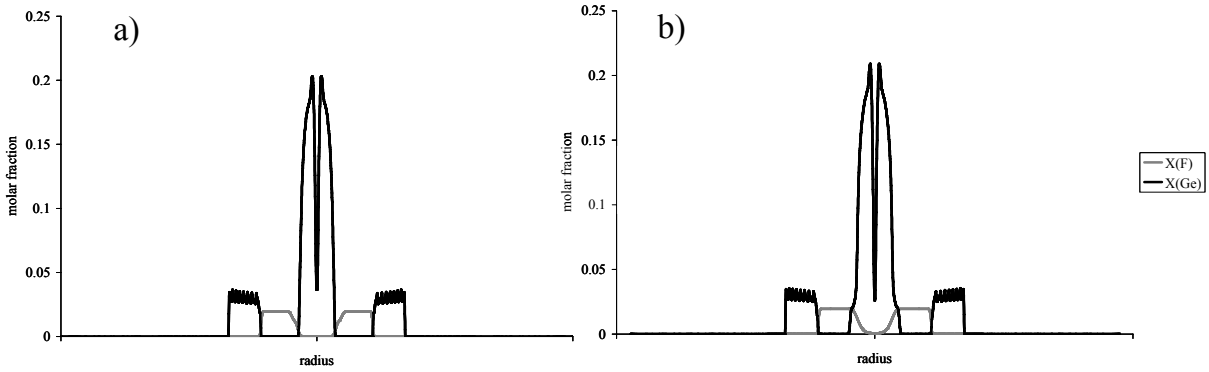

Figure 25 – Concentration profiles of F and Ge in the reference fiber (a) and the viscosity matched fiber (b)

The optical properties of the two fibers are listed in Table 11 showing that the wave guiding properties of the two fibers are very similar. The main difference between the two fibers is the attenuation, with the attenuation of the viscosity-matched fiber being 0.2 dB/km higher than that of the reference fiber. Due to the higher concentration of the dopants in the core and trench regions, the Rayleigh scattering of the viscosity-matched fiber will be larger than of the reference fiber. The total dopant concentration is at no part of the index profile of the viscosity-matched fiber more than 5% higher than the reference fiber. A 5% increase of total dopant concentration will correspond to an increase of the Rayleigh scattering of the viscosity-matched fiber of 0.01 dB/km

[Tsujikawa et.al. 1994]. This is not enough to account for the 0.2 dB/km added attenuation of the viscosity-matched fiber.

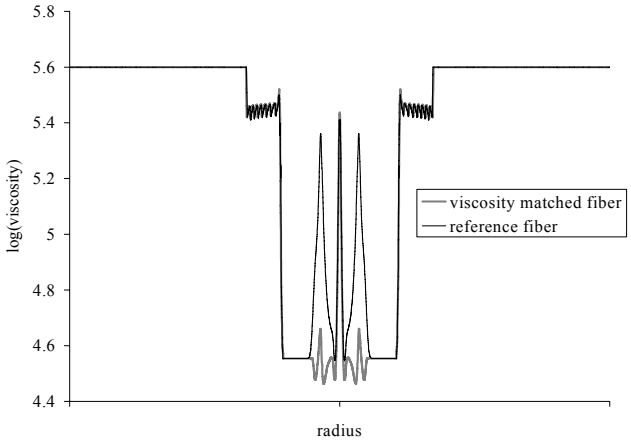

Figure 26 – Viscosity profiles of reference and viscosity matched fibers.

	Dispersion [ps/(nm km)]	Cutoff wavelength [nm]	Effective area [μm^2]	RDS [nm^{-1}]	Attenuation [dB/km]
Reference fiber	-252	1512	22.2	0.0045	0.554
Viscosity matched fiber	-243	1507	21.9	0.0042	0.754

Table 11 – Optical properties as measured at 1550 nm of the fibers for the viscosity matching experiment.

The difference in the measured attenuation of 0.2 dB/km of the two fibers having similar index profiles but differing viscosity profiles shows that the anomalous loss is not only dependent on the index profile parameters, but also on the dopant concentrations. If the estimated viscosity profile of the viscosity-matched fiber is correct it can furthermore be concluded that the anomalous loss is not caused by a viscosity mismatch at the core boundary as suggested by Likhachev [2003, 2004].

5.4 Predicting the attenuation of high index fibers

It has now been established that the dopant concentration profile affects the attenuation of optical fibers. In the following, a model for predicting the attenuation coefficient at 1550 nm of high index fibers based on information on profile parameters and draw conditions will be presented. Such a model is needed for optimizing the performance of dispersion compensating fibers (chapter 6).

5.4.1 The loss model

As discussed in chapter 3, the attenuation in optical fibers can be expressed as a sum of several components. For the high index fibers discussed presently some assumptions can be made to simplify the expression.

It is assumed that absorption bands from defects or the water peak do not contribute to the attenuation at 1550 nm. As long as the water peak of an optical fiber is less than 0.5 dB/km at 1385 nm, it will contribute with less than 0.004 dB/km to the attenuation at 1550 nm [Bredol et.al 1990]. Typical high index fibers produced at OFS Denmark have waterpeaks of less than 0.2 dB/km (with the background loss subtracted).
Since the content of Ge in the fibers is high, the IR vibrational absorptions are assumed not to contribute to the attenuation at 1550 nm. Furthermore, the analysis of the attenuation can reasonably be limited to fibers with negligible waveguide dependent losses, since for most practical applications these losses should be minimized at 1550 nm. The only mechanisms contributing to the attenuation at 1550 nm are the Rayleigh scattering loss, the Urbach edge absorptions and the anomalous scattering loss. The total attenuation of fibers having a high index difference can thus be written as:

$$\alpha = \alpha_{Rayleigh} + \alpha_{Urbach} + \alpha_{Anomalous} \qquad \text{Equation 26}$$

All components of Equation 26 can be expressed as functions of the core index difference (Δn_{core}):
The Rayleigh scattering is given as [Ohashi et.al 1992b]:

$$\alpha_{Rayleigh} = A_{Rayleigh} \frac{\left(1 + C_{Rayleigh} \Delta n_{core}\right)}{\lambda^4} \qquad \text{Equation 27}$$

In which $A_{Rayleigh}$ is a constant [dB μm^4/km] giving the weight of the Rayleigh scattering loss in the expression for the total attenuation, $C_{Rayleigh}$ is a constant that will be determined during the calibration of the model.
The Urbach absorption loss can be expressed as:

$$\alpha_{UV} = A_{Urbach} \Delta n_{core} \exp\left[g\left(E - E_0\right)\right] \qquad \text{Equation 28}$$

In which A_{Urbach} is a constant [dB/km] giving the weight of the Urbach absorption loss in the expression for the total attenuation, g is a constant that depends on temperature and E_0 is a constant comparable to the band gap. In the present work, E_0 is assumed independent of the Ge-concentration.

The final contribution to the attenuation of fibers having a high Δn_{core} is the anomalous loss:

$$\alpha_{anomalous} = A_{Anomalous} \Delta n_{core}^2 \frac{\gamma^2}{d_{core} \lambda^3 (\gamma + 2)^2} \frac{T_{draw}}{F_{draw}} f(\Delta n_{core}) \qquad \text{Equation 29}$$

$A_{Anomalous}$ is a constant [dB μm^4 g/(km K)] giving the weight of the anomalous loss in the expression for the total attenuation. The first part of Equation 29 is from Equation 19. The dependence of the attenuation on the draw tension is as found in [Ainslie 1983]. $f(\Delta n_{core})$ is a function of the core index that will be discussed in the confidential part of this report. The loss has been chosen to depend on the wavelength as $1/\lambda^3$ as for a step index fiber as listed in Table 9.

	Profile factor ($x\ 10^{-5}$)	Δn_{core} ($x\ 10^{-3}$)	Draw Tension (g)	Draw temperature (°C)	$f(\Delta n_{core})$	Measured attenuation @ 1550 nm [dB/km]	Calculated Rayleigh scattering loss [dB/km]	Calculated Urbach absorption loss [dB/km]	Calculated Anomalous loss (first model) [dB/km]	Total calculated attenuation (first model) [dB/km]
Fiber 1 (graded core - reference fiber)	15.1	28	220	2060	4.0	***0.554***	0.281	0.051	0.227	***0.559***
Fiber 2 (graded core)	14.6	29	220	2100	4.3	***0.570***	0.286	0.052	0.238	***0.576***
Fiber 3 (graded core)	13.0	27	225	2080	3.8	***0.471***	0.276	0.049	0.182	***0.506***
Fiber 4 (graded core)	12.8	27	220	2100	3.6	***0.477***	0.276	0.049	0.174	***0.499***
Fiber 5 (graded core)	15.6	30	220	2020	4.5	***0.595***	0.291	0.054	0.261	***0.606***
Fiber 6 (graded core)	16.4	30	220	2020	4.5	***0.628***	0.291	0.054	0.274	***0.620***
Fiber 7 (graded core)	16.8	30	350	1990	4.5	***0.528***	0.291	0.054	0.174	***0.520***
Fiber 8 (graded core)	13.4	27	220	2030	3.8	***0.465***	0.276	0.049	0.187	***0.512***
Fiber 9 (graded core)	0.4	7	100	2200	1.3	***0.204***	0.175	0.013	0.005	***0.193***
Fiber 10 (graded core)	1.6	12	220	2050	1.7	***0.228***	0.201	0.022	0.010	***0.232***
Fiber 11 (graded core)	6.0	28	220	2100	4.0	***0.420***	0.281	0.051	0.092	***0.423***
Fiber 12 (graded core)	4.0	19	200	1980	2.4	***0.271***	0.236	0.034	0.038	***0.308***
Fiber 13 (graded core)	1.2	8	120	2180	1.4	***0.198***	0.181	0.014	0.012	***0.207***
Fiber 14 (graded core)	1.8	12	220	2070	1.7	***0.242***	0.201	0.022	0.011	***0.234***
Fiber 15 (step index)	16.9	23	230	2020	3.0	***0.575***	0.256	0.042	0.178	***0.476***
Fiber 16 (step index)	15.4	22	225	2040	2.8	***0.414***	0.251	0.040	0.158	***0.449***
Fiber 17 (step index)	20.9	26	220	2020	3.6	***0.584***	0.271	0.047	0.274	***0.592***
Fiber 18 (step index)	13.8	22	225	2040	2.8	***0.401***	0.251	0.040	0.142	***0.432***
Fiber 19 (step index)	18.7	24	225	2010	3.1	***0.632***	0.258	0.042	0.207	***0.507***
Fiber 20 (viscosity match)	15.1	28	220	2050	4.0	***0.754***	0.288	0.051	0.226	***0.565***

Table 12 – Input for the loss model (Equation 26), measured attenuation at 1550 nm as well as calculated contributions to the total attenuation at 1550.

In order to determine the constants of Equation 27 - Equation 29, Equation 26 is fitted to the measured attenuation of a set of fibers as given in Table 12 (fiber 1-14) using a least squares fitting routine The resulting values for the constants are given in Table 13. All fibers listed in Table 12 are either fibers in production at OFS Denmark, or fibers made for experiments. The fibers have been chosen to have as large as possible variation of core index within the group. The values for the draw conditions listed represent the values used for each type of fiber. The reference fiber used for the viscosity matching experiment is listed as fiber 1. Fiber 6 and 7 are drawn under different draw conditions, but have essentially same index profile since they come from the same preform.

The correlation between measured and calculated values for the attenuation is good as shown in Figure 27 with a maximum difference between calculated and measured attenuation coefficients as low as 0.04 dB/km.

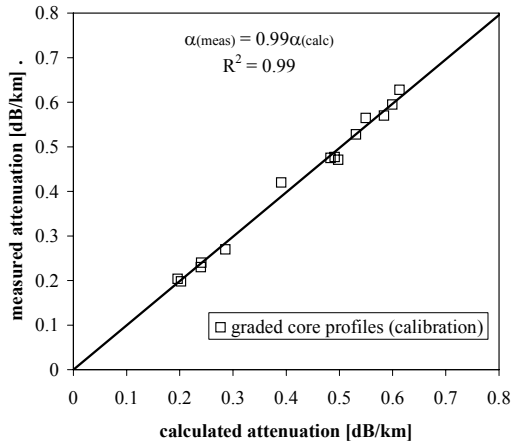

Figure 27 – The correlation between calculated and measured values for the attenuation of the fibers listed in Table 12.

$A_{Rayleigh}$ [dB μm^4 /km]	0.81
$C_{Rayleigh}$	35.8
A_{Urbach} [dB/km]	16.500
E_0 [eV]	5.5
g [eV^{-1}]	4.97
$A_{Anomalous}$ [dB μm^4 g/(km K)]	35.4

Table 13 – Constants of Equation 27 - Equation 29 found by fitting Equation 26 to the measured attenuation data of fibers in Table 12

The Rayleigh scattering coefficient found by fitting Equation 26 to the measured values of the attenuation coefficients (Table 12) $A_{Rayleigh}$ having a value of 0.81 dB μm^4/km is comparable to the values found in the literature with the value of $A_{Rayleigh}$ being calculated to 0.63 dB μm^4/km by Lines for a silica glass with T_f = 1450°C

[1994], determined through $1/\lambda^4$ fit to measured spectral attenuation to 0.76 dB μm^4/km by Tajima et.al. [1994], to 0.79 dB μm^4/km Dianov et.al.[1997] and Ohashi et.al.[1992a] found the value to be 0.8 dB μm^4/km. Since it has been shown that $A_{Rayleigh}$ depends linearly on the fictive temperature of the glass [Lines 1994,Tsujikawa 2000], the differences in $A_{Rayleigh}$ observed can be explained by differences in drawing conditions. The value of $C_{Rayleigh}$ has been determined to be 35.8, which is comparable to the value found by Ohashi et.al.[1992a] of 30 and the value of 48 found by Dianov et.al [1997].

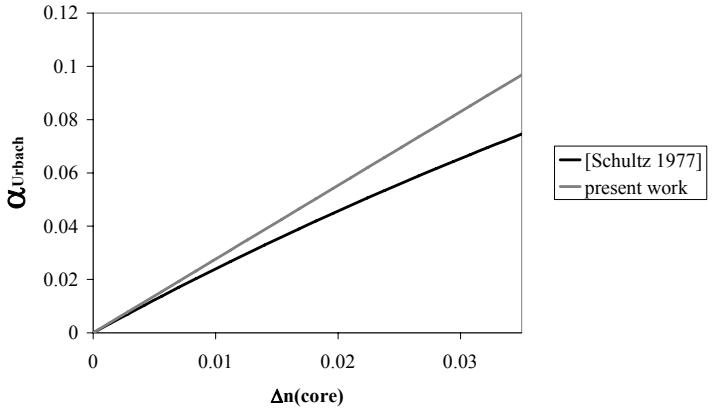

Figure 28 – Comparing α_{Urbach} at 1550 nm as calculated in this work with the α_{Urbach} determined by Schultz [1977]

The Urbach loss accounts for less than 10% of the total loss of the fibers. Figure 28 shows α_{Urbach} as a function of Δn_{core} determined here compared to α_{Urbach} as determined by Schultz [1977]. The largest deviation between the two expressions for α_{Urbach} is observed at $\Delta n_{core} > 0.035$ for which the difference between the two expressions is 0.02 dB/km.

The values for the Rayleigh scattering and Anomalous loss given in Table 12 are comparable for the fibers having a high $\Delta n_{core.}$ Measured values of the attenuation coefficients of the fibers of Table 12 are shown in Figure 21 along with the calculated dependence of the Urbach and Rayleigh loss on Ge-concentration.

Of the draw conditions listed, especially the draw temperature is associated with some uncertainty. T_{draw} of Equation 29 is the temperature of the glass during the drawing of the fiber. T_{draw} listed in Table 12 is a value measured inside the oven used for heating the preform during draw. If the ratio between the measured T_{draw} in the oven and the temperature experienced by the fiber is constant, this error will be accounted for during the calibration of the model. If the difference is an offset, it will introduce an error into the model. The draw temperature is however not a very sensitive parameter. As can be seen from Table 12 that while F_{draw} can be more than doubled, the variation of T_{draw} is less than 10%. Consequently, changes of F_{draw} affects the anomalous loss more than changes of T_{draw}.

The validity of the model is tested by calculating the attenuation of a set of fibers that have not been used for calibrating and comparing these values with the measured

values. The result is shown as the grey points in Figure 29 and shows that the model can also predict the attenuation coefficients of fibers that were not used for the calibration of the model.

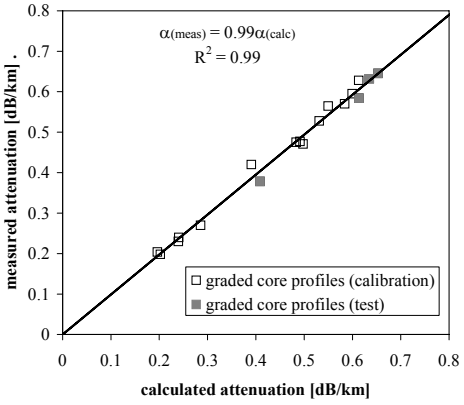

Figure 29 – The correlation between calculated and measured values for the attenuation when including the fibers with graded cores for which the model was tested.

So far the model has only been used for calculating the attenuation of fibers having graded core index. In Table 12 the profile parameters, draw conditions and resulting attenuation coefficients are also given for fibers having a step index profile and for the viscosity matched fiber. As shown in Figure 30 in which these fibers are included, the correlation between the measured and calculated attenuation coefficients leads to an R^2 value as low as 0.88 and a deviation between calculated and measured values as large as 0.1 dB/km for the step index fibers and 0.2 dB/km for the viscosity matched fiber.

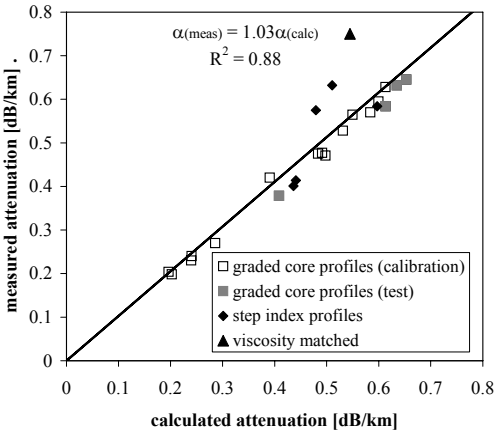

Figure 30 – The correlation between calculated and measured values for the attenuation when the values for step index fibers and the viscosity-matched fiber are included.

To some extend, the large difference between the calculated and measured values for the attenuation coefficient for the step index fibers can be explained by the fact that actual step index fibers are not well described by Equation 18. The ideal step index fiber would have a core exponent, $\gamma = \infty$ but due to diffusion of dopants during production, it is not possible to manufacture an ideal step index fiber and furthermore, Equation 18 does not give a very good description of an actual step index profile as shown in Figure 31. The figure shows the best possible fit of Equation 18 to a fiber having a graded core index and to a fiber with a step index profile. Both index profiles show the center dip characteristic of the MCVD process, so for radii up to 0.4 r_{core} Equation 18 is not expected to give a good description of the refractive index profile of either fiber. For radii > 0.4 r_{core}, Equation 18 gives a good description of the fiber with a graded core index profile but not of the fiber having a step index profile.

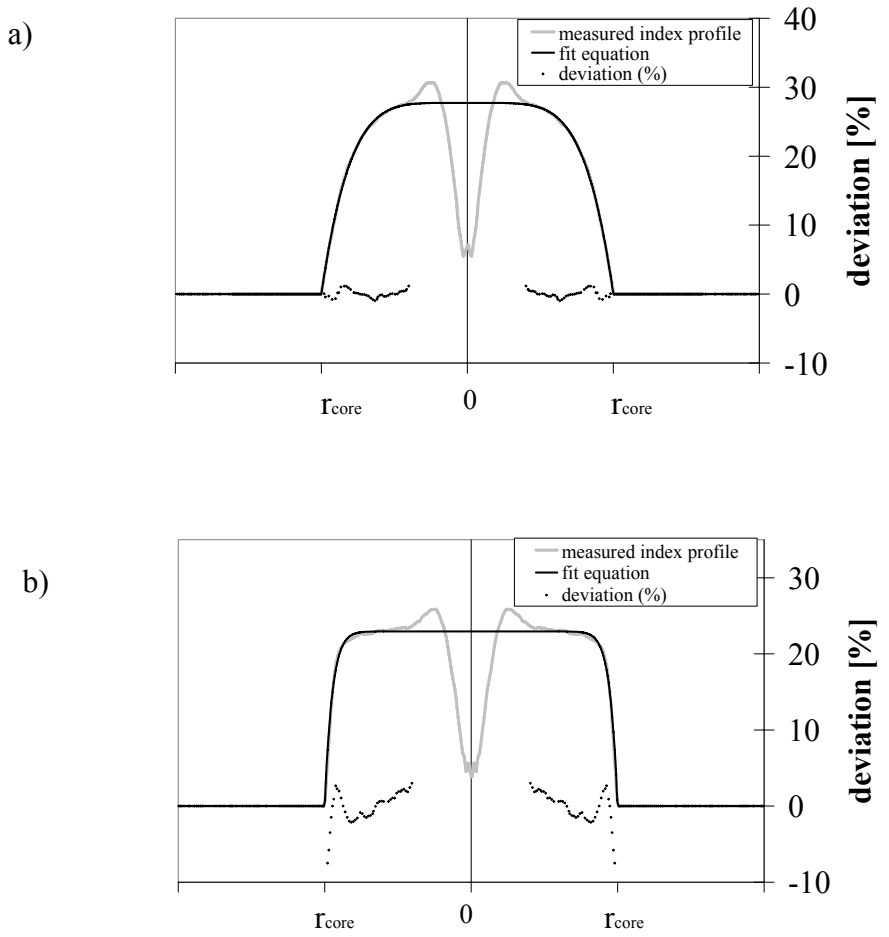

Figure 31 – Fitting Equation 18 to fibers having
a) - a graded core index with $\gamma = 5.4$ or
b) - a step index profile with $\gamma = 20$

That the loss model cannot calculate the attenuation coefficient of the viscosity matched fiber is as expected, since all index parameters used as input to the calculation of the attenuation coefficient of the viscosity matched and the reference

fiber are the same and the two fibers are drawn under the same conditions. So, according to the model, the anomalous loss for these two fibers should be the same. As discussed previously, the increased dopant concentration in the viscosity matched fiber can only account for an 3.5% increase of the Rayleigh scattering which is not enough to explain the difference in measured attenuation of the reference and viscosity matched fibers of 0.2 dB/km. This difference between the measured attenuation of the fibers is attributed to differences between the anomalous loss of the two fibers.

The inability of the model to predict the attenuation coefficient of fibers with either step index profiles or the viscosity-matched profile, leads to the observation that the model should only be used for fibers having index profiles that are well described by Equation 18 and similar dopant distributions to the fibers for which the model is calibrated.

5.4.2 Improving the loss model

The inability of the model to predict the attenuation of the above mentioned fiber types also leads to an improvement of the model in which the formalism of Equation 18 is no longer used. Instead the entire index profile (*n(r)*) as well as the viscosity profile ($\eta(r)$) and the mode field distribution (*E(r)*) is included in the expression for the anomalous loss:

$$\alpha_{anomalous} = A_{anomalous} \frac{\Delta n^2}{d_{core}\lambda^3} \frac{T_{draw}}{F_{draw}} I_{Anomalous} \qquad \text{Equation 30}$$

With $I_{Anomalous}$ being an integral given as:

$$I_{anomalous} = \int_{-r}^{r} f\left[\eta(r), n(r), E(r)\right] r dr \qquad \text{Equation 31}$$

Inside the integral is a function of the viscosity profile, the index profile and the mode field distribution. The function describes the contribution to the anomalous loss from each point along the fiber radius and is integrated in order to give the anomalous loss contribution across the index profile. The refractive index profile is measured, the mode field distribution can be calculated by solving the scalar wave equation (chapter 6) and a good estimate of the viscosity profile can be obtained by using the procedure described in section 5.3. The function will be discussed further in the confidential part of this report.

By using the improved model for the anomalous loss (Equation 30) when fitting Equation 26 to the measured attenuation coefficients of the fibers in Table 12 a good correlation between the calculated and measured attenuation coefficients can be obtained as shown in Figure 32. The amplitudes for the Rayleigh scattering and the Urbach absorption loss are kept constant (values in Table 13). The resulting $A_{anomalous}$ for the improved model is 2.1 [dB μm^4 g /(km K)].

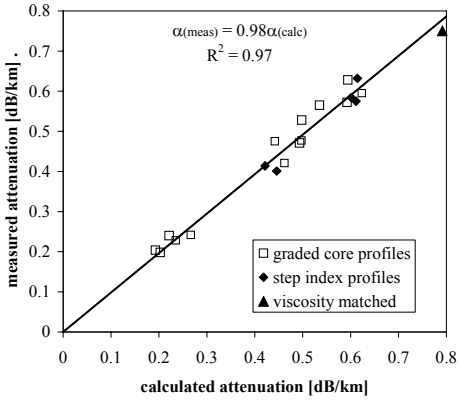

Figure 32 – The correlation between calculated and measured values for the attenuation when Equation 30 is included in the loss model instead of Equation 29. Values for fibers having graded core index as well as step index fibers and the viscosity matched fiber are included

The radial contribution to the anomalous loss as given by the function $f[\eta(r), n(r), E(r)]$ is shown for the reference fiber (fiber 1) in Figure 33 along with the refractive index profile of the same fiber. The main radial contribution to the anomalous loss comes from radial positions for which $r \approx r_{core}$. This is in accordance with the results obtained by Likhachev et.al [2003] in their study of few-modes fibers, that modes having a high power fraction at the core-cladding interface will experience a higher anomalous loss than modes having a smaller fraction of the power at the core-cladding interface.

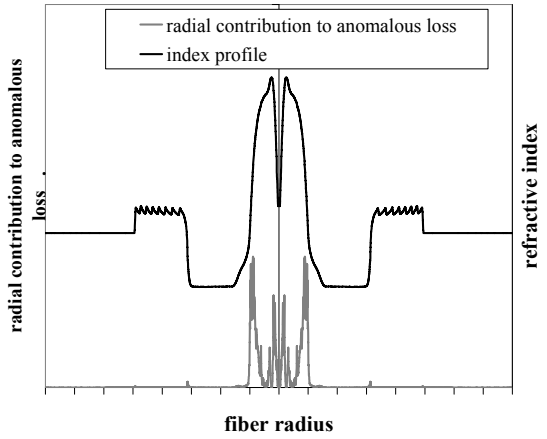

Figure 33 – Refractive index profile and radial contribution to the anomalous loss as determined by $f[\eta(r), n(r), E(r)]$

In Figure 34 the radial contribution to the anomalous loss is shown as a function of the normalized radius for 3 different fibers from Table 12: The reference fiber (fiber 1), a step index fiber (fiber 16) and the viscosity matched fiber (fiber 20). The value of $I_{Anomalous}$ for both the step index fiber and the viscosity-matched fiber is 13.1 while the value for the reference fiber is 6.6.

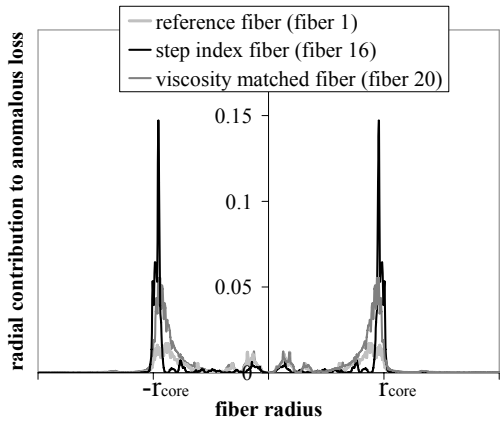

Figure 34 – Radial contribution to the anomalous loss of 3 fibers from Table 12: Reference fiber (fiber 1), a step index fiber (fiber 16) and the viscosity matched fiber (fiber 20).

5.5 Comparing the models

The strength of the first proposed model in which the anomalous loss is given by Equation 29 is its simplicity since the only input needed on profile parameters are the core index difference, the core diameter and the core exponent. The weakness of the model is its inability to predict the attenuation in fibers having very different refractive index profiles from those for which the model has been calibrated. As long as the model is used for fibers having refractive index profiles similar to those fibers for which the model was calibrated, some interesting trends can however be observed:

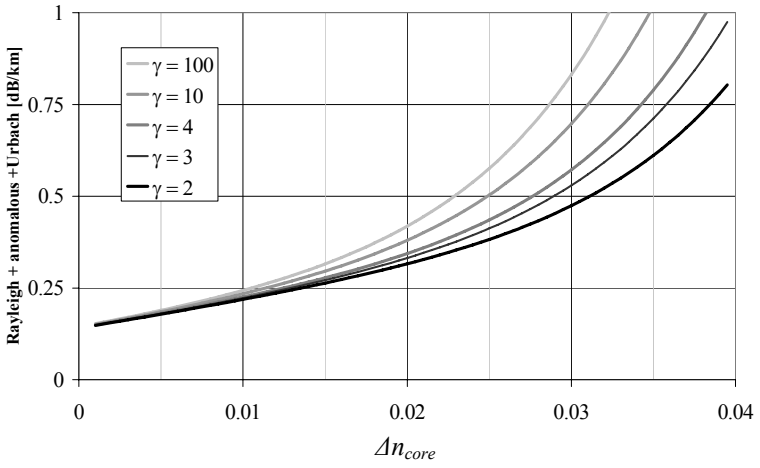

Figure 35 – Calculated attenuation at 1550 nm of high index fibers as a function of core index. The core exponent γ is varied between 2 and 100. The core diameter is 2.6µm, the draw temperature is 2100 °C and the draw tension 220g.

Figure 35 shows calculated total attenuation at 1550 nm as a function of Δn_{core}. The draw temperature is 2100°C, the draw tension is 200 g, the core diameter is 2.6 µm

and the core exponent is varied from $\gamma = 2$ to $\gamma = 100$. The figure shows that decreasing the core exponent can thus counteract the increase of attenuation seen on increasing the core index.

As all input to the first model can easily be obtained from the index profile (assuming that draw conditions are not varied) the model is well suited for the optimization of the loss performance of dispersion compensating fibers as will be described in chapter 6.

Since the improved model in which the anomalous loss as given by Equation 30 includes information on the entire index profile, viscosity profile and mode field distribution the simplicity of the first model is lost. Instead knowledge on how the refractive index profile can be modified in order to reduce the anomalous loss is gained. The refractive index profile and the viscosity profile cannot be engineered completely independently since they both depend on the dopant profile, however it is possible through the knowledge gained from Equation 30 to design fibers with a reduced anomalous loss.

5.6 Fiber designs inspired by the improved loss model

In order to investigate the effect on the anomalous loss of engineering the refractive index and viscosity profile of optical fibers, an experiment has been performed in which four fibers have been designed. The first fiber is included as reference fiber since it has an index profile with a graded core similar to those of Table 12 (fiber 1-14). The index and viscosity profiles of the other three fibers have been varied to test whether the radial contribution to the anomalous loss calculated on the basis of the index profile, viscosity profile and the mode field distribution as described by the function within the integral of Equation 31, can be minimized by an optimization of the viscosity and refractive index profile. A reduction of $I_{Anomalous}$ should result in a reduction of the attenuation coefficient of the fibers. The refractive index profiles of the four fibers have been designed to have the same wave guiding properties and consequently the same mode field distribution. The design strategies for the four fibers will be discussed further in the confidential part of this report.

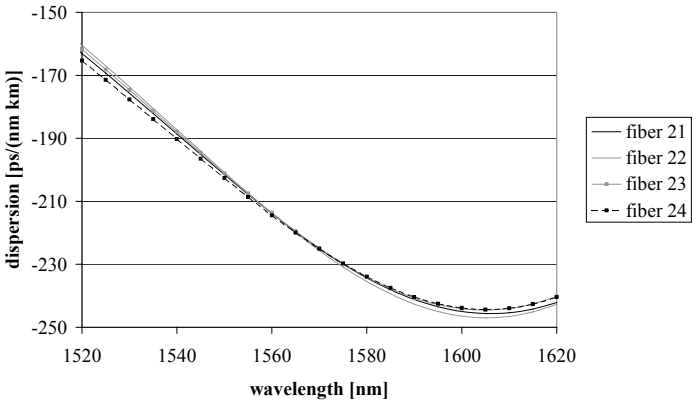

Figure 36 – Dispersion of fibers 21-24 (Table 14)

The measured dispersion coefficients as functions of wavelength for the four fibers are shown in Figure 36 showing that even though there are small differences in the refractive index profiles of the four fibers, the resulting dispersion curves are very similar.

The radial contributions to the anomalous loss are given in Figure 37 along with the index profiles of the four fibers. Table 14 gives the profile parameters, anomalous loss integral and draw conditions needed for calculating the attenuation coefficients of the fibers as well as the measured and calculated attenuation coefficients.

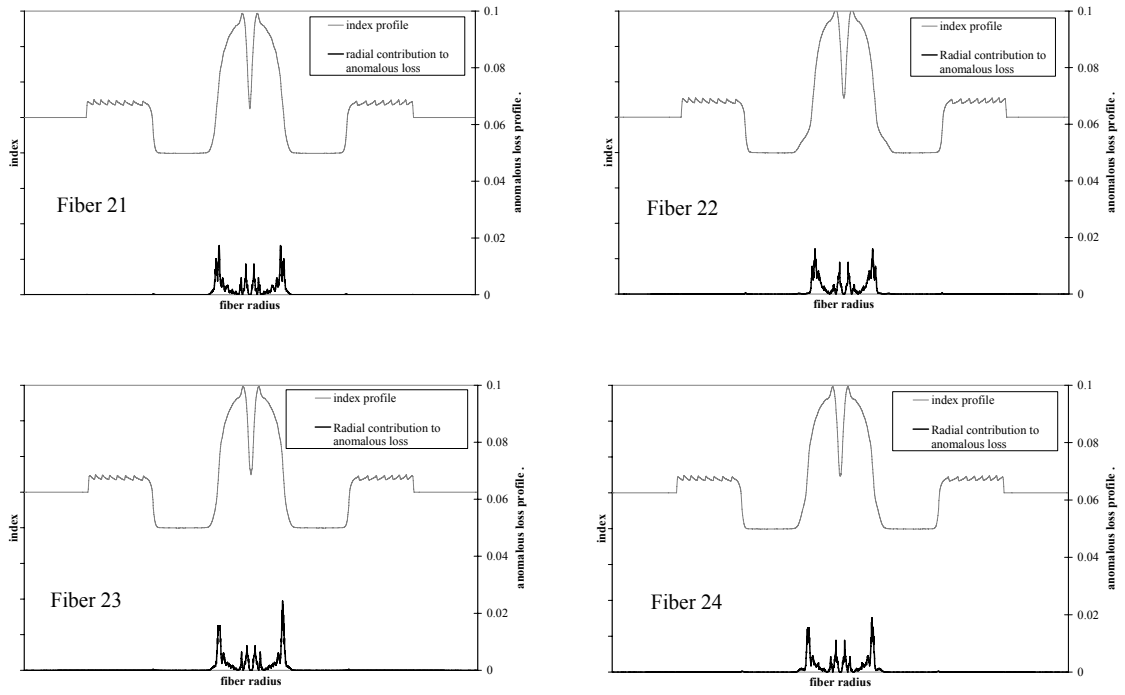

Figure 37 – Index profiles and radial contribution to the anomalous loss for the fibers 21-24 (Table 14)

	Loss integral	$\Delta n_{core}^2/d_{core}$ [μm^{-1}]	Draw tension [g]	Draw temperature [°C]	Calculated Attenuation @ 1550 nm [dB/km]	Measured attenuation @ 1550 nm [dB/km]
Fiber 21	5.4	$4.35 \cdot 10^{-4}$	220	2060	0.475	0.543
Fiber 22	5.6	$4.93 \cdot 10^{-4}$	220	2065	0.511	0.579
Fiber 23	5.9	$4.25 \cdot 10^{-4}$	220	2060	0.481	0.552
Fiber 24	5.1	$4.23 \cdot 10^{-4}$	220	2050	0.458	0.525

Table 14 – Attenuation parameters of four fibers with differing viscosity profiles across the core boundary.

The correlation between the measured and calculated attenuation coefficients for the four fibers is good except for an offset of 0.06 dB/km (Figure 38). Since the offset is observed for all the fibers including the reference fiber that has an refractive index profile similar to that of fibers for which the model has been shown to predict the

attenuation accurately (Figure 32), it is possible that the offset is not due to the model. One possible source of the offset could be the draw conditions. The attenuation offset corresponds to an offset of the measured tension of 60g. Another source of the offset could be a contamination as that described in chapter 4, but the attenuation spectra of none of the fibers support this theory. At this point the source of the offset between the measured and calculated attenuation is unexplained.

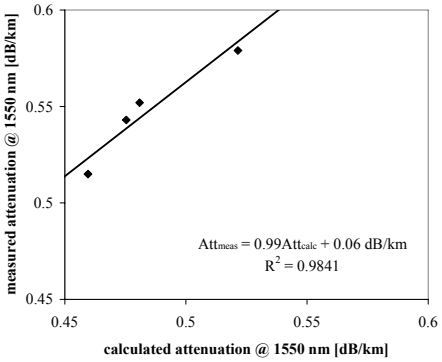

Figure 38 – Calculated and measured attenuation for the 5 fibers of Table 14.

It has thus been shown that, beside an offset of 0.06 dB/km, the improved model for calculating the anomalous loss (Equation 30) is useful for giving guidelines on how to lower the attenuation in high index optical fibers without affecting the wave guiding properties.

5.7 Conclusion on attenuation in high index fibers

In this chapter, the high attenuation coefficients of fibers having a high Δn_{core} have been investigated. Through the experiment with the viscosity-matched fiber it has been shown that the dopant concentration profile of the fiber affects the anomalous loss. Furthermore two models for predicting the attenuation coefficient of optical fibers on the basis of the refractive index profile has been proposed.

The first model predicts the attenuation coefficient based on input on profile parameters such as Δn_{core}, core diameter and core exponent and draw conditions such as draw tension and temperature. The model is based on existing models for the Rayleigh scattering loss, the Urbach absorption and anomalous loss. The amplitude of the contribution from each loss mechanism to the total attenuation is calibrated by fitting the expression for the total attenuation to the measured attenuation for a series of fibers having graded cores. The model is shown to be able to predict the attenuation of a series of fibers that have not been used for the calibration of the model. The model is however unable to predict the attenuation for step index fibers or the viscosity matched fiber.

In order to improve the model, the expression for the anomalous loss has been modified to include a function of the viscosity profile, the refractive index profile and

the mode field distribution. The strength of the improved model is that it has been shown to be able to predict the attenuation of fibers having graded core indexes as well as step index profiles. The weakness of the model is that it is more complex than the first proposed model, since in order to obtain an accurate viscosity profile of the fiber, the diffusion of dopants during production must be calculated.

Since the improved model contains information on the refractive index profile, the viscosity profile and the mode field distribution, it can be used to investigate how these parameters affect the attenuation in optical fibers. The model has been used to give guidelines as to how the design of a dispersion compensating fiber can be improved in order to lower the attenuation. Four fibers designed using the model have been manufactured and the attenuation coefficients measured. The resulting attenuation coefficients of the four fibers follow the trend predicted by the improved model.

6. Optimizing dispersion compensating fibers

6.1 Introduction

One of the most wide spread uses of high index fibers is for dispersion compensating fibers. More than 100000 dispersion compensating fiber modules are deployed in optical communications systems worldwide. In this chapter the application and design principles of dispersion compensating fibers will be discussed with special emphasis on low attenuation dispersion compensating fiber modules. In the last part of the chapter, results on the design and realization of two dispersion-compensating fibers for low attenuation dispersion compensating fiber modules will be presented.

As the name implies, dispersion compensating fibers (DCF) are used in optical communication systems to compensate the dispersion accumulated in a transmission fiber. They can either be used as a part of the span or as discrete dispersion compensating modules placed within the amplifier as shown in Figure 39. In whichever way they are used, dispersion-compensating fibers are fibers with a negative dispersion coefficient. The dispersion compensating fibers treated in this work will all be fibers for dispersion compensating fiber modules.

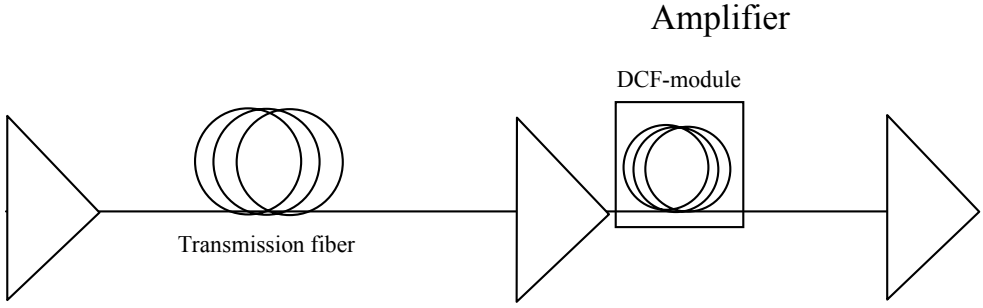

Figure 39 – The conventional use of a dispersion compensating fiber module (DCF-module). The DCF-module is placed in the amplifier between two amplification stages.

The only requirement to dispersion compensating fiber modules when they were first introduced into the market in the mid ’90, was for them to have a negative dispersion coefficient. As the bit rate of optical communication systems continually increases,

other requirements have followed such as the requirement for low loss, low nonlinearity or the ability of broadband dispersion compensation.

When designing dispersion compensating fibers there are many expectations to be met. The end users' expectation to the dispersion compensating fiber module is for the module to be able to deliver broadband dispersion compensation without significantly adding loss or nonlinearities to the system. Another expectation of the end users is that the optical properties of the module are stable when the operating conditions with respect to temperature and humidity changes. As to the expectations to the physical appearance of the module, the dispersion compensating fiber module normally consists of the dispersion compensating fiber wound onto a metallic spool with connectors spliced onto each end of the fiber.

Besides meeting the expectations of the end users, the manufacturer also has some requirements to the design of the dispersion compensating fiber. One of the most important requirements here is for the design to be robust, so the small variations in the index profile, which are unavoidable during the manufacturing process, will not severely affect the optical properties of the fiber.

6.2 Designing dispersion compensating fibers

This section will present the basic theory needed for understanding the design of dispersion compensating fibers. The theory will be published in [Wandel & Kristensen 2005]. The dispersion compensating fibers discussed here are all designed to have a negative dispersion coefficient in the wavelength range used for telecommunication systems (C+L band; 1510-1610 nm). The negative dispersion coefficient is obtained by controlling the waveguide dispersion.

All fibers in this work have triple clad index profile with a core surrounded by a down-doped region (trench) followed by a raised ring. The basic fiber profile is given in Figure 40a. Since both the indexes and widths of all three layers in the triple clad index profile can be varied during the design process, there is an almost unlimited number of possible designs and to understand the effect of changing each profile parameter can be a challenge.

6.2.1 The super mode approach to fiber design

Super mode theory can be an efficient tool for gaining an intuitive understanding of how changes in the refractive index profile of a fiber affect the propagation properties [Schneider & West, 2002].

Dispersion is related to the second derivative of the propagation constant (β) by:

$$D = \frac{-2\pi c}{\lambda^2}\frac{d^2\beta}{d\omega^2} \qquad \text{Equation 32}$$

The second derivative of β is given by:

$$\frac{d^2\beta}{d\omega^2} = \frac{1}{c}\left(2\frac{dn_e}{d\omega} + \omega\frac{d^2n_e}{d\omega^2}\right) \qquad \text{Equation 33}$$

With ω being the frequency and n_e the effective index. β can be expressed in terms of the free space wave number (k_0) and n_e:

$$\beta = k_0 n_e \qquad \text{Equation 34}$$

With k_0 defined as:

$$k_0 = \frac{\omega}{c} = \frac{2\pi}{\lambda} \qquad \text{Equation 35}$$

And n_e as:

$$n_e = \Delta n_e + n_0 \qquad \text{Equation 36}$$

Δn_e being the effective index difference and n_0 the refractive index of the cladding. When only considering the second term in Equation 33 the dispersion can be expressed as:

$$D = \frac{-2\pi c}{\lambda^2}\frac{d^2 k_0 \Delta n_e}{d\omega^2} + \frac{-2\pi c}{\lambda^2}\frac{d^2 k_0 n_0}{d\omega^2} = D_{waveguide} + D_{material} \qquad \text{Equation 37}$$

In which the first term gives the waveguide dispersion and the second term the material dispersion. The waveguide dispersion is thus given by the second derivative of the effective index difference [Agraval, 1997].

With the super mode theory, the propagation properties in a fiber with a triple clad index profile are understood by considering separately the two guiding regions, the core and the ring as shown in Figure 40 b+c. The index profile of the core guide (b) has been obtained by removing the ring from the triple clad index profile of Figure 40a, while the index profile of the ring profile (c) has been obtained by removing the core part from the index profile of Figure 40a.

The effective index of the combined mode can be described by:

$$n_e = \frac{n_{e(core)} + n_{e(ring)}}{2} \pm \sqrt{\kappa^2 + \left(\frac{(n_{e(core)} - n_{e(ring)})^2}{4}\right)} \qquad \text{Equation 38}$$

with $n_{e(core)}$ being the effective index of the core mode, $n_{e(ring)}$ being the effective index of the ring mode and κ the coupling strength between the two modes [Schneider & West, 2002].

At the short wavelengths the effective index of the LP_{01} mode approaches that of the core mode, indicating that the mode is mainly confined to the core while at higher wavelengths it approaches that of the ring indicating that the mode at these wavelengths is mainly confined to the ring.

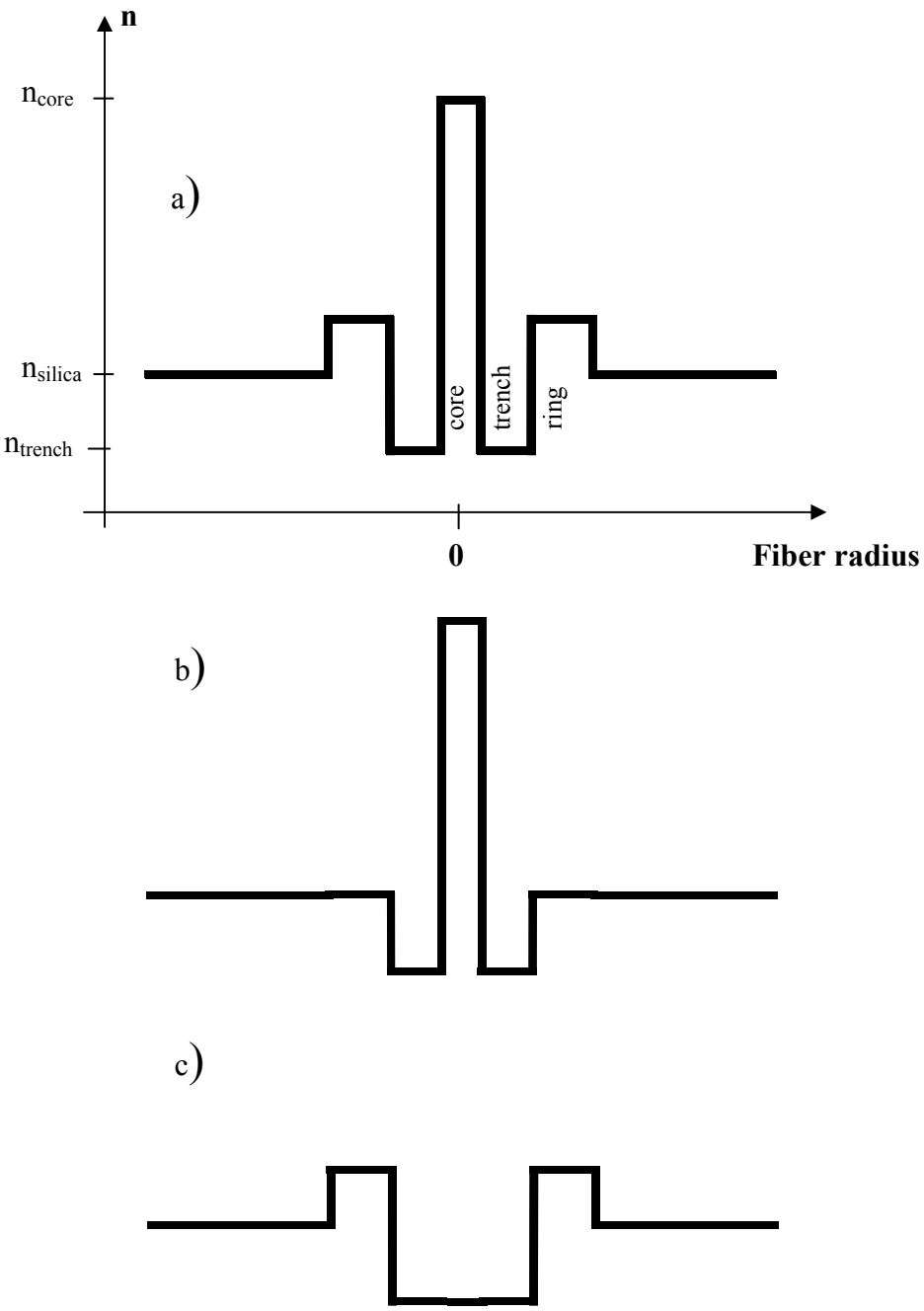

Figure 40 – Triple clad index profile.
a): The core is surrounded by the deeply down-doped trench followed by a raised ring. The core and ring are doped with germanium in order to increase the refractive index with respect to silica while the trench is doped with fluorine to lower the refractive index.
b): The index profile of the core guide
c): The index profile of the ring guide

In Figure 41 the point where the core and ring mode intersect is defined as the crossover point. The curvature of the effective index difference, and consequently the dispersion of the combined mode are given by the coupling strength κ. A low coupling strength signifies small interaction between the core and the ring mode and

the curvature of the effective index difference will be high at the crossover point. The opposite is the case for high coupling strength.

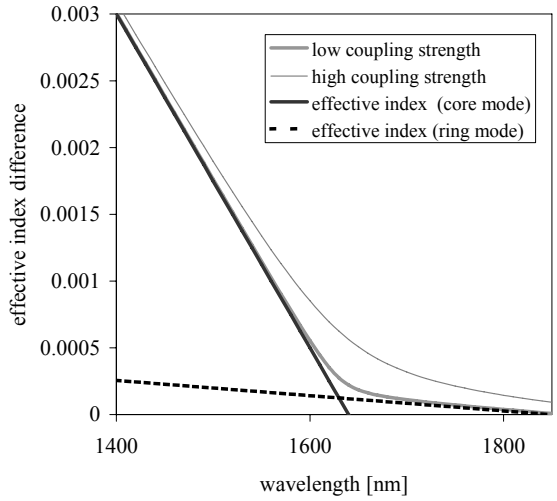

Figure 41 – Effective index differences for core-, ring- and LP_{01} modes.
The LP_{01} mode is shown for high and low coupling strengths between the core and ring modes. A high coupling strength results in a low curvature at the crossover point while a low coupling strength results in a high curvature.

The minimum of the dispersion of the LP_{01} mode occurs where the curvature of the effective index difference reaches a maximum (Figure 42). Since the dispersion is given by the second derivative of the effective index difference, the negative dispersion coefficient can be increased by reducing the coupling strength between the core and the ring mode thus increasing the curvature of the effective index difference. This can be done by either increasing the width or by decreasing the refractive index of the non-guiding trench layer of the triple clad index profile.

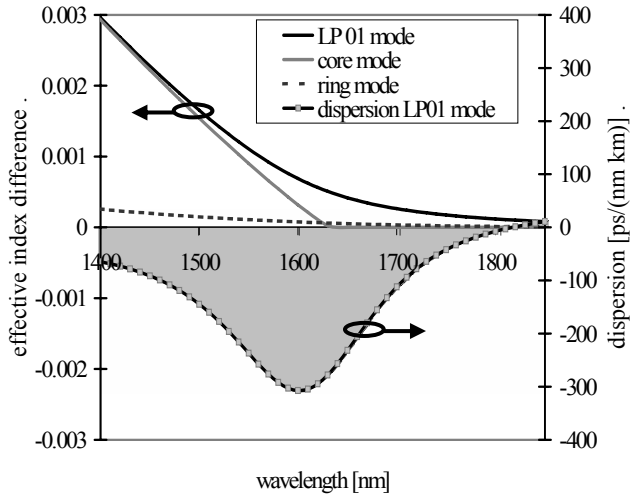

Figure 42 – The effective index difference of the core, ring and LP_{01} mode along with the resulting dispersion.

The first derivative of the propagation constant with respect to wavelength is the group delay. Consequently, the area above the dispersion curve (shaded gray in Figure 42) must be equal to the difference between the group delay at the short and long wavelength side of the minimum of the dispersion curve. Since at shorter wavelengths the group delay of the LP_{01} mode approaches that of the core mode and at longer wavelengths that of the ring mode, the area above the dispersion curve must remain unchanged for fiber designs having the same slopes of Δn_e for the core and ring mode but differing coupling strengths between the modes. The consequence for this is that if the coupling strength between the modes is decreased by increasing the non-guiding area (trench), thereby increasing the negative dispersion coefficient, then in order for the area above the dispersion curve to remain constant, the dispersion curve must become steep and narrow.

6.2.2 Scaling of the triple clad index profile:

The wave guiding properties and thereby the dispersion curve of an optical fiber can be changed by changing the widths and indexes of the layers of the triple clad index profile [Kristensen, 2004].
The scalar wave equation can be written as:

$$\nabla_{r,\theta}^2 \varphi + \frac{4\pi^2}{\lambda^2} 2n_0 \Delta n \varphi = \frac{4\pi^2}{\lambda^2} 2n_0 \Delta n_e \varphi \qquad \text{Equation 39}$$

With $\nabla_{r,\theta}^2$ being the laplacian operator, Δn the refractive index difference, Δn_e the effective index difference and φ the scalar electric field. Terms in the order of Δn_e^2 and Δn^2 have been neglected.
If the scalar wave equation (Equation 39) is written for two different fiber profiles that are related to each other by:

$$\Delta n^* = a\,\Delta n \qquad \text{Equation 40}$$

And by a scaling of radial distances by:

$$r^* = b\,r \qquad \text{Equation 41}$$

with the superscript * denoting the scaled profile, a the index scale factor and b the radius scale factor, the scalar wave equation for the two index profiles will be the same when Δn_e is scaled as:

$$\Delta n_e^* = a\,\Delta n_e \qquad \text{Equation 42}$$

And the wavelength (λ) is scaled as:

$$\lambda^* = b\sqrt{a}\,\lambda \qquad \text{Equation 43}$$

Consequently the dispersion scales as:

$$D^*_{waveguide} = \frac{-2\pi c}{\lambda^*}\frac{d^2 k_0^* \Delta n_e^*}{d\omega^{*2}} = \frac{\sqrt{a}}{b}\frac{-2\pi c}{\lambda}\frac{d^2 k_0 \Delta n_e}{d\omega^2} = \frac{\sqrt{a}}{b} D_{waveguide}$$ Equation 44

The dispersion slope as:

$$S^*_{waveguide} = \frac{dD^*_{waveguide}}{d\lambda^*} = \frac{d\left(\frac{\sqrt{a}}{b} D_{waveguide}\right)}{d(b\sqrt{a}\lambda)} = \frac{1}{b^2} S_{waveguide}$$ Equation 45

If the radius scale factor b is related to the index scale factor a by:

$$b = \frac{1}{\sqrt{a}}$$ Equation 46

The relative dispersion slopes of the two fibers will be the same:

$$RDS^*_{waveguide} = RDS_{waveguide}$$ Equation 47

A consequence of this is that the effective index can be changed significantly without changing the waveguide dispersion [Kristensen 2004].

The scaling of the triple clad index profile that has been outlined here only affects the waveguide dispersion. The neglect of the material dispersion will introduce a small error on the dispersion.

The scaling of the profile can be performed on all layers of the triple clad index profile or on either of the guiding regions. By scaling only the core region by decreasing the core diameter, the intersection between the effective indexes of the core and ring mode (Figure 41) and thereby the point of minimum dispersion can be moved to shorter wavelengths thereby translating the dispersion curve with respect to wavelength.

The magnitude of the shift in λ upon scaling of the index profile can be used as a measure of the sensitivity of a design to the small variations in the index profile that are unavoidable during the manufacturing of optical fibers.

By changing the width of the trench, the slope of the effective index difference for the core and ring modes remains largely unchanged. Consequently, the area under the dispersion curve is the same for fibers with different widths of the trench, but a significant change in the slope of the dispersion curve is seen.

6.2.3 Dispersion tailoring

One of the strengths of dispersion compensating fibers is that they can compensate the dispersion of the transmission fibers over a large wavelength range. The residual dispersion, which is the remaining dispersion after compensation, can be used as a measure of the performance of the dispersion compensating fiber in a given

wavelength range. A low residual dispersion will signify high performance of the dispersion compensating fiber. It has been shown that the theoretical tolerance on the residual dispersion for a non return to zero (NRZ) signal assuming a 1 dB eye-closure penalty is around 60 ps/nm at 40 Gb/s [Nelson, 2003].
The dispersion of any fiber or combination of fibers can be modeled by a Taylor expansion around a center wavelength (λ_0) as:

$$D\ (\lambda) = D(\lambda_0) + D^{'}(\lambda_0)(\lambda - \lambda_0) + \frac{1}{2}D^{''}(\lambda_0)(\lambda - \lambda_0)^2 + \frac{1}{6}D^{'''}(\lambda_0)(\lambda - \lambda_0)^3 \ldots\ldots\ldots\ldots \quad \text{Equation 48}$$

where *D'* is the first derivative of the dispersion (the dispersion slope: *S*), *D''* the second derivative of the dispersion (the dispersion curvature), and *D'''* the third derivative of the dispersion. In most transmission fibers, the dispersion is dominated by the material dispersion, and in the wavelength range considered here it can be described by including only the first two terms of Equation 48. However, as seen from Figure 43, in order to give a good description of the dispersion of a dispersion compensating fiber, higher order terms need to be included as well.

In order to obtain a low residual dispersion, not only the dispersion of the dispersion compensating fiber should match that of the transmission fiber, but also the dispersion slopes should be matched while all higher order terms of Equation 48 for the dispersion compensating fiber should be as low as possible. It has been shown that in order to obtain slope match, the relative dispersion slope (*RDS*), which is defined as the ratio of dispersion slope (*S*) to dispersion (*D*), for the dispersion compensating fiber and for the transmission fiber should be the same [Grüner-Nielsen et al. 2000].

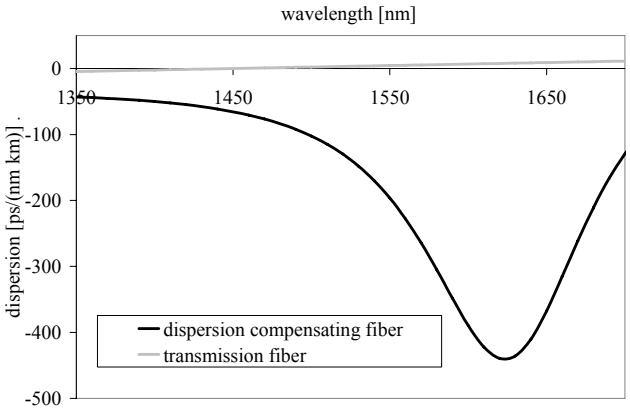

Figure 43 – The dispersion as function of wavelength for dispersion compensating fiber and transmission fiber in the wavelength range 1350- 1700 nm

That perfect dispersion compensation would be obtained by matching the slopes of the two fibers would only be true if higher order terms from Equation 48 such as the curvature were not needed to describe the dispersion of the dispersion compensating fiber. It is only true that slope match gives the lowest possible residual dispersion when the dispersion curvature is not considered.

As mentioned previously, since the dispersion of the transmission fiber is well described by the first two terms in Equation 48, all higher order terms, and thereby the curvature – and relative dispersion curvature for the dispersion compensating fiber should be as small as possible in order to obtain a low total dispersion curvature and thereby a low residual dispersion. The dispersion properties of the most commonly used transmission fibers are given in Table 15. The values are given at 1550 nm unless otherwise stated.

	Dispersion [ps/nm·km]	**Dispersion slope [ps/nm^2·km]**	**RDS [nm^{-1}]**
Standard single-mode optical fiber (SSMF) ITU: G.652	16.5	0.058	0.0036
Non-zero dispersion-shifted single-mode optical fiber (NZDF): ITU: G.655			
TrueWave® *REACH* fiber	7.1	0.042	0.0058
TeraLight* fiber	8	0.058	0.0073
TrueWave® RS fiber	4.5	0.045	0.010
ELEAF* fiber	4.2	0.085	0.02
Dispersion shifted single-mode optical fiber (DSF) (@1590 nm) ITU:G.653	2.8	0.07	0.025

Table 15 – Dispersion properties of transmission fibers.
The values are given at 1550 nm unless otherwise stated.

Figure 44 shows the residual dispersion of 4 links of the same type as shown in Figure 39. The transmission fiber is a TrueWave® RS (Table 15) and the four different dispersion compensating fibers are all realized fibers.

The residual dispersion of the link is calculated from the measured dispersions of the transmission and dispersion compensating fibers.

The residual dispersion variation is one way to measure the quality of the dispersion compensation. Another is usable bandwidth, which can be defined as the bandwidth for which the residual dispersion variation is below a given value [Rathje et.al.2002]. In Figure 44 the usable bandwidth is shown as the bandwidth for which the residual dispersion variation is within 0.2 ps/(nm km) corresponding to a theoretical transmission length of 300 km of a NRZ signal at 40 Gb/s assuming the transmission length to be limited by the dispersion only [Nelson 2003].

In Figure 44a the *RDS* of the transmission fiber is different from the *RDS* of the dispersion compensating fiber and the usable bandwidth is limited to 12 nm by the slope mismatch.

In Figure 44b the dispersion slopes of the two fibers are matched resulting in a usable bandwidth that is only limited by the dispersion curvature of the dispersion compensating fiber. By reducing the curvature of the dispersion compensating fiber and keeping the slopes matched, an improvement in usable bandwidth can be obtained as shown in Figure 44c, but the improvement is only from the usable bandwidth of 51 nm from Figure 44b to the usable bandwidth of 57 nm in Figure 44c. The largest usable bandwidth can be obtained if the curvature of the dispersion compensating fiber is minimized while allowing a small slope mismatch as shown in Figure 44d. This figure shows the same dispersion compensating fiber as in Figure 44c but the

transmission fiber of Figure 44d has a slightly lower dispersion slope. This overcompensation of the dispersion slope results in a usable bandwidth of 82 nm and is an example of how slope match is not always desirable in order to obtain a large usable bandwidth. By increasing the RDS of the dispersion compensating fiber slightly, the usable bandwidth can be increased even further

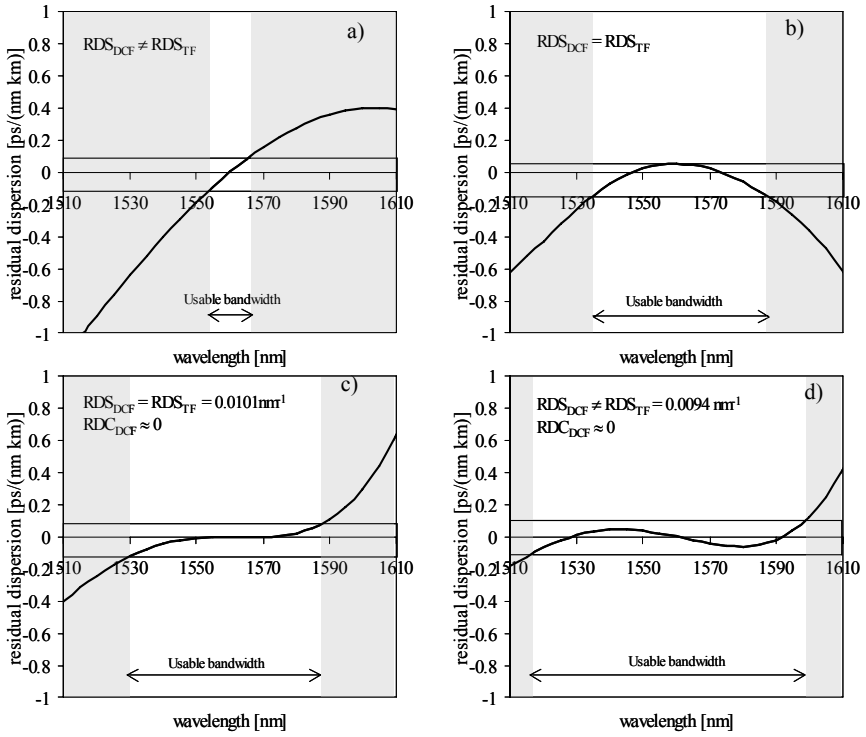

Figure 44 – Residual dispersion variation and usable bandwidth of 4 links consisting of a NZDF (TrueWave®RS) and a dispersion compensating fiber. The usable bandwidth is defined here as the bandwidth for which the residual dispersion is within 0.2 ps/(nm km).
a) *RDS* of the transmission fiber and the dispersion compensating fiber do not match.
b) *RDS* of the transmission fiber and the dispersion compensating fiber are matched
c) *RDS* of the transmission fiber and the dispersion compensating fiber are matched. The curvature of the dispersion compensating fiber is low.
d) *RDS* of the transmission fiber is slightly lower than the RDS of the dispersion compensating fiber. The curvature of the dispersion compensating fiber is low.

Whether the slopes should be perfectly matched for dispersion compensating fibers with low curvature depends of course on the requirements to the residual dispersion. In Figure 44c, even though the usable bandwidth as defined above is smaller than in Figure 44d, the residual dispersion variation from 1550 nm – 1570 nm is less than 0.01 ps/(nm km) and for some applications a low residual dispersion is more important than a large usable bandwidth.

In Figure 45 the dispersion, dispersion slope and dispersion curvature are shown as functions of wavelength. The dispersion curvature has been scaled with a factor of 10 in order to be plotted on the same axis as the slope. Two important points are marked in the figure: The inflection point where the sign of the curvature changes is where the

lowest residual dispersion can be obtained due to the low curvature, and the point of minimum dispersion where the dispersion slope changes sign is where the highest negative dispersion can be obtained. It should be noted that the dispersion curvature reaches its maximum value at the point of minimum dispersion resulting in a high residual dispersion for dispersion compensating fibers operated at this point of the dispersion curve.

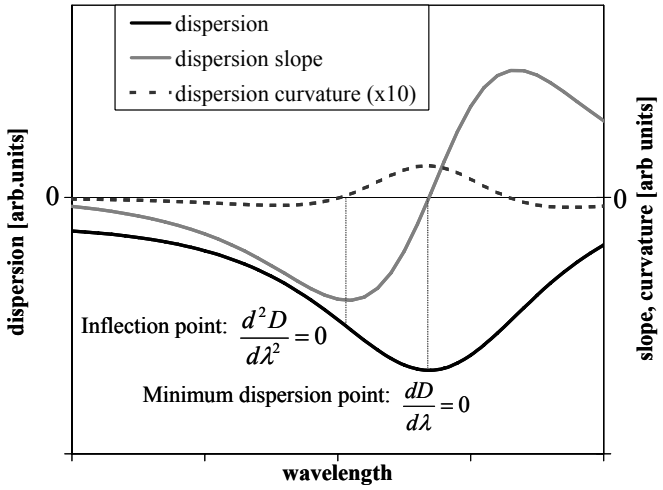

Figure 45 – Dispersion, dispersion slope and dispersion curvature for a dispersion compensating fiber. The dispersion curvature has been scaled with a factor of 10 in order to be plotted on the same axis as the dispersion slope.

6.2.4 Waveguide dependent attenuation

In chapter 3 it was briefly mentioned that the wave guiding properties of the fiber affects the attenuation as well. In the previous chapter it was discussed how the design of the index profile and the choice of dopant concentrations affect the attenuation of high index fibers, primarily through the anomalous loss. In this section the basic mechanisms for the waveguide dependent losses, macro and micro bend losses will be discussed.

Macro bend losses

Understanding the mechanisms for macro bend losses are important for any kind of fiber, but for dispersion compensating fibers that are typically used on a spool whose inner diameter should be as small as possible in order to minimize the volume of the component, the macro bend losses must be controlled carefully.
The propagation in a bend fiber is often described using the equivalent index profile (n_{equ}) [Andreasen 1987]:

$$n_{equ}^2 = n^2(r)\left[1+2\frac{r}{R}\cos(\phi)\right] \qquad \text{Equation 49}$$

with $n(r)$ being the refractive index profile, r and ϕ the cylindrical coordinates of the fiber and R the bend radius of the fiber. The radius where the effective index

intersects the equivalent index profile is the radiation caustic (r_c) outside which the field becomes radiating (Figure 46).

The macro bend losses can be minimized by either increasing the effective index of the mode, thereby increasing r_c, or by reducing the effective area, thereby reducing the field present at r_c. A side effect of increasing the effective index of the LP_{01} mode is that also higher order modes will be more confined to the core and consequently their cut off wavelengths are increased. If the fiber supports higher order modes as well as the fundamental mode, the light traveling in different modes can interfere, causing noise through multi path interference (MPI).

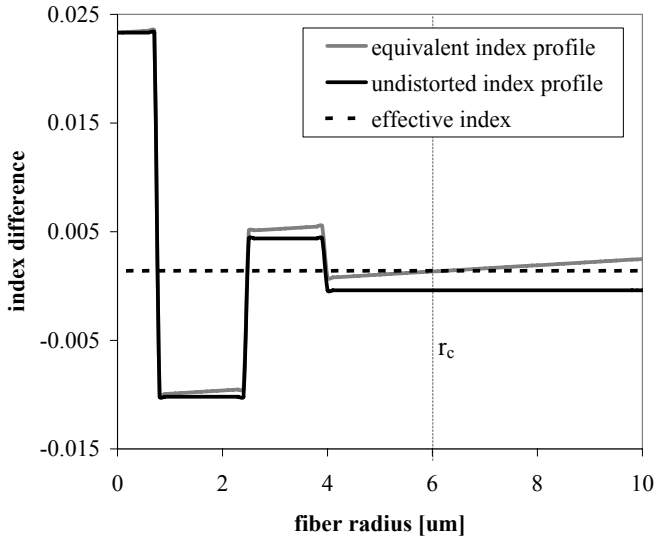

Figure 46 – The undistorted index profile and the equivalent index profile for a bend fiber. The vertical dotted line marks the radiation caustic r_c, the radius outside which the mode becomes radiating

Micro bend losses

The fiber in a module experiences not only the macroscopic bend loss induced by the bend radius of the fiber on the module. Another source of attenuation is the micro bend loss originating from the microscopic deformations caused by the pressure from the other fibers in the package.

The micro bend loss of the fiber is important not only for the overall attenuation of the fiber, but also for the performance of the dispersion compensating fiber module when subjected to temperature changes. When the dispersion compensating fiber module is subjected to an increase of temperature, the metallic spool on which the fiber is wound, will expand. The fiber will experience a pressure from the other turns of the fiber, which will act as a surface with a deformation power spectrum Φ. This leads to micro bend loss (α_{micro}) that can be expressed as [Marcuse, 1984]:

$$\alpha_{micro} \propto \sum_{p} C_{1p}^2 \Phi(\Delta\beta_{1p}) \qquad \text{Equation 50}$$

where C_{1p} are the coupling coefficients between the LP_{01} mode and the cladding modes, LP_{1p} , (p = 1, 2,……) and Φ is the deformation power spectrum of the fiber axis at spatial frequencies $\Delta\beta_{1p}$ corresponding to the difference in propagation constants between the LP_{01} and cladding modes. ($\Delta\beta_{1p} = \beta_{01} - \beta_{1p}$)
The deformation spectrum experienced by the fiber depends on the stiffness of the fiber as well as on the ability of the coating to absorb the deformation. This leads to an expression for the micro bend loss of a fiber that experiences a linear pressure (F) onto a surface with the deformation spectrum Φ[Gloge, 1975]:

$$\alpha_{micro} \propto \frac{DF}{H^2\sigma}\sum_{p=1}^{\infty} C_{1p}^2 \frac{1}{(\Delta\beta_{1p})^8}\Phi_s(\Delta\beta_{1p}) \qquad \text{Equation 51}$$

with σ being related to the RMS value of the surface deformation, H the flexural rigidity (stiffness) and D the lateral rigidity of a coated fiber. The terms in front of the summation are all related to the mechanical properties of the fiber, whereas the terms inside the summation are related to the fiber index profile and the deformation spectrum.

Equation 51 shows that by increasing the fiber diameter and thereby the stiffness of the fiber, the micro bend losses can be reduced. Another possibility for reducing the micro bend losses is to change the ability of the coating to protect the fiber from deformation by absorbing the pressure. Both strategies have been reported to have been used successfully to compensate for a fiber design highly sensitive to micro bend loss [Tsukitani et al., 2002; Hatayama, 2003; Kato et al., 2001] but neither will be pursued here. The strategy pursued here will be that of being able to understand and minimize the micro bend loss of the fiber design through control of the effective index difference. As the terms inside the summation show, the micro bend loss depends strongly on the difference in propagation constants ($\Delta\beta_{1p}$). So by choosing a design with large effective index difference, the micro bend loss can be minimized.

6.2.5 Calibrating the model

The optical properties of the fiber designs presented in this work have all been calculated using an OFS modeling tool that solves the scalar wave equation using a finite elements formulation to obtain β and the fields of the guided modes on the basis of the preform index profile, the cross sectional area of the jacketing tube and the fiber diameter. The model for calculating the micro bend loss is based on [Petermann, 1976] and the output value for the micro bend loss calculation is normalized to a reference fiber. The value for the micro bend loss is thus a measure of how much higher or lower the micro bend loss is compared to the reference fiber, which is a depressed cladding fiber[1].

When the preform is drawn into fiber, the refractive index profile changes due to stresses and strain built into the material [Yablon, 2004]. Consequently, the optical properties calculated on the basis of the preform index profile will differ from those calculated on the basis of the real fiber index profile. This deviation can be minimized by a calibration of the model in which the measured optical properties of a fiber are

[1] Private communication: Manual for modelling tool; G.Gnacadja, OFS

compared to the corresponding properties calculated for varying draw induced index changes. The draw induced index changes obtained in this way will not only contain the index changes that have occurred during draw, but also any systematic errors in the measurement of the preform index profile.

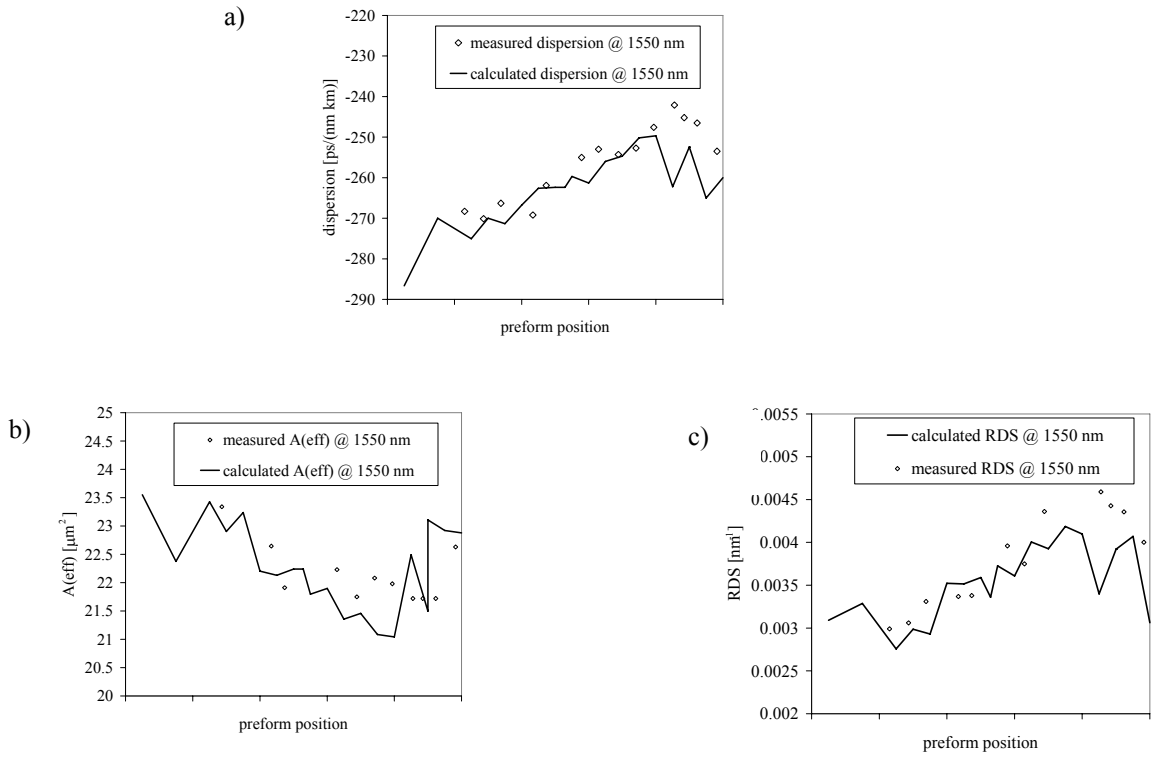

Figure 47 – Calibration of the model for calculating the wave guiding properties of the fiber
a) Measured and simulated values for the dispersion at 1550 nm along a preform
b) Measured and simulated values for the effective area at 1550 nm along a preform
c) Measured and simulated values for the *RDS* at 1550 nm along a preform

The validity of the model is controlled by comparing measured optical properties to the calculated properties for fiber from a couple of preforms. Figure 47a-c shows the measured and calculated values for dispersion, effective area and *RDS* along a preform. The index profile used as an input for the model is measured at several positions along the preform. The simulation have been performed with a constant area of the jacketing tube which is probably the reason why the measured and simulated values deviates for fiber from the end of the preform in which the variation in cross sectional area of the jacketing tube is known to have considerable variation along the length.

Since the draw induced index changes depend on material properties of the fiber such as the viscosity, the set of draw induced index changes found for one fiber design are not necessarily valid for another design if the refractive indexes and consequently the dopant concentrations and viscosities have changed.

6.3 Dispersion compensating fibers with a high figure of merit.

While dispersion compensating fiber modules are used in systems in order to control the dispersion of the system thereby increasing performance, they decrease the performance of the system with respect to loss by increasing the need for amplification thereby degrading signal to noise ratio and adding to the cost of the system. The added attenuation from a dispersion compensating fiber module to the system ($A_{DCFmodule}$) is expressed as:

$$A_{DCF\,\mathrm{mod}\,ule} = L_{DCF}\alpha_{DCF} + A_{splice} + A_{connector} \qquad \text{Equation 52}$$

L_{DCF} is the length of dispersion compensating fiber in the module [km], α_{DCF} is the attenuation coefficient of the dispersion compensating fiber [dB/km], A_{splice} is the splice loss [dB] and $A_{connector}$ is the loss of the connector [dB]. The length of dispersion compensating fiber needed in the module is found as:

$$L_{DCF} = \frac{D_{tot}}{D_{DCF}} \qquad \text{Equation 53}$$

With D_{tot} being the total dispersion of the module (= the dispersion accumulated on the length of transmission fiber in the span) and D_{DCF} the dispersion coefficient of the dispersion compensating fiber. From Equation 52 and Equation 53 it is seen that the attenuation of a dispersion-compensating module can be reduced by increasing the dispersion coefficient thereby reducing the length of dispersion compensating fiber needed or by decreasing the attenuation coefficient of the fiber. This leads to a description of the performance of the dispersion-compensating module with respect to the added loss to the system by a figure of merit (FOM) given by:

$$FOM = \frac{-D_{DCF}}{\alpha_{DCF}} \qquad \text{Equation 54}$$

A high *FOM* signifies that a dispersion compensating fiber module adds less loss to the system. A high *FOM* can be obtained by either increasing the negative dispersion coefficient or by decreasing the attenuation coefficient of the dispersion compensating fiber.

The remainder of this chapter will be describing the design and realization of dispersion compensating fibers with high *FOM*.

As mentioned earlier, the *RDS* of the dispersion compensating fiber must match that of the transmission fiber in order to compensate the dispersion over a wide wavelength range. Consequently different fiber designs are needed for dispersion compensating fibers for NZDSF and SSMF transmission fibers (Table 15). Since the dispersion coefficient on NZDSF is much lower (4-5 ps/(nm km)) than on SSMF (16-17 ps/(nm km)), the accumulated dispersion on NZDSF is much smaller than for SSMF. On 100 km of SSMF a dispersion of 1650 ps/nm will be accumulated

compared to the 450 ps/nm accumulated on 100 km of NZDSF. The need of dispersion compensation for NZDSF fibers is thus smaller and shorter lengths of fibers will be needed, making a high *FOM* less important for dispersion compensating fibers for NZDSF than for the dispersion compensating fibers for SSMF.

The designs for high *FOM* dispersion compensating fibers discussed here will all be for compensating the dispersion of SSMF having an *RDS* of 0.0035 nm^{-1}.
Two fiber designs will be discussed. The first is the first attempt at making a dispersion compensating fiber with a high *FOM*. The high *FOM* for this fiber has been obtained by making a fiber with a very negative dispersion coefficient. This fiber is currently being manufactured at OFS Denmark. The second fiber design discussed here is an improvement of the first high *FOM* fiber. The main improvements are with respect to the bend loss sensitivity and the attenuation coefficient.

Dispersion compensating fibers with high *FOM* or high negative dispersion coefficients have been demonstrated previously. In [Auguste et al., 2000] a fiber having a dispersion coefficient of –1800 ps/(nm km) is reported, but the attenuation of this fiber is not well documented so the *FOM* is not known. Other reports include a fiber with a dispersion of –295 ps/(nm km), a *FOM* of 418 ps/(nm dB) and an *RDS* of 0.0004 nm^{-1} [Hawtof et al., 1996]. Another fiber has a negative dispersion of –302 ps/(nm km), a *FOM* of 459 ps/(nm dB) and a *RDS* of 0.0097 nm^{-1} [Wandel et al., 2001]. None of the high *FOM* fibers mentioned in the literature have slope match to SSMF. The last mentioned fiber has slope match to the low slope NZDSF.

6.4 First generation high *FOM* dispersion compensating fiber

The strategy for achieving a high *FOM* has been to increase the negative dispersion coefficient compared to that for standard dispersion compensating fibers. The primary goal for the design process has been to design a fiber with a very negative dispersion and to investigate which draw backs this will present with respect to other related optical properties such as bend loss performance and the sensitivity of the optical properties to variations in core diameter.

6.4.1 Design strategy

With the starting point for the design process being a standard dispersion compensating fiber for SSMF, the first step of increasing the negative dispersion coefficient is to make the dispersion curve deeper by increasing the negative index of the non-guiding area of the index profile – the trench, thereby reducing the coupling strength between the two guiding regions – the core and the ring. As discussed previously, this operation will not only make the dispersion curve deeper, it will also make the dispersion curve narrower as long as the slopes of the effective index differences of the core and ring modes remains unchanged. The consequence is a higher residual dispersion due to the increased dispersion curvature.

a)

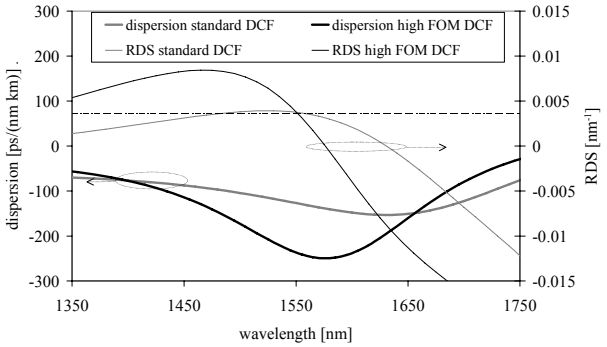

b)

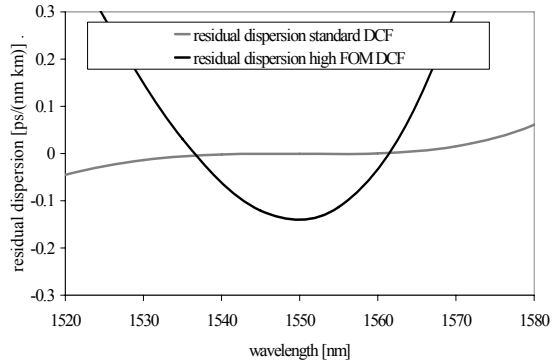

c)

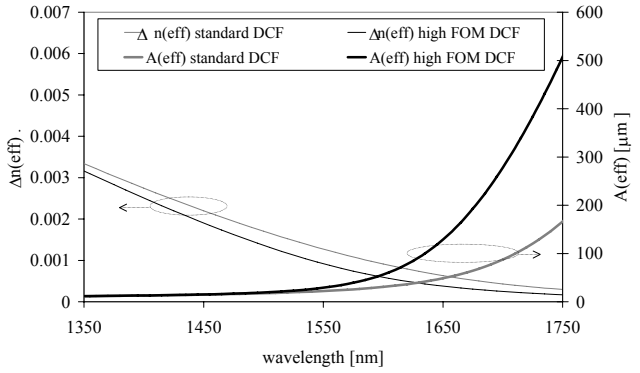

Figure 48
a) Modeled dispersion and *RDS* as functions of wavelength for the standard dispersion compensating fiber and the high *FOM* dispersion compensating fiber.
b) Modeled residual dispersion of a link consisting of SSMF and DCF
c) Modeled effective index difference and effective area as functions of wavelength for a standard dispersion compensating fiber and a high *FOM* dispersion compensating fiber

By increasing the core radius, the dispersion curve has been moved with respect to wavelength in order to obtain slope match to SSMF at 1550 nm. The dispersion and *RDS* curves of both the resulting high *FOM* dispersion compensating fiber and a standard dispersion compensating fiber [Qian et.al.2002] are given in Figure 48a. Of the two fibers, only the high *FOM* dispersion compensating has been developed as a part of this work. The standard dispersion compensating fiber is merely shown for comparison since it, as an established product, was used as a reference point for the

high *FOM* fiber. Index profiles of the two fiber designs are given in Figure 49. Both fibers have step index profiles.

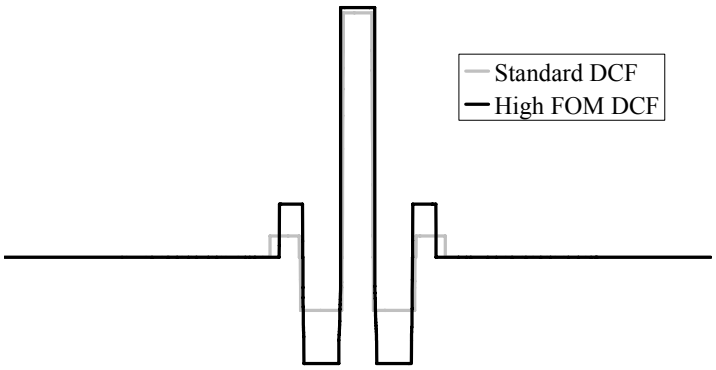

Figure 49 – Refractive index profiles of a standard dispersion compensating fiber and of the high *FOM* dispersion compensating fiber designed in this work

6.4.2 Fiber results

Typical measured optical properties of the two dispersion-compensating fibers are given in Table 16. The values are given at 1550 nm unless otherwise noted.

	Dispersion (ps/(nm km))	**Attenuation (dB/km)**	***FOM*** **(ps/(nm dB))**	**Residual dispersion variation (1530- 1565 nm) (ps/(nm km))**
Standard DCF	-120	0.43	280	± 0.05
High *FOM* DCF	-250	0.58	430	± 0.2

Table 16 – Typical values for the optical properties of standard and high *FOM* dispersion compensating fibers measured at 1550 nm unless otherwise noted.

Even though the dispersion coefficient of the high *FOM* fiber has been more than doubled compared to the standard dispersion compensating fiber, the *FOM* has only been increased from 280 ps/(nm dB) to 430 ps/(nm dB) due to the higher attenuation of the high *FOM* fiber.

The higher attenuation measured in the high *FOM* fiber is explained by an increased anomalous loss caused partly by the higher index difference between the core and the trench and partly by the increased F concentration in the trench which will increase the diffusion of F into the core and consequently affect the viscosity profile of the fiber (section 5.4).

For the standard dispersion compensating fiber, the operating wavelength of 1550 nm is very close to the inflection point of the dispersion curve and a very low residual dispersion of ± 0.05 ps/(nm km) can be obtained in the wavelength range 1530 nm –

1620 nm. For the high *FOM* dispersion compensating fiber, the operating wavelength of 1550 nm is close to the minimum dispersion point of the dispersion curve and the residual dispersion is consequently larger due to the high dispersion curvature. The residual dispersion in the C-band can be kept within ± 0.2 ps/(nm km) (Figure 48b).

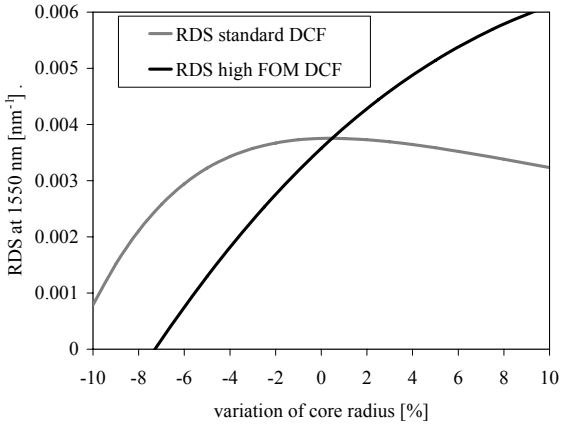

Figure 50 – The sensitivity of the *RDS* to variations of core radius (simulation).

Another result of the high dispersion curvature is a high sensitivity of the *RDS* of the high *FOM* fiber to variations in core diameter. In Figure 50 the *RDS* for the two dispersion compensating fibers is shown as a function of variations of core radius (in %) and it is seen that while a variation of the core radius of ±3% will lead to a variation of the *RDS* for the standard dispersion compensating fiber between 0.0035 and 0.0037 nm^{-1}, the same variation of the core radius will for the high *FOM* dispersion compensating fiber lead to a variation between 0.0023 and 0.0045 nm^{-1}. The large variation of the *RDS* value with core diameter will lead to a large variation of the residual dispersion across the C-band (Figure 51).

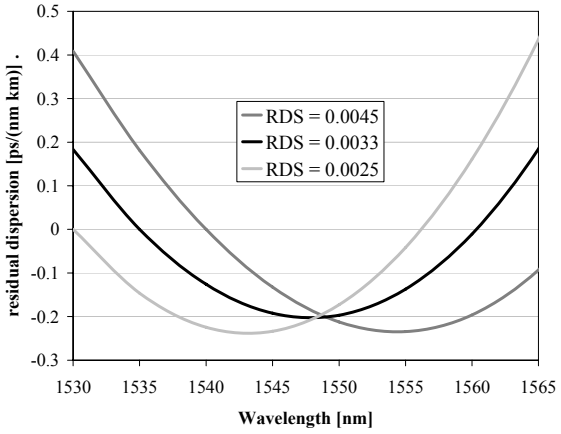

Figure 51 – Residual dispersion for a link (Figure 39) consisting of SSMF having an *RDS* of 0.0035nm^{-1} and one of 3 high *FOM* dispersion compensating fibers having *RDS* values ranging from 0.0025 nm^{-1} to 0.0045 nm^{-1}.

Another trade off is found in Figure 48c in which the effective index differences and the effective areas of the two fibers are shown as functions of wavelength. Due to the smaller coupling strength between core and ring mode for the high *FOM* fiber, the effective index difference of the LP_{01} mode follows the effective indexes for the core and ring mode more closely resulting in a lower effective index difference compared to the standard dispersion compensating fiber. The consequence of a lower effective index difference is higher micro and macro bend losses for the high *FOM* fiber.

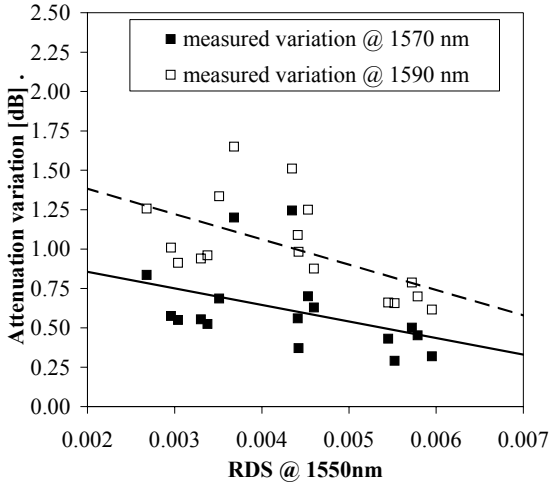

Figure 52 – Variations in attenuation of high *FOM* dispersion compensating fiber modules when subjected to temperature changes between -5 °C and 60°C.

It has been shown that there is a linear relationship between the measured micro bend loss of a dispersion compensating fiber and the measured variations in the attenuation when the dispersion compensating fiber module is subjected to temperature variations[2]. The variation is here defined as the difference between the maximum and minimum measured attenuation at a given wavelength when the module is subjected to temperature changes. As the effective index difference decreases on going to longer wavelengths, the micro bend losses and consequently the attenuation variations during temperature cycling increases. As shown in Figure 52 the attenuation variations increases when going from 1570 nm to 1590 nm. Furthermore, as the *RDS* value increases, corresponding to a movement of the operating wavelength to shorter wavelengths on the dispersion curve, away from the wavelength of minimum dispersion, the attenuation variation decreases due to the increased effective index.

The relation seen in Figure 52 between the *RDS* and the attenuation variations is thus through the relationship between the two parameters and the effective index difference.

6.4.3 Applications of dispersion compensating fiber with high *FOM*

The high *FOM* fiber is currently deployed in communication systems by several system houses. The fiber has furthermore been used for dispersion compensating Raman amplifiers (DCRAs) in an experiment in which the use of Raman-pumped

[2] Private communication, Lars Grüner-Nielsen ,OFS Denmark

dispersion compensating fiber amplifiers for multiplespan, terminal-only dispersion compensation of 40 x 10 Gb/s C-band channels over 6 x 80 km of SSMF fiber was demonstrated [Nelson et al. 2005]. The high *FOM* fiber was chosen for the experiment, as the low attenuation of the module was more important than a low residual dispersion. The low attenuation of the dispersion compensating fiber module was also the reason why the high *FOM* dispersion compensating fiber was chosen to be used in an experiment to test how the capacity of a CWDM system could be increased from 40 to 100 Gb/s [Thiele et.al 2003].

6.4.4 Conclusion on the first high *FOM* fiber

It has been demonstrated that it is possible to make a dispersion compensating fiber with slope match to SSMF having a record high *FOM* of 430 ps/(nm dB). The high *FOM* has been obtained by increasing the negative dispersion coefficient of the fiber.

One of the major trade offs for increasing the negative dispersion coefficient in order to achieve a high *FOM* has been a higher residual dispersion due to the higher dispersion curvature when the operating wavelength moves close to the minimum dispersion point of the dispersion curve. The high curvature also results in larger sensitivity of the *RDS* to variations in core diameter.

Another trade off for the negative dispersion is the increased micro bend loss sensitivity due to the lower effective index difference caused by the lower coupling strength between the core and the ring mode. The high micro bend loss results in large variations of the attenuation when the dispersion compensating fiber module is subjected to temperature changes.

For some applications, the record low attenuation and low nonlinearities of the module are more important than residual dispersion and variations of the attenuation due to temperature changes. It has thus been shown that by pushing the limits for acceptable micro bend loss and design sensibility to variations during manufacturing, the *FOM* of a dispersion compensating fiber can be substantially increased.

6.5 Second generation high *FOM* dispersion compensating fiber

The results obtained with the high *FOM* fiber are interesting since they show that it is possible to greatly increase the negative dispersion coefficient from around -120 ps/(nm km), which is the standard value in most dispersion compensating fibers to a dispersion coefficient as high as –250 ps/(nm km). But as shown, the very high negative dispersion coefficient comes at the cost of increased residual dispersion due to higher dispersion curvature and increased micro and macro bend loss sensitivity due to a low effective index difference. For the second high *FOM* fiber, the goal is to investigate whether all the trade offs encountered with the first high *FOM* fiber are inevitable and to find a manufacturable fiber design for a dispersion compensating fiber with a *FOM* > 500 ps/(nm dB).

6.5.1 Residual dispersion

One of the trade offs encountered with the first high *FOM* fiber is the high residual dispersion caused by the high dispersion curvature. A design search using the

optimizer function within the OFS modeling tool has been performed. The input to the design search is an input fiber profile, target values for dispersion, *RDS*, micro and macro bend losses and information on the range in which the profile parameters are allowed to vary. Since the object of the design search has been to eventually design a dispersion compensating fiber with a high *FOM*, the upper limit for the core index difference has been set to 0.03. Figure 35 shows that if the core index is higher than 0.03, an attenuation of less than 0.5 dB/km is difficult to obtain. The target values for the design search are given in Table 17 along with the values for the designs found during the search. The residual dispersions of the designs are shown in Figure 53 along with the residual dispersion of the first high *FOM* fiber for comparison.

	Dispersion [ps/(nm km)]	***RDS*** **[nm^{-1}]**	**Normalized micro bend loss**	**Cut off wavelength [nm]**
Target values	*-250*	*0.0035*	*< 100*	*< 1600 nm*
Design 1	-240	0.0037	55	1555
Design 2	-248	0.0036	53	1575
Design 3	-241	0.0036	52	1590
Design 4	-242	0.0036	56	1580

Table 17 – Target values and resulting design for design search

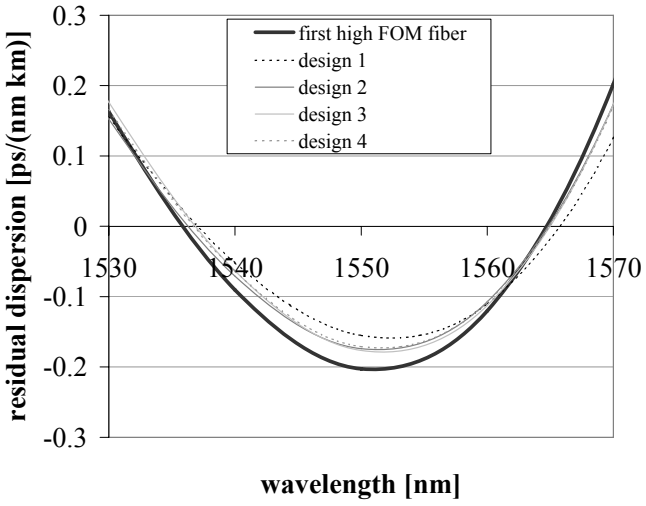

Figure 53 – Residual dispersion for the first high *FOM* fiber compared to the residual dispersion of the fibers being the results of the design search

As shown in Figure 53 none of the designs found during the design search has a significantly lower dispersion curvature than the first high *FOM* fiber. This is explained by the fact that as the core index has to be kept low in order to maintain low attenuation, the slopes of the effective index of the core and ring modes are not changed significantly and the area above the dispersion curve must remain constant. A dispersion of –250 ps/(nm km) must thus result in a high dispersion curvature.

6.5.2 Understanding the relation between *FOM* and micro bend loss

Accepting the high residual dispersion, improvements might be found regarding the micro and macro bend loss of the high *FOM* fiber. Both micro and macro bend losses are due to the low effective index difference which can be increased by increasing the core index of the high *FOM* fiber. However, a higher core index will lead to a higher attenuation and possibly also to a lower *FOM* unless the negative dispersion is increased correspondingly.

It was shown (in chapter 5.6) that the attenuation of high index fibers can be reduced by grading the index of the core. The question is how this grading of the core index affects the effective index difference and the dispersion coefficient of the fiber. It is expected that the effective index will be lower as the core exponent is decreased since the average refractive index of the core is reduced.

The effect on the dispersion coefficient and micro bend loss of changing the core exponent of the fiber can be evaluated using the OFS modeling tool for solving the scalar wave equation. If the design search is restricted to index profiles with similar viscosity profiles at the core boundary, the first loss model developed in this project (chapter 5.4) can be used for the determination of the attenuation coefficient for the fiber design. With the micro bend loss, the dispersion and the attenuation coefficients thus determined, it is possible to optimize the design for a high *FOM* fiber having low micro bend loss.

It is known from experience with the design of dispersion compensating fibers that the normalized micro bend loss factor for a dispersion compensating fiber should be no higher than 100 in order to avoid large attenuation variations when the dispersion compensating module is subjected to temperature changes.

A triple clad refractive index profile with a graded core index (design 2 of Table 17) is chosen as the starting point for the design optimization. It is possible to vary indexes and widths of all layers of the refractive index profile. However, for the present purpose of achieving an understanding of the mechanisms relating the *FOM* and the micro bend loss, only one or two parameters at a time will be allowed to vary while the others are kept constant.

With refractive indexes and widths of all layers of the refractive index profile kept constant and only allowing the core exponent (γ) to vary, the effect of the core exponent on the *FOM* and micro bend loss is investigated. Each point in Figure 54 represents a fiber design. As expected, the grading of the core results in a lower effective index difference and a higher normalized micro bend loss. The maximum in the *FOM* of 550 ps/(nm dB) for γ=5 is mainly due to the effect of the core exponent on the dispersion coefficient where lowering the effective index corresponds to going to longer wavelengths on the dispersion curve in Figure 42. The points in Figure 54 all seems to be situated along the same curve resembling a dispersion curve (turned upside-down). The effect on the *FOM* is of course modified by the effect of grading the core index on the attenuation. The interesting point is how universal this curve is. Is it possible to translate this curve by changing the widths and indexes of some or all of the layers in the triple clad index profile?

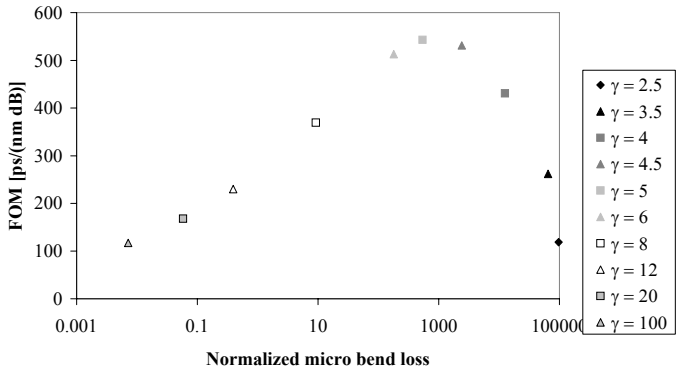

Figure 54 – The simulated relation between the figure of merit and the micro bend loss factor for a series of fiber designs where indexes and widths of all layers have been kept constant while varying the core exponent γ between 2.5 and 100.

Figure 55 shows the effect of not only varying the core exponent but also varying the core width. The effect of varying the core width on the effective index and the dispersion is very similar to the effect seen upon varying the core exponent so by changing the core width, the effect on the dispersion and of changing the exponent can be supplemented.

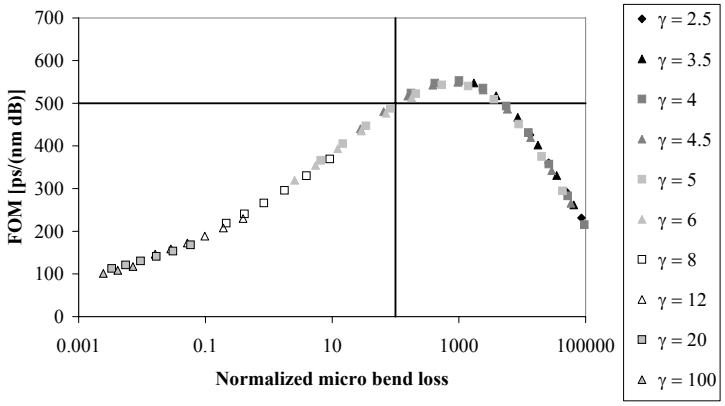

Figure 55 – The simulated relationship between the micro bend loss and the *FOM* when not only the core exponent but also the core width is changed.

A similar effect is seen upon changing the core index. The main difference being that the effect on the attenuation and consequently the *FOM* of changing the core index is much larger, making the curve less smooth.

In order for a design to fulfill the goals set up for an improved high *FOM* fiber, the design should fall within the upper left hand corner in Figure 55. That is with a *FOM* > 500 ps/(nm dB) and a normalized micro bend loss < 100. None of the simulated designs shown so far meet the requirements.

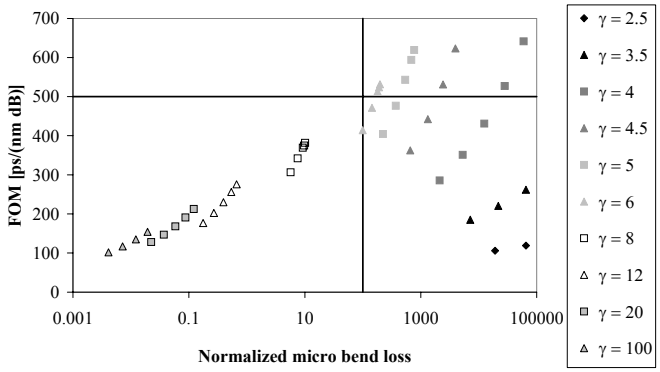

Figure 56 – The simulated relationship between the micro bend loss and the *FOM* when not only the core exponent but also the trench width is changed.

The effect of varying the width of the trench has also been investigated (Figure 56). Changing the width of the trench layer has a different effect on the relation between the *FOM* and the micro bend loss than the changes in the core parameters had. One major difference is that in the loss model used for calculating the attenuation, the width of the trench has no effect on the attenuation. Another effect is that increasing the width of the trench reduces the coupling strength between the core and the ring mode, increasing the curvature of the effective index difference and thereby the minimum negative dispersion.

Since the slope of the effective index of neither the core mode nor the ring mode has been changed, the area under the dispersion curve remains constant so increasing the width of the core will not only result in a the higher negative dispersion but also in a more narrow dispersion curve.

To complete the analysis, the effect of changing the width of the ring has been investigated as well (Figure 57). The largest effect is seen for designs with $\gamma < 5$ where an increase in the width of the ring results in largely unchanged micro bend losses but in a great reduction of the *FOM*. However, these designs all have micro bend losses that are much higher than the maximum allowed micro bend loss of 100.

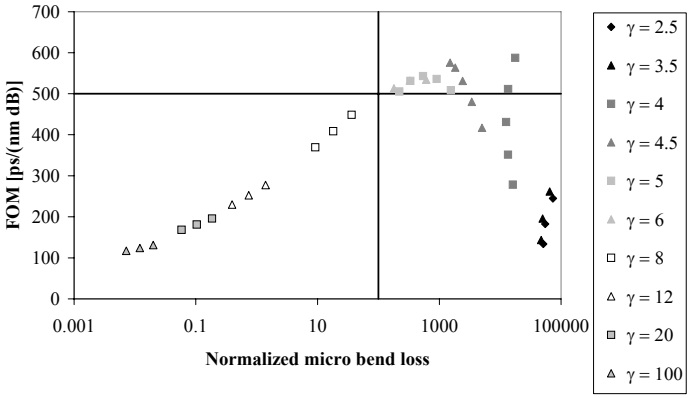

Figure 57 – The simulated relationship between the micro bend loss and the *FOM* when not only the core exponent but also the ring width is changed

Allowing all parameters of the refractive index profile to vary gives the result shown in Figure 58. The figure is much too busy to convey much understanding of how changing the individual profile parameters can affect the relation between the *FOM* and the micro bend loss. The two important conclusions to be drawn from Figure 58 are that several designs exist having not only a *FOM* > 500 ps/(nm dB) but also a micro bend loss < 100. Figure 59 shows a plot of these designs.

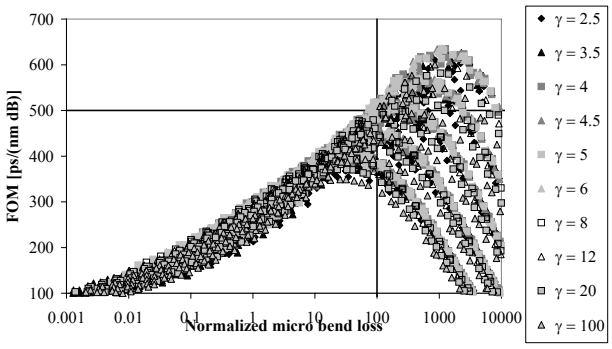

Figure 58 – The simulated relationship between the micro bend loss and the *FOM* when all parameters of the triple clad index profile are varied.

These designs fulfilling the requirements to the improved high *FOM* fiber all have a core exponent between 3.5 and 6. It should be kept in mind that this analysis has only been performed for designs having a graded core, but with no other optimizations of the viscosity profile or the slope of the refractive index profile at the core boundary. It is thus very likely that a higher *FOM* can be obtained by optimizing the fiber design with respect to viscosity and refractive index profile.

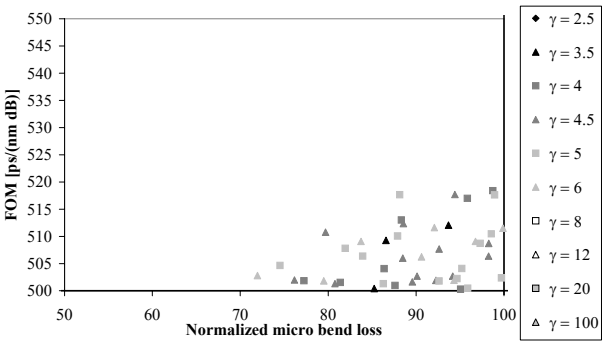

Figure 59 – Detail of Figure 58. The designs fulfilling the requirements to the improved high *FOM* fiber: *FOM* > 500 ps/(nm dB) and a normalized micro bend loss < 100

Another conclusion to be drawn from Figure 58 is that if the requirement to the micro bend loss performance of the design can be relaxed, a *FOM* higher than 500 ps/(nm dB) can easily be obtained. A way to relax this requirement could be to increase the fiber diameter or possibly by modifying the coating's ability to absorb deformations. No experiments have been performed to test the validity of this conclusion.

6.5.3 Fiber results on improved high *FOM* dispersion compensating fiber

In order to test the results from the design search a design has been chosen for realization.
The design chosen has a core index of 0.028 and a core exponent of 4.5. A fiber with this design will, according to the models, have a *FOM* of 506 ps/(nm dB) and an *RDS* of 0.0035 nm^{-1}.
As it turned out, the realized fiber had a higher core exponent of 5.5 resulting in a dispersion coefficient of only –248 ps/(nm km) instead of the expected –258 ps/(nm km) and an attenuation of 0.53 dB/km instead of the expected 0.51 dB/km resulting in a *FOM* of 470 ps/(nm dB). Even though the target value for *FOM* of 500 ps/(nm dB) was not reached, the realized fiber has some very interesting properties, especially compared to the first high *FOM* fiber. Details of the design and of the realized fiber are given in Table 18.

	Core index	**Core exponent**	**Dispersion [ps/(nm km)]**	**Attenuation [dB/km]**	***FOM* [ps/(nm dB)]**	**Normalized micro bend loss**
Design	0.028	4.5	-258	0.51	506	89
Realized fiber	0.028	5.5	-248	0.53	470	42

Table 18 – Profile parameters and calculated values for dispersion, attenuation, *FOM* and the normalized micro bend loss for the chosen fiber design and for the realized high *FOM* dispersion compensating fiber.

The residual dispersions of the first and of the improved high *FOM* fibers are very similar as shown in Figure 60. The differences are due to differences in *RDS* rather than differences in the dispersion curvature. Since the first *FOM* fiber has an attenuation of 0.58 dB/km and a normalized micro bend loss of 520, it has now been shown that it is indeed possible to improve both the *FOM* and the micro bend loss without increasing the residual dispersion.

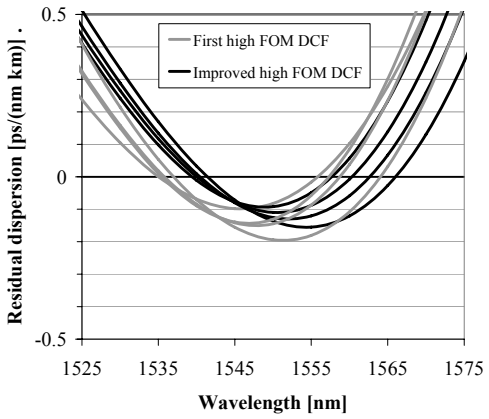

Figure 60 – Typical residual dispersion based on measured dispersion of the first and the improved high *FOM* dispersion compensating fibers.

6.5.4 Further improvements for high *FOM* dispersion compensating fibers

It has been shown that it is possible to improve both the *FOM* and the micro bend loss of dispersion compensating fibers without increasing the residual dispersion. This has been achieved by performing a systematical design search in which both the wave guiding properties and the attenuation of the fiber was taken into account. Further improvements are however possible.

By choosing one of the designs from Figure 59 it is possible to achieve the *FOM* > 500 ps/(nm dB) with only a minor increase of the micro bend loss. Furthermore, as shown in chapter 5.6 it is possible to obtain the same dispersion properties for fibers with differing viscosity profiles and refractive index profiles, so an optimization of the attenuation coefficient without decreasing the high negative dispersion coefficient is also possible thereby offering the possibility of a dispersion compensating fiber having an even higher *FOM*.

6.6 Conclusions on design of high *FOM* fibers

In this chapter the trade offs regarding the design of high *FOM* dispersion compensating fibers have been presented. The main trade offs have been found to be between parameters such as a very negative dispersion coefficient and low micro bend losses or between the very negative dispersion coefficient and the residual dispersion.

The first high *FOM* fiber produced has a high *FOM* of 430 ps/(nm dB) but also high micro bend losses leading to large attenuation variations when the dispersion compensating fiber module is subjected to temperature changes. This fiber is currently employed in optical communication systems in which a high *FOM* is more important than low residual dispersion or low variation of the attenuation when the module is subjected to temperature changes.

By performing a systematical design search an improved design for a high *FOM* dispersion compensating fiber has been found. This has led to the design of a dispersion compensating fiber having a high *FOM* of 470 ps/(nm dB) which is the highest *FOM* reported for a dispersion compensating fiber with slope match to SSMF. The fiber has a micro bend loss, which is more than 10 times lower than the first high *FOM* fiber.

If the conclusions from chapter 5.6 on how to tailor the refractive index profile to achieve a lower anomalous loss are applied, a further reduction of the attenuation coefficient should be possible, resulting in an increased *FOM*.

7. Conclusion

In this work some important aspects on attenuation in optical fibers have been investigated.

The unusually high attenuation of a group of transmission fibers has been measured in the wavelength range (290 nm – 1700nm). The measurements of the spectral attenuation in a wide wavelength range have been proven to be a valuable tool for analyzing the attenuation in optical fibers. Strong evidence point to Ni to be the cause of the high attenuation observed in these fibers.

The main achievement presented in this work is the model for predicting the attenuation in high index fibers. Two versions of the model have been presented, each with its strengths and weaknesses.

The strength of the first model for predicting the attenuation of high index fibers is that the attenuation of high index fibers can be predicted simply on the basis of the index profile and knowledge of draw conditions. This makes this model highly useful for the design of dispersion compensating fibers with high *FOM*. Without this model for predicting the attenuation, in order to determine the attenuation resulting from a given fiber design, the fiber will have to be manufactured first, and only then can the attenuation be measured. With the model, the attenuation can be predicted with good accuracy on the basis of the index profile, thus making the design process much simpler, faster and less expensive.

The weakness of the first model is that it can only predict the attenuation of fibers having similar viscosity profiles as those for which it was calibrated. This drawback has led to the improvement of the model.

Since it has been shown that not only the index profile but also the viscosity profile and the mode field distribution affects the attenuation of high index fibers, the model for predicting the attenuation has been expanded to include the viscosity profile, the refractive index, and the mode field distribution.

The strength of this improved model is its ability to provide guidelines as to how the viscosity profile and the refractive index profile must be engineered in order to lower the attenuation of high index fibers. The model has been used for the design of a series of high index fibers with varying viscosity and refractive index profiles. It has been shown that by controlling the viscosity profile as well as the refractive index profile, the attenuation of high index fibers can be reduced.

The weakness of the improved model is its complexity especially with respect to the determination of the viscosity profiles. The viscosity profiles are calculated on the basis of the dopant profiles, which must be estimated through calculations of diffusion of dopants during processing. That the viscosities are based on an estimate is a serious weakness of the model. The model has however been shown to be able to predict with high accuracy the attenuation of high index fibers having very different viscosity profiles at the core boundary.

Another important result is the development of dispersion compensating fibers having a high figure of merit (*FOM*) signifying a high ratio between the negative dispersion coefficient and the attenuation coefficient of the dispersion compensating fiber. A high *FOM* is needed for dispersion compensating modules with low loss.

The trade offs encountered when designing high *FOM* fibers have been investigated and it has been found that the main trade offs are between achieving at the same time a very negative dispersion coefficient, a low attenuation coefficient, and low micro bend loss. The first model for predicting the attenuation of high index fibers has been applied in the search for a design of a dispersion compensating fiber having a high *FOM* and low micro bend loss. As a result of the design search, fibers having a record high *FOM* of 470 ps/(nm dB) have been realized.

8. References

Agraval,G.P.; *Fiber-optic communication systems*; John Wiley & Sons, Inc (1997)

Ainslie,B.J., J.K.Beales, C.R.Day, J.D.Rush; Interplay of design parameters and fabrication conditions of the on the performance of monomode fibers made by MCVD; *IEEE Journal of Quantum Electronics* (1981), vol qe-17, no 6, 854-857

Ainslie,B.J., K.J.Beales, D.M.Cooper, C.R.Day, J.D.Rush; Drawing dependent loss in single mode fibers; *Proceedings of 1982 Optical Fiber Communications*, paper THEE6

Ainslie,B.J., K.J.Beales, D.M.Cooper, C.R.Day; Sensitivity of the performance of monomode fibres to the fabrication conditions; *Proceedings of the SPIE* 425 (1983) 15-21

Andreasen,S.B.; New bending loss formula explaining bends on the loss curve; *Electronics letters*, Vol 23, 21 (1987) pp1138-1139

Angell,C.A; Formation of glasses from liquids and biopolymers; *Science* (1995), vol 267, 1924-1935

Antonyuk,B.P., V.B.Antonyuk, A.A.Frolov; Charge transfer excitons in Ge-doped silica fibres and their response to static electric field; *Optics Communications* 174 (2000) 427

Auguste,J.L, R.Jindal, J.-M.Blondy, M.Clapeau, J.Marcou, B.Dussardier; -1800 ps/(nm km) chromatic dispersion at 1.55 micron in dual concentric core fibre *Electronics letters*, 2000, Vol 36, 20 p1689

Bauch, H., V.Paquet, W.Siefert; Properties of PICVD-Fibers with pure SiO_2-core: The influence of the preform collapse process *Journal of optical Communications*, 8 (1987) p140

Bell,R.J**.**, D.C.Hibbins-Butler; Acoustic and optical modes in vitreous silica, germania and beryllium fluoride; *Journal of physics C: Solid state physics* (1975), vol 8, 787-792

Bell,R.J., P.Dean, D.C. Hibbins-Butler; Normal mode assignments in vitreous silica, germania and beryllium fluoride; *Journal of Physics C: Solid state physics* (1971), vol 4, 1214-1220

Bredol,M., D.Leers, L.Boisselaar, M.Hutjens; Improved model for OH absorption in optical fibers; *Journal of Lightwave Technology* (1990), vol 8, no 10, 1536-1539

Brehm,C., P.Dupont, G.Lavanant, P.Ledoux, C.Le Sergent, C.Reinaudo; Improved drawing conditions for very low loss 1.55 my dispersion shifted fiber; *Fiber and integrated optics* (1988), Vol 7, pp333-341

Burns,R.G., W.S.Fyfe; Site of preference energy and selective uptake of transition-metal ions from a Magma; *Science* vol 144 (1964) 1001

Chang, K.H., D.Kalish, M.I.Pearsall; New hydrogen aging loss mechanism in the 1400 nm window; *Proceedings of 1999 Optical Fiber Communication*, post deadline paper PD22.1

Cheng,X., Y.Jaluria; Effect of furnace design on high speed optical fiber drawing; *Proceedings of the 49th International Wire and Cable Symposium*, 479-484

Choudhury,S.R., Y.Jaleuria, S.H-K.Lee; A computational method for generating the free-surface neck-down profile for glass flow in optical fiber drawing; *Numerical Heat Transfer* (1999), Part A, 35, 1-24

Choudhury,S.R., Y.Jaleuria; Practical aspects in the drawing of an optical fiber; *Journal of materials research* (1998), vol 13, no 2, 483-493

Cotton,F.A., G.Wilkinson, P.L.Gaus; Basic inorganic chemistry (3rd ed.); *John Wiley & Sons, Inc*. (1995)

Crank,J.; The mathematics of diffusion, 2nd ed.; *Oxford Science Publications* (1975)

Davey,S.T, D.L.Williams, D.M.Spirit, B.J.Ainslie; The fabrication of low loss high NA silica fibres for Raman Applications; *SPIE* Vol 1171(1989) 181-191+A81
Dianov,E.M., V.M.Mashinsky,V.B.Neustruev, O.D.Sazhin; Origin of excess loss in single-mode optical fibers with high GeO_2-doped silica core; *Optical Fiber Technology* (1997) vol 3, 77-86
Dow, J.D.; Urbach's Rule; In: Optical properties of Highly Transparent Solids, *Plenum Press*, New York (1975)
Garret,I., C.J.Todd; Components and system for long-wavelength monomode fibre transmission; *Optical and Quantum Electronics* (1982), vol 14, 95-143
Geissberger,A.E., F.L.Galeener; Raman studies of vitreous SiO_2 versus fictive temperature; *Physical Review B* (1983), vol 28, no 6, 3266-3288
Gitter,M., W.Vogel; Absorptionsspektren, magnetische Eigenschaften und Koordinationsverhalten von Ni(II) in Gläsern; *Wiss.Ztschr.Friedrich-Schiller-Univ. Jena, Math.-Nat*.R.28.Jg.(1979), H. 2/3
Gloge,D.; Optical-fiber packaging and its influence on fiber straightness and loss; *The Bell system technical journal*, vol 54, 2,(1975) 245-263
Grüner-Nielsen,L., S.N.Knudsen, B.Edvold, T.Veng, D.Magnussen, C.C.Larsen, H.Damsgaard; Dispersion compensating fibers; *Optical fiber technology*; Vol6, no 2 (2000+A38) 164-180
Guenot,P., P.Nouchi, B.Poumellec; Influence of drawing temperature on light scattering properties of single mode Fibers; *Proceedings 1999 Optical Fiber Communications*, Paper ThG2
Hass, M.; Raman spectra of vitreous silica, germania and sodium silicate glasses; *Journal of physics and chemistry of solids* (1970), vol 31, no 3, 415-422
Hatayama,H., M.Hirano, T.Yokokawa, T.Kato, M.Onishi, E.Sasaoka; Dispersion compensating fiber for large-Aeff NZ-DSF with low residual dispersion by the technique of suppressing the micro-bending loss; *Proceedings of 2003 European Conference on Optical Communications*, Paper We 4.P.32
Hawtof,D.W., G.E.Berkey, A.J.Antos; High figure of merit dispersion compensating fiber; *Proceeding of 1996 Optical Fiber Communications*, Paper D6
Humbach,O., H.Fabian, U.Grzesik, U.Haken, W.Heitmann; Analysis of OH absorption in synthetic silica; *Journal of Non-crystalline Solids*(1996), vol 203, 19-26
ITU-T Recommendation G.652
ITU-T Recommendation G.655
ITU-T Recommendation G.692
Kaiser,P.; Contamination of furnace-drawn silica fibers; *Applied Optics*, Vol 16, no3 (1977) 701
Kanamori,H., H. Yokota, G.Tanaka, M.Watanake, Y.Ishiguro, I.Yashida, T.Kakii, S.Hoh, Y.Asano, S.Tanaka; Transmission characteristics and reliability of pure-silica-core single-moded fibers; *Journal of Lightwave Technology*(1986) vol 4, no 8, 1144-1150
Kapron,F.P., D.B.Keck, R.D.Maurer; Radiation losses in glass optical waveguides; *Applied Physics Letters* (1970), vol 17, no 10, 423-425
Kato,T., M.Hirano, K.Fukuda, A.Tada, M.Onishi, M.Nishimura; Design optimization of dispersion compensating fiber for NZ-DSF considering nonlinearity and packaging performance; Proceeding of 2001 Optical Fiber Communications, Paper TuS6
Kato,T., M.Hirano, M.Onishi, M.Nishimura; Ultra-low nonlinearity low-loss pure silica core fibre for long-haul WDM transmission; *Electronics Letters* (1999), vol 35, 1615
Kirchhof,J., P.Kleinert, A.Funke, B.Knappe, H-.R.Müller; About the smoothing of concentration fluctuations by diffusion in the glass systems SiO_2/GeO_2 and $SiO_2/GeO_2/B_2O_3$; *Cryst.Res.Technol*, 22, 6 (1987) K105-108

Kirchhof,J., S.Unger, B.Knappe, J.Vobian; Interaction of germanium and fluorine in the preparation of optical waveguides; *Proceeding of 1994 Optical Fiber Communications*, Poster WK11
Kirchhof,J., S.Unger, K.-F.Klein, B.Knappe; Diffusion behaviour of fluorine in silica glass; *Journal of non-crystalline solids* 181 (1995) 266-273
Kristensen, M.; Refractive Index Engineering in silica glass; Dissertation for Doctor Technices; Research Center COM, *Technical University of Denmark* (2003)
Kristensen,P.; Design of dispersion compensating fibers; Proceedings of 2004 European Conference on Optical Communications, Paper We 3.31
Kyoto,M., Y.Ohoga, S.Ishikawa, Y.Ishiguro; Characterisation of fluorine-doped silica glasses; *Journal of materials science* 28 (1993) 2738-2744
Likhachev,M.E., M.M.Bubnov, S.L.Semenov, V.F.Khopin, M.Yu. Salganskii; Optical Losses in single-mode and multi-mode fibres heavily doped with GeO_2 and P_2O_5; *Quantum Electronics* 34 (3) (2004) 241-246
Likhachev,M.E., M.M.Bubnov, S.L.Semenov, V.V.Shvetsov, V.F.Khopin; Mechanisms of optical losses in fibres with a high concentration of germanium dioxide; *Quantum Electronics* 33 (7) (2003) 633-638
Lines, M.E.; Scattering loss in optic fiber materials. I. A new parameterization; *Journal of Applied Physics* (1984), vol 55, no 11, 4052-4057
Lines,M.E., W.A.Reed; D.J.DiGiovanni; J.R.Hamblin; Explanation of anomalous loss in high delta singlemode fibers; *Electronic letters*; Vol 35 (1999) p1009-10
Lines,M.E.; Can the minimum attenuation of fused silica be significantly reduced by small compositional variations? I: Alkali metal dopants; *Journal of Non-Crystalline Solids* 171 (1994) 209-218
Lyytikäinen,K.. S.T.Huntington, A.L.G.Carter, P.McNamara, S.Fleming; Dopant diffusion during optical fiber drawing; *Optics Express*, vol 22, No 6 (2004) 972-977
MacChesney, J.B., P.B.O'Connor, H.M.Presby; *Proc.IEEE* 62, 1278-1279 (1974)
Mahinsky, V.M., E.M.Dianov, V.B.Neustruev, S.V.Lavrichev, A.N.Guryanov; V.F.Khopin; N.N.Vechkanov,O.D.Sazhin; UV absorption and excess optical loss in preforms and fibers with high germanium content; *Proceedings of the SPIE* (1994), 2290, 105-112
Marcuse,D.; Microdeformation losses of single-mode fibers; *Applied Optics*, Vol23, No7, (1984) 1082-1091
Mazumder,P., S.L.Logunov, S.Raghavan; Analysis of excess scattering in optical fibers; *Journal of Applied Physics* (2004), vol 96, no 8, 4042-4049
Miya,T., Y.Terunuma, T.Hosaka, T.Myashita; Ultimate low-loss single-mode fibre at 1.55 μm; *Electronics Letters* (1979), vol 15, no 4, 106-108
Möncke,D., D.Ehrt, H.Eckert, V.Mertens; Influence of melting and annealing conditions on the structure of borosilicate glasses; *Physics and Chemistry of Glasses*, vol 44, no2 (2003) pp113-116
Möncke,D., D.Ehrt; Influence of melting and annealing conditions on the optical spectra of a borosilicate glass doped with CoO and NiO Glass; *Sci.Technol*, vol75, no 4 (2002) pp163
Möncke,D., D.Ehrt; Radiation-induced defects in CoO- and NiO-doped fluoride, phosphate, silicate and borosilicate glasses; *Glass science Technology* (2002), vol 75, no 5, 243-253
Nagayama,K., T.Saitoh, M.Kakui, K.Kawasaki, M. Matsui, H. Takermizawa, H.Myiaki, Y.Ooga, I.Tscichiya, Y.Chigwa; Ultra low loss (0.151 dB/km) fiber and its impact on submarine transmission systems, *Proceedings of 2002 Optical Fiber Communications* , post deadline paper FA-10

Nagel,S.R.; Optical fiber - the expanding medium; *IEEE Circuits and Devices Magazine* (1989), vol 5, no 2, 36-45
Neeves, A.E; Experimental apparatus for measurement of the angular, polarization and wavelength dependence of light scattering from the visible to the infrared in bulk glass samples; *Applied Optics,* vol31, No12 (1992) 2072
Nelson,C., W.B.White; Transition metal ions in silicate melts. Part 3. Nickel in quenched oxide glasses; *Physics and chemistry of glasses*, Vol34, No5 (1993) p219
Nelson,L.E., C.G.Jørgensen, M.Du, T.Loadholt, D.Peckham; Raman-pumped dispersion compensating fiber amplifiers for terminal-only compensation of 6 x 80 km, 10 Gb/s WDM transmission; *Proceedings of 2005 European Conference on Optical Communications*, Paper Mo. 4.2.2
Nelson,L.E.; Optical Fibers for High-capacity WDM, Long-Haul systems IEICE trans. *Electron*, Vol E86-C (2003) 693
Neustruev,V.B.; Colour centres in germanosilicate glass and optical fibres; *J.Phys; Conden. Matters* (1994) vol 6, 6901-6936
Ohashi,M**.**, K.Shiraki, K.Tajima; Optical loss property of silica-based single mode fibers; *Journal of Lightwave technology* (1992); vol 10, no.5, 539
Ohashi,M., M.Tateda, K.Shiraki, K.Tajima; Imperfection loss reduction in viscosity-matched optical fibers; *IEEE Photonics Technology Letters* (1993), vol 5, no 7, 812-814
Ohashi,M., M.Tateda, K.Tajima, K.Shiraki; Fluorine concentration dependence of viscosity in F-doped silica glass; *Electronics Letters* (1992) vol 28, no 11, 1008-1010
Paek,U.C., C.M.Schroeder, C.R.Kurkjian; Determination of the viscosity of high silica glasses during fibre drawing; *Glass Technology* (1988), vol 29, no 6, 263-266
Paek,U.C., C.R.Kurkjian; Calculation of cooling rate and induced stresses in drawing of optical fibers; *Journal of the American Ceramic Society*, vol 58 (1975) no 7-8, 330-335
Paek,U.C., R.B.Runk; Physical behavior of the neck-down region during furnace drawing of optical fibers; *Journal of applied physics* 49 (8) (1978) 4417-4422
Paek,U.C.; High-speed high-strength fiber drawing; *Journal of Lightwave Technology* (1986), vol. LT-4, no8, 1048-1060
Pasquarello,A., R.Car; Identification of raman defect lines as signatures of ring structures in vitrous silica; *Physical Review B* (1998), vol 80, no 23, 5145-5147
Petermann,K.; Theory of microbending loss in monomode fibers with arbitrary index profile; *Archiv für Elektronik und Übertragungstechnik*, vol 30, no 9 (1976) pp337-342
Qian,Y., S.Dyrbøl, J.S.Andersen, PB.Gaarde, C.G.Jørgsensen, B.Pálsdóttir, L. Grüner-Nielsen; Bi-directionality pumped discrete raman amplifier with optimised dispersion compensation for non-shifted transmission fibre; *Proceedings of the 2002 European Conference on Optical Communications,* paper 4.1.6
Rathje,J., L.Grüner-Nielsen; Relationship between relative dispersion slope of a transmission fiber and the useable bandwidth after dispersion compensating; *Proceedings of the 2002 European Conference on Optical Communications*, paper P1.23
Rawson,E.G.; Analysis of Scattering from Fiber Waveguides with Irregular Core Surfaces; *Applied Optics*, Vol13, No10 (1974) 2370-2377
Roberts, P.J., F.Couny, H.Sabert, B.J.Mangan, D.P.Williams, L.Farr, M.V.Mason, A.Tomlinson; Ultimate low loss of hollow-core photonic crystal fibres; *Optics Express* (2005) Vol 13, no 1, 236-244
Schneider,V.M., J.A.West; Analysis of wideband dispersion slope compensating optical fibres by supermode theory; Electronics Letters vol 38, No 7 (2002) 306-307
Schultz,P.C.; Ultraviolet absorption of titanium and germanium in fused silica; *Proceedings of XI International Congress on Glass* (1977); vol 13, 155-163

Schultz,P.G.; Optical absorption of the transition elements in vitreous silica; *J.Am.Ceram.Soc* 57 [7] (1973)
Shelby,J.E.; Introduction to glass science and technology, 2nd ed.; *The Royal Society of Chemistry* (2005)
Shiraki,K. M.Ohashi, K.Tajima, M.Tateda, K.Tsujikawa; Viscosity of F and GeO2 codoped silica glass; *Electronics letters* vol29, No14, (1993) 1263-1265
Shiraki,K., M.Ohashi; Scattering property of fluorine doped silica glasses; *Electronic letters*, 1992, Vol28, No 17, p 1565
Skuja,L., K.Kajihara, Y.Ikuta, M.Hirano,H.Hosomo; Urbach absorption edge of silica: reduction of glassy disorder by fluorine doping; *Journal of non-crystalline solids* (2004), vol 345&346, 328-331
Skuja,L.; Optically active oxygen-deficiency-related centres in amorphous silicon dioxide; *Journal of Non-crystalline Solids* (1998), vol 239, 16-48
Stone,J.; Interactions of hydrogen and deuterium with silica optical fibers: A review; *Journal of Lightwave Technology* (1987), vol LT-5, no 5, 712-733
Stone;J., G.E.Walrafen; Overtone vibrations of OH groups in fused silica optical fibers; *Journal of Chemical Physics* (1982), vol 76, no 4, 1712-1722
Suzuki, T., Y.Ohishi; Broadband near-infrared emission from nickel in zinc-alumino-silicate glass; *Proceedings of XX International Conference on Glass*, 2004, Paper O-14-004
Tajima,K., M.Tateda, M.Ohashi; Viscosity of GeO2-doped silica glasses; *Journal of Lightwave Technology*, Vol 12, no 3 (1994) pp 411
Tajima,K., Y.Miyajima; Viscosity-matched P_2O_5-SiO_2 core single mode fiber; *Proceedings of the 1997 Optical Fiber Communications*, paper TuB5
Tateda,M., M.Ohashi, K.Tajima, K.Shiraki; Design of viscosity-matched optical fibers; *IEEE photonics technology letters* vol 4, No 9 (1992)
Thiele,H.J., L.E.Nelson, S.K.Das; Capacity enhanced coarse WDM transmission using 10 Gbit/s sources and DWDM overlay; *Electronics Letters* (2003), vol 39, no 17, 1264-1266
Tsujikawa,K., K. Tajima, M.Ohashi; Rayleigh scattering reduction method for silica based optical fiber; *Journal of lightwave technology*, Vol18 (2000), No11, p1528,
Tsujikawa,K., M.Ohashi, K.Shiraki, M.Tateda; Scattering property of F and GeO_2 codoped silica glasses; *Electronic letters*, 1994 vol 30, No4, 351
Tsukitani,M., M.Matsui, K.Nagayama, E.Sasaoka; Ultra Low Nonlinearity Pure-Silica-Core Fiber with an Effective area of 211 μm2 and transmission Loss of 0.159 dB/km; *Proceedings of 2002 European Conference on Optical Communications*, Paper 3.2.2
Turner,W.H., J.A.Turner; Ligand-Field spectra and structure of Nickel in Silicate glasses; *Journal of the American Ceramic society*, Vol55 No4 (1972) p201
Urbach,F.; The Long-Wavelength edge of photographic sensitivity and of the electronic absorption of solids; *Phys.Rev.Letters* 92 (1953) p1324
Vasiljev,V.N., G.N.Dulnev, V.D.Namuchic; The flow of a highly viscous liquid with a free surface; *Glass technology*, Vol30, no 2 (1989) 83-90
Wandel,M., Kristensen,P.;Fiber design for high figure of merit and high slope dispersion compensating fibers; *J.Opt.Fiber.Commun.Rep* 2.1-36 (2005), Springer Science and Business Media Inc. Accepted for publication
Wandel,M., T.Veng, Q.Le, L.Grüner-Nielsen; Dispersion compensating fibre with a high figure of merit; *Proceedings of 2001 European Conference on Optical Communications*, Paper PD.A.1.4
Wandel,M; L. Grüner-Nielsen; Measurement and modelling of absorption due to defects in optical fibres; *Proceedings of the XX International Congress on Glass* (2004), paper 0-14-003

White,W.B., D.S.Knight; Transition metal ion species in glass: A comparison of optical absorption and luminescence evidence; *Mat. Res. Soc. Symp.* (1986), vol 61,
Yablon, A.; Stresses and Strains Frozen into Optical Fibers; *Proceedings of 2004 Optical Fiber Communications*, Paper TuB1

9. Publications:

M.Wandel, P.Kristensen; Fiber designs for high figure of merit and high slope dispersion compensating fibers; J.Opt.Commun. Rep.2, 1-36 (2005) – accepted for publication

L. Grüner-Nielsen, M. Wandel, P. Kristensen, C. Jørgensen, L. V. Jørgensen, B. Edvold, B. Pálsdóttir and D. Jakobsen; "Dispersion Compensating Fibers"; Journal of Lightwave Technology, Vol. 23, No. 11; 2005 – accepted for publication

*K.Rottwitt, H.Ou, M.Wandel; "Nonlinear germanium nanocluster doped planar waveguides", Proc.SPIE, Vol 5971 (2005) 83-90

M.Wandel, L.Grüner-Nielsen; "Measurement and modeling of absorption due to defects in silica based optical fibers"; Proceedings of XX International Congress on Glass (2004) paper O-14-007

Patents:

US.Pat-no: 6.654.531: L.Grüner-Nielsen, P.Kristensen, Q.Le, M.Wandel; Dispersion Compensating Module

US.Pat-no: 6.498.887: L.Grüner-Nielsen, P.Kristensen, Q.Le, M.Wandel; Dispersion compensating fiber having a high relative dispersion slope.

*) Outside the scope of this thesis.